

APPLIED COMPUTER SCIENCE

**VOL.13, No.1,
2017**



ISSN1895-3735

www.acs.pollub.pl

APPLIED COMPUTER SCIENCE

The Journal is a peer-reviewed, international, multidisciplinary journal covering a broad spectrum of topics of computer application in production engineering, technology, management and economy.

The main purpose of Applied Computer Science is to publish the results of cutting-edge research advancing the concepts, theories and implementation of novel solutions in computer technology. Papers presenting original research results related to applications of computer technology in production engineering, management, economy and technology are welcomed.

We welcome original papers written in English. The Journal also publishes technical briefs, discussions of previously published papers, book reviews, and editorials. Especially we welcome papers which deals with the problem of computer applications in such areas as:

- manufacturing,
- engineering,
- technology,
- designing,
- organization,
- management,
- economics,
- innovations,
- competitiveness,
- quality and costs.

The Journal is published quarterly and is indexed in: BazTech, Cabell's Directory, CNKI Scholar (China National Knowledge Infrastructure), ERIH PLUS, Index Copernicus, J-Gate, Google Scholar, TEMA Technik und Management.

Letters to the Editor-in-Chief or Editorial Secretary are highly encouraged.

CONTENTS

Paweł MAGRYTA

**AERODYNAMIC RESEARCH OF THE OVERPRESSURE
DEVICE FOR INDIVIDUAL TRANSPORT..... 5**

Tytus TULWIN

MODELLING OF A LARGE ROTARY HEAT EXCHANGER.....20

Yuriy TRYUS, Nataliya ANTIPOVA,
Kateryna ZHURAVEL, Grygoriy ZASPA

**INFORMATION TECHNOLOGY OF STOCK INDEXES
FORECASTING ON THE BASE OF FUZZY NEURAL
NETWORKS..... 29**

Stanisław BŁAWUCKI, Kazimierz ZALESKI

**CONSTRUCTION AND TECHNOLOGICAL ANALYSIS
OF THE BROACH BLADE SHAPE USING
THE FINITE ELEMENT METHOD..... 41**

Michał BIAŁY, Marcin SZLACHETKA

**CRANK-PISTON MODEL OF INTERNAL COMBUSTION
ENGINE USING CAD/CAM/CAE IN THE MSC ADAMS..... 51**

Evans BAIDOO

**FIREWORKS ALGORITHM FOR UNCONSTRAINED
FUNCTION OPTIMIZATION PROBLEMS..... 61**

Paweł PIEŚKO, Magdalena ZAWADA-MICHAŁOWSKA

**USEFULNESS OF MODAL ANALYSIS
FOR EVALUATION OF MILLING PROCESS STABILITY..... 75**

Tomasz CHMIELEWSKI, Katarzyna ZIELIŃSKA

**SURVEY OF REMOTELY CONTROLLED LABORATORIES
FOR RESEARCH AND EDUCATION..... 85**

aviation propulsion, CFD, 3D structure, aerodynamic drag

Paweł MAGRYTA*

AERODYNAMIC RESEARCH OF THE OVERPRESSURE DEVICE FOR INDIVIDUAL TRANSPORT

Abstract

Paper proposes a solution of overpressure device for individual transport, the purpose of which is to accumulate the overpressure in a certain geometric area, through the use of specially designed three-dimensional structures. In order to verify the underlying assumptions of the idea, it was decided to perform a simulation study of air flow stream within the proposed unit. These studies were done in Star CD – Pro Star 3.2 software. Further studies were carried out on the actual real model. The verification was performed to compare and identify the main parameters of air flow through the three-dimensional structure.

1. INTRODUCTION

Nowadays, many urban agglomerations are trying to fight the problem of limited possibilities of improving the population transport. Commonly known transportation methods are based on ground movement, such as automobiles or rail. However, the close location of buildings in the cities centers prevents the further growth of this type of network connection (Gössling, 2016). There is also the possibility of transferring the transport into the underground, but the underground urban infrastructure of cities also has its limitations. More often, the new idea is an attempt to transfer the individual urban transport in the realm of air (Ambarwatia, Verhaeghe, Arem & Pel, 2017). This is facilitated by the development of the individual air transport devices, as well as the possibility

* Department of Thermodynamics, Fluid Mechanics and Aviation Propulsion Systems, Faculty of Mechanical Engineering, Lublin University of Technology, Nadbystrzycka Street 36, 20-618 Lublin, Poland, +48 815384764, e-mail: p.magryta@pollub.pl

to use ever newer technologies and materials, particularly in the field of electrical energy storage. The use of internal combustion engines to drive the individual means of transport seems to be impossible because of the noise and pollution that accompany their work. However, the use of the flying vehicle equipped with a conventional propellers drive also has several disadvantages. Standard propellers drives tend to be too loud. Therefore, there is need to design a new type of propulsion system, based on the principle of jet systems or airbag flying ship (Decker, Fleischer, Meyer-Soylu & Jens, 2013).

The main idea for the research contained in this work was the improvement of the air propulsion system, precisely, to create a new compressed air system which would replace engines used in flying vehicles. In this order, research simulations of air flow in a simulation model, in the STAR CD – Pro Star 3.2 software has been carried out. Additionally a geometric model in a Catia V5 virtual environment has been made (Welyczko, 2005). A final stage of work was the implementation of real model and the verification of the simulation results (Magryta, 2009).

2. SIMULATION

2.1. Simulation introduction

The main aspect of the design and purpose of the presented device was to obtain very high pressures and mass flows values of air stream. The initial objectives of the project focused on the idea of creating a model in which it would be possible to perform simulation studies, and subsequent execution on real model and check the pressures and flows values in real conditions.

The simulations were mainly based on the phenomenon of air flow contact to the one of the model walls, allowing for the further stabilization of the flow conditions, what gives a high values of pressure and mass flows, which was a primary design goal (Nedeff, Bejenariu, Lazar & Agop, 2013; Smirnova and Zvyaguin, 2011). Such a solution seemed to be very accurate idea, which created the possibility of obtaining high operating parameters, at the expense of very low power consumption (Magryta, 2009).

2.2. Boundary conditions

Simulations were made in the STAR CD – Pro Star 3.2 software, which allows for three-dimensional simulation of fluid flow (CFD). By using this application, it was possible to registry the changes in pressure and velocity versus simulation time, and the mass flows in some selected points of the simulation model (*Report I/02/2006*, 2006).

For the calculation carried out in the STAR – CD, it is necessary to create a suitable model with the appropriate computing grid. The adopted computing grid has a number of computing cells approx. 3500. It should be noted, that at the nozzle inlet, the grid was heavily concentrated, to enable accurate recording of pressure, velocity and mass flows values. View of computational grid is shown in figure 1. The blue lines (walls) are marked additionally, they limited the flow of air outside of the simulation model. In fact, in the place of these lines, in the STAR – CD, a boundary conditions restricting the air flows were added. While the orange arrow indicates the direction of the compressed air inlet to the simulation model (Magryta, 2009).

The main objective adopted in the design of the device, was to restrict the air flow through the sides and top of the model, what caused the accumulation of overpressure in the upper zone and the separation of its lower pressure zone by incoming air stream. It would cause overpressure, which reacts to the upper wall, what would be used as a thrust in the propulsion system (Hu, Lin, Fu & Wang, 2017; Juraeva, Ryu, Jeong & Song, 2016; Moureh & Yataghene, 2016).

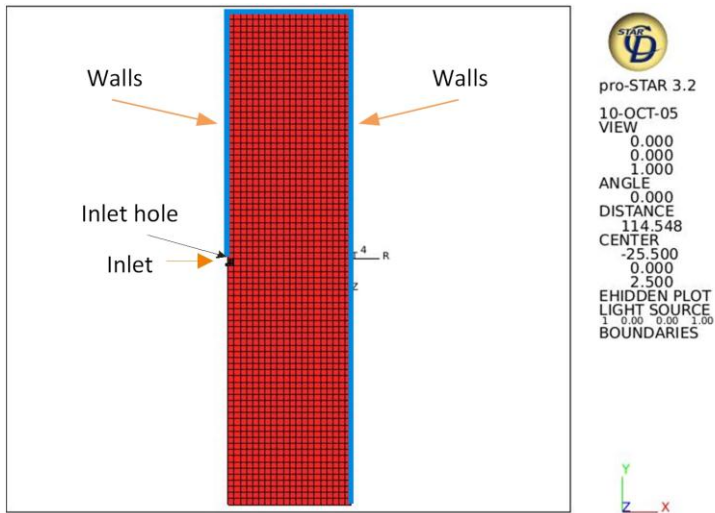


Fig. 1. Computing grid

2.3. Simulation results

The simulation was performed under the steady state conditions. The pressure in the inlet nozzle was linearly increased from zero to a predetermined value (0.25 and 0.5 bar). In both cases the vector map of the pressure and velocity were recorded, at the time from the start of the simulation to 0.08 sec. This time is due to the fact that after 0.08 seconds, the flow stabilizes and further simulations would be useless. As mentioned earlier, tests were conducted

for two different values of inlet pressure, however, because of the results size, it was decided to present the distribution of vector map of pressure and velocity flows only at the conditions of 0.5 bar pressure, as is shown in figures 2–9. (Magryta, 2009).

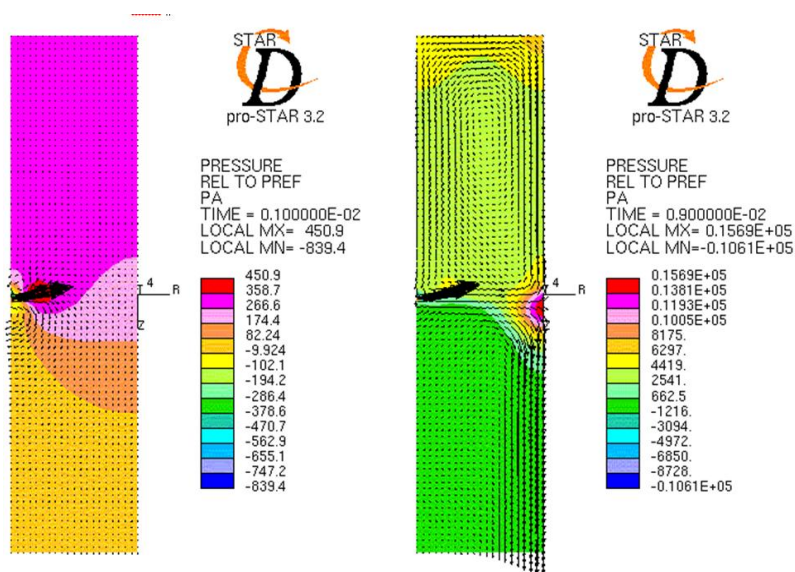


Fig. 2. Vector map of pressure, pressure 0.5 bar, time 0.001–0.009 sec.

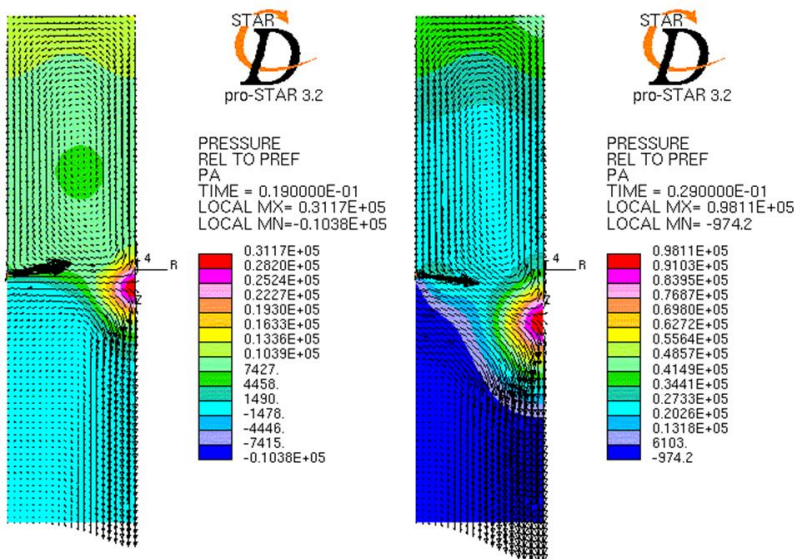


Fig. 3. Vector map of pressure, pressure 0.5 bar, time 0.019–0.029 sec.

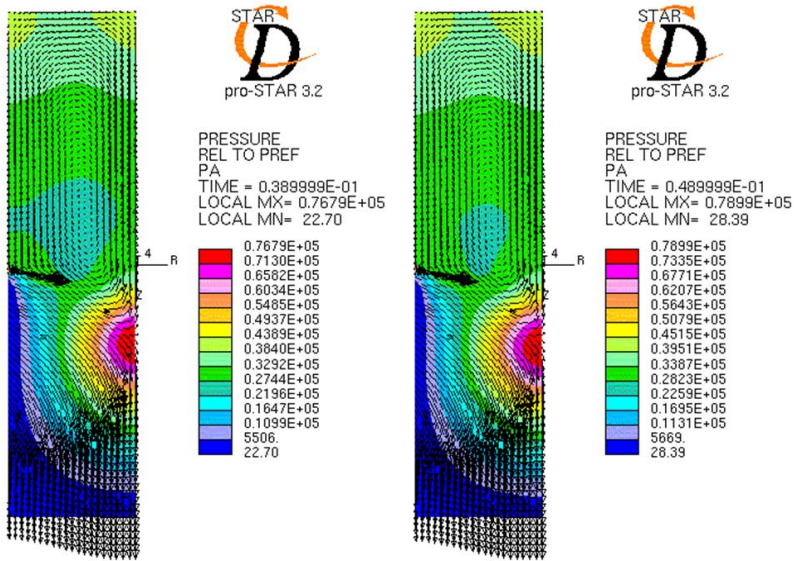


Fig. 4. Vector map of pressure, pressure 0.5 bar, time 0.031–0.049 sec.

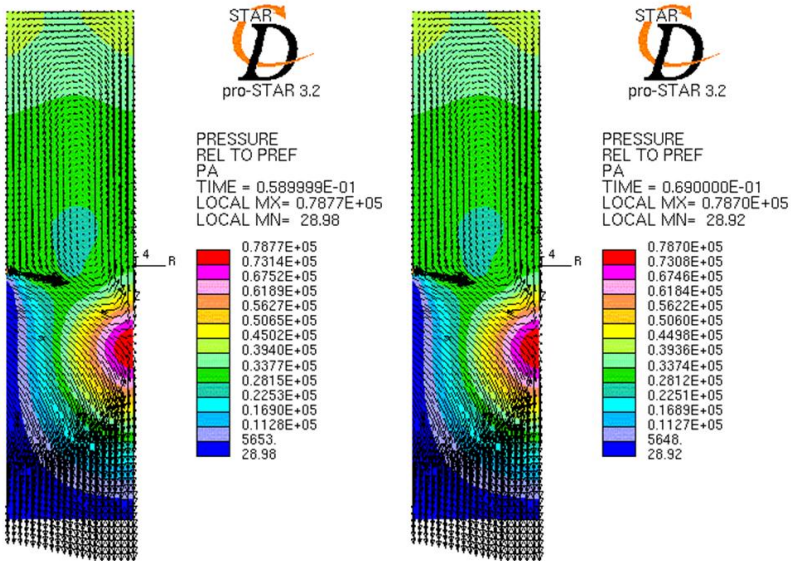


Fig. 5. Vector map of pressure, pressure 0.5 bar, time 0.059–0.069 sec.

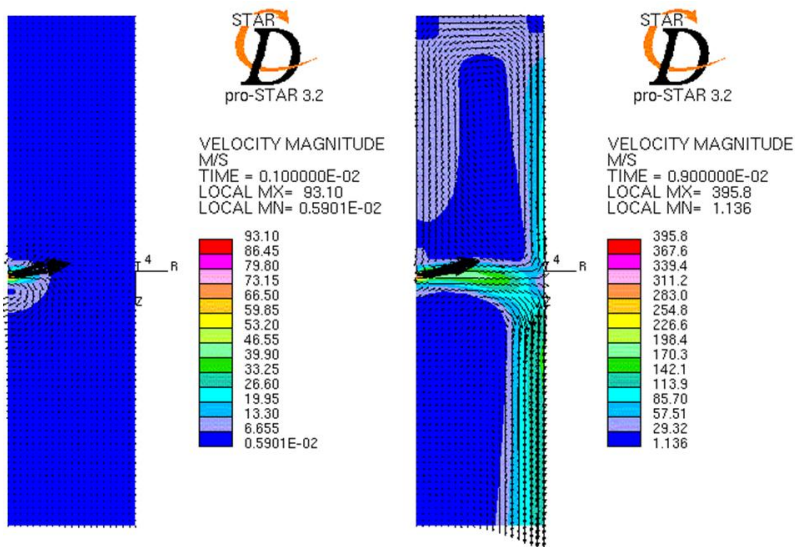


Fig. 6. Vector map of velocity flow, pressure 0.5 bar, time 0.001–0.009 sec.

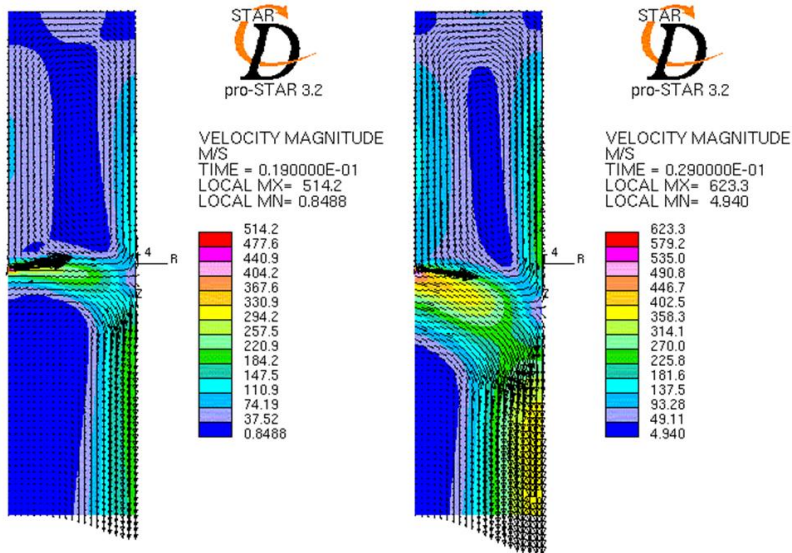


Fig. 7. Vector map of velocity flow, pressure 0.5 bar, time 0.019–0.029 sec.

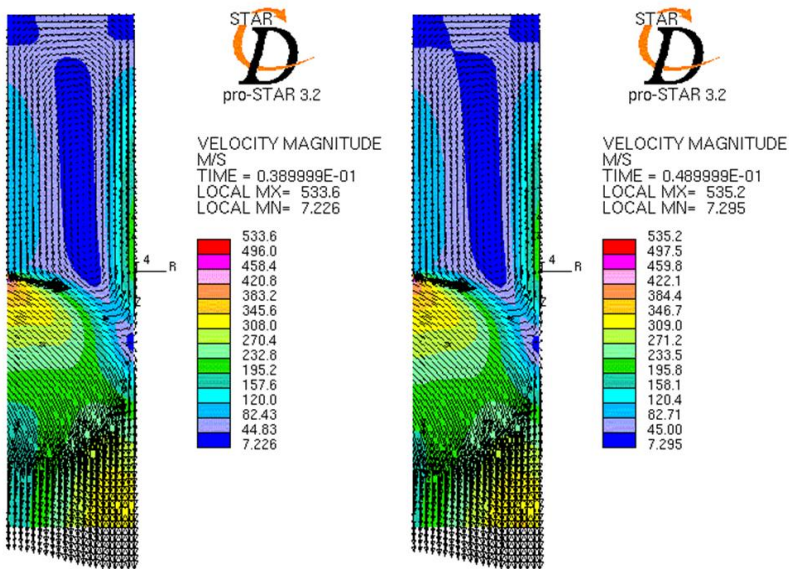


Fig. 8. Vector map of velocity flow, pressure 0.5 bar, time 0.031–0.049 sec.

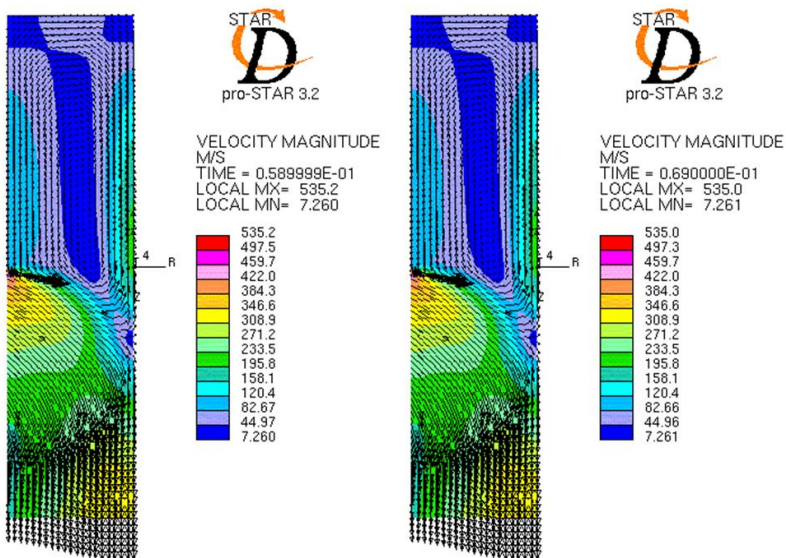


Fig. 9. Vector map of velocity flow, pressure 0.5 bar, time 0.059–0.069 sec.

During the simulation, the pressure, velocity and mass flows in the respective measuring points of the simulation model were recorded.

The pressure at the inlet nozzle and at the measuring point on the top of the device were recorded (Magryta, 2009). Figure 10 shows the characteristic of the pressure at the inlet nozzle and at the top side of the model.

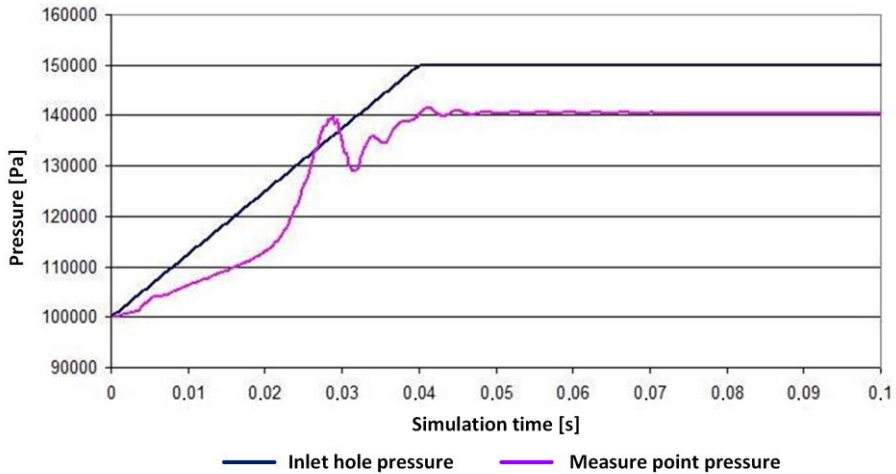


Fig. 10. Characteristic of the pressure at the measuring points during the simulation, in the case of supply of 0.5 bar pressure

All presented results of simulation conducted in the STAR – CD Pro-star 3.2 show clearly, that it is possible to obtain high values of pressure at the top part of the device. The whole concept of creating this kind of the model proved to be correct. After stabilization of conditions, the air flow adopted a laminar flow stream and the phenomenon of contacting airflow to one of the walls occurs. Such a shape of the stream and a large flow rate are blocking the possibility of air leakage beyond the closed top part of the model. All these phenomena mean that at the upper wall of the model a large pressure value is distributed uniformly over the length of the top wall. As can be seen from the distribution of the vector field of the pressure, it is possible to obtain a pressure of approx. 40,000 Pa, with the inlet pressure of 0.5 bar. The top wall of device has internal dimensions of 50 x 10 mm, so its surface is 500 mm². It can be said that such a small airbag is able to lift the approx. 2 kg of mass. Since the results of simulation confirm previously established hypotheses concerning the behavior of the air stream, the author began to create a real model, as shown in the following chapters of the work (Magryta, 2009).

3. EXPERIMENTAL RESEARCH

3.1. CAD model

In order to optimize the real model construction, it was decided to use a Catia v5. The main assumptions of the real model are:

- ability to test multiple geometrical settings,
- simplicity of the design,
- easiness of the real model assembly,
- possibility of setting multiple dimensions of the height of the inlet nozzle,
- short time of real model production,
- complete seal of real model,
- ability to measure pressure in many points,
- ability to measure the weight of the entire device during testing (Camba, Contero & Company, 2016; Zhu, Li & Martin, 2016).

View of the final geometric model in the Catia v5 software is shown in figure 11.

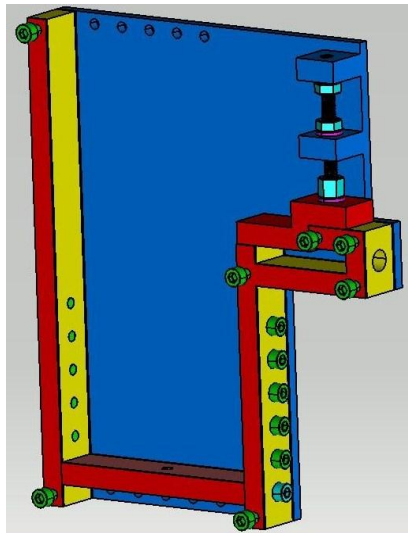


Fig. 11. View of the model without the front cover

3.2. Real Model

Most of the requirements and assumptions about the real model has been already fulfilled during the virtual design. According to calculations made in the Catia v5, the total mass of the model (assuming it will be made of steel) would be 6 kg. In order to reduce this value, front and back cover were made of aluminum sheet

2017 PA6, with a thickness of 5 mm. This value of the thickness has allowed to avoid the deformation of the whole covers, especially during the assembly of the model (Przybylski & Deja, 2007). The total mass of the real model was reduced to a value of 2.8 kg (Magryta, 2009).

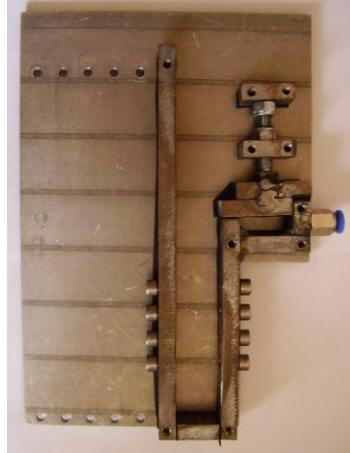


Fig. 12. Finished model in one of the actual geometric settings, excluding the front cover

3.3. Research test bench

Schematic diagram of the test bench is shown in figure 13.

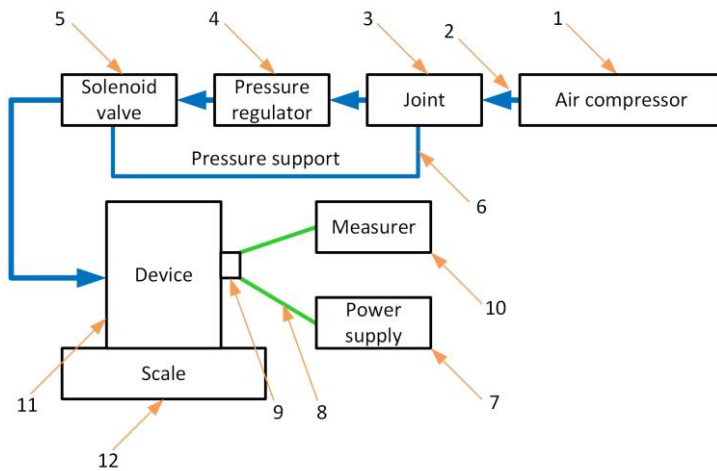


Fig. 13. Schematic diagram of test bench: 1 – air compressor, 2 – pressure line, 3 – joint, 4 – pressure regulator, 5 – solenoid valve, 6 – pressure support, 7 – power supply, 8 – powerline, 9 – pressure sensor, 10 – measurer, 11 – device, 12 – scale

Research carried out on the real model were based on certain assumptions resulting from the construction of the test bench, as well as the limitations of the hardware devices used during the tests. As is apparent from the simulation model, large pressure values at the measurement points, should be obtained even at the inlet pressure of 0.25 and 0.5 bar. In fact, after completely sealing of real model and the initiation of compressed air supply with such a values of pressure, it was impossible to obtain comparable results to the simulation model. However, if pressure at the inlet was higher, the values of obtain overpressure was bigger. Therefore the same pressure at the inlet nozzle of 2.2 bar was established, for all studies. Measurements were made at five different values of the height of the inlet nozzle (0.3, 0.6, 0.9, 1.2, 1.95 mm) and the position of pressure measuring point correspond to the position selected during simulation tests (Magryta, 2009).

3.4. Experimental research results

The only value that we can compare between the simulation study and real research is the actual pressure value at the measurement point on the upper side of the model. Compared to the simulation test, a weight values were read out from the scale, that has been added to the real model tests. In order to fully reflect the capabilities of the real model, a total of 180 measurements at five different positions of the inlet nozzle were made.

For comparison, the relationship between registered overpressure at the measuring point and the width and height of the chamber in which the pressure was accumulated, at two heights of the nozzle 0.3 mm (Figure 14) and 0.6 mm has been presented (Figure 15).

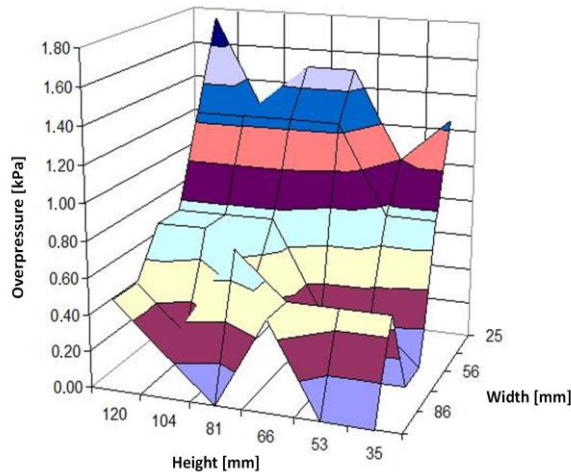


Fig. 14. Three-dimensional graph showing the variation of the level of overpressure at different geometric setup for the inlet nozzle 0.3 mm (own study)

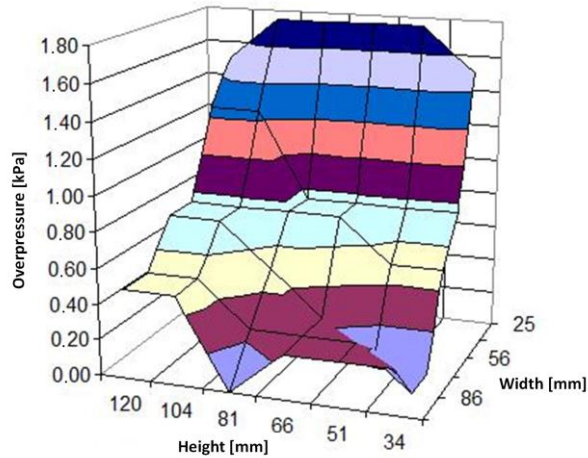


Fig. 15. Three-dimensional graph showing the variation of the level of overpressure at different geometric setup for the inlet nozzle 0.6 mm

A next measured value was so-called lift force, this value was recorded on a laboratory scale placed under the real model. The results of these measurements, analogous to results of pressure measurements, are shown in figures 16 (for the inlet nozzle 0.3 mm) and 17 (for the inlet nozzle 0.6 mm). Values read from the scale, are appropriately reduced by the mass of the real model, what gives the value of the actual lift force (Magryta, 2009).

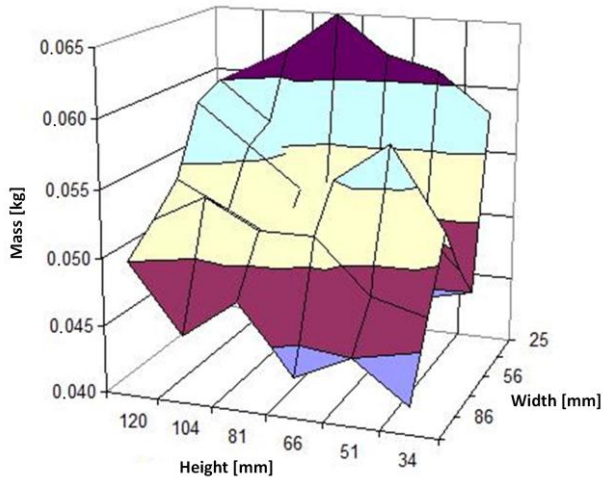


Fig. 16. Three-dimensional graph showing the variation of the level of lift force at different geometric setup for the inlet nozzle 0.3 mm

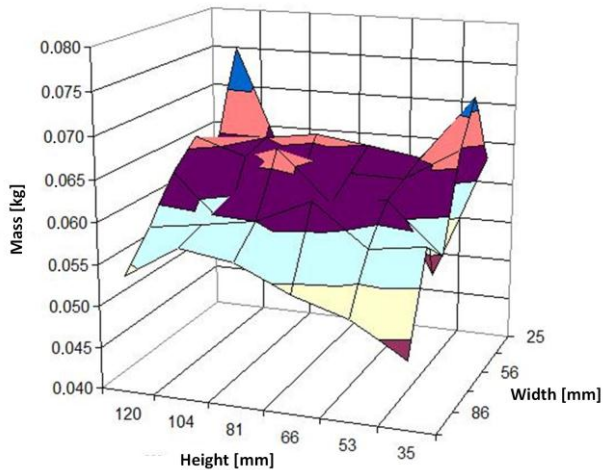


Fig. 17. Three-dimensional graph showing the variation of the level of lift force at different geometric setup for the inlet nozzle 0.6 mm

4. CONCLUSIONS

As follows from the conducted studies, it was failed to reproduce the full flow conditions conducted in simulation tests on a real object. Although the STAR – CD software takes into account all kinds of phenomena of local flow disturbances, changes in temperature, mixing, etc., all kinds of dimensions and boundary conditions given in this application are treated by the computer system in an ideal manner (Nazarewicz, Szlachetka & Wendeker, 2006). For example, setting of the wall, assumption that all connections are 100% tightness and all applied dimensions of the model are perfect and not subjected to any deviation. What is true, that in the real model it was able to fully seal the device, but the behavior of ideal dimensions of all geometric elements, such as walls, nozzle or covers: the front and rear, was very difficult. The maximum deviation resulting from the imperfections of the implementation of the real model could be 1 mm, but such a value in the point of inlet nozzle could cause some distortion of the air flow. According to the author, this was the main cause of such low pressures values at the measurement point.

In summary, the work provide accurate simulations of flow of compressed air through a simulation model in the STAR – CD software, creation of a structural model in the Catia v5 software, creation of a real model and tests on real model. And these are the main conclusions and suggestions for further research on this model:

- simulations carried out in the STAR – CD Pro Star 3.2 shows a very high potential in model in terms of obtaining high pressures and mass flows,

- Catia v5 software makes very easy to optimize the design of real model what is stated in Skarka & Mazurek (2005),
- despite the execution of possible high accuracy of real model, it was failed to reproduce the perfect geometry settings of walls and inlet nozzle,
- it was possible to fully seal the real model, by using the rubber seals of a thickness of 1 mm and 2 mm,
- results obtained from the real test differs from the values obtained in the simulation tests, what is a result of inaccuracy of real model, which obviously affects the course of the air flows,
- for further implementation of the model, it is proposed to make dozens of sets of geometry settings of device, and several inlet nozzles, with the use of the CNC processing machine, which would increase the accuracy of, real model (Magryta, 2009).

The maximum pressure values obtained for certain conditions was 2 kPa. This value is too low to exploit the apparatus as flying vehicle. However, both the model simulation and actual real tests, show a linear relationship with the value received between the overpressure and boundary conditions which have been presented in the work.

This work was funded by the Polish Ministry of Science and Higher Education.

REFERENCES

- Ambarwati, L., Verhaeghe, R., Arem, B., & Pel, A. J. (2017). Assessment of transport performance index for urban transport development strategies — Incorporating residents' preferences. *Environmental Impact Assessment Review*, 63, 107-115. doi:10.1016/j.eiar.2016.10.004
- Camba, J. D., Contero, M., & Company, P. (2016). Parametric CAD modeling: An analysis of strategies for design reusability. *Computer-Aided Design*, 74, 18–31. doi:10.1016/j.cad.2016.01.003
- Decker, M., Fleischer, T., Meyer-Soylu, S., & Jens, S. (2013). *Personal air vehicles as a new option for commuting in Europe: vision or illusion?* European Transport Conference 2013.
- Gössling, S. (2016). Urban transport justice. *Journal of Transport Geography*, 54, 1–9. doi:10.1016/j.jtrangeo.2016.05.002
- Hu, S.-C., Lin, T., Fu, B.-R., & Wang, T.-Y. (2017). Air curtain application in a purged unified pod. *Applied Thermal Engineering*, 111, 1179–1183. doi:10.1016/j.applthermaleng.2016.10.022
- Juraeva, M., Ryu, K. J., Jeongc, S.-H., & Song, D. J. (2016). Influences of the train-wind and air-curtain to reduce the particle concentration inside a subway tunnel. *Tunnelling and Underground Space Technology*, 52, 23-29. doi:10.1016/j.tust.2015.11.008
- Lublin University of Technology. (2006). *Report I/02/2006. Badania symulacyjne doświadczalnego układu wtryskowego silnika lotniczego K9-E*. Project 03605/CT12-6/2005.
- Magryta, P. (2009). *Simulation Research of the Aerodynamic contumacy of three-dimensional structures*. MSC Thesis, 3–4. Lublin University of Technology.
- Moureh, J., & Yataghene, M. (2016). Numerical and experimental study of airflow patterns and global exchanges through an air curtain subjected to external lateral flow. *Experimental Thermal and Fluid Science*, 74, 308–323. doi:10.1016/j.expthermflusci.2015.11.028

- Nazarewicz, A., Szlachetka, M., & Wendeker, M. (2006). Wykorzystanie programu Star – CD do modelowania zjawisk w silnikach spalinowych. In *Informatyka w technice. Tom I*. Lubelskie Towarzystwo Naukowe.
- Nedeff, V., Bejenariu, C., Lazar, G., & Agop, M. (2013). Generalized lift force for complex fluid. *Powder Technology*, 235, 685–695. doi: 10.1016/j.powtec.2012.11.027
- Przybylski, W., & Deja, M. (2007). *Komputerowo wspomagane wytwarzanie maszyn*. Warszawa: Wydawnictwo WNT.
- Smirnova, M. N., & Zvyaguin, A. V. (2011). Theoretical solution for the lift force of “ecranoplan” moving near rigid surface. *Acta Astronautica*, 68(11–12), 1676–1680. doi:10.1016/j.actaastro.2010.12.006
- Skarka, W., & Mazurek, A. (2005). *Catia – podstawy modelowania i zapisu konstrukcji*. Wydawnictwo Helion.
- Węłyczko, A. (2005). *Catia v5 – Przykłady efektywnego zastosowania systemu w projektowaniu mechanicznym*. Wydawnictwo Helion.
- Zhu, L., Li, M., & Martin, R. R. (2016). Direct simulation for CAD models undergoing parametric modifications. *Computer-Aided Design*, 78, 3–13. doi:10.1016/j.cad.2016.05.006

Tytus TULWIN*

MODELLING OF A LARGE ROTARY HEAT EXCHANGER

Abstract

The first simulation consists of a partial cut-out of gas flow canal between the heat exchanger fins. The simulation is steady state and mainly provides the information about the heat transfer coefficient and pressure drop across the canal. The second simulation takes into account the complete system of rotary heat exchanger. It is a transient simulation with moving mesh. Then the heat transfer and air flow parameters are presented as a porous volume with a heat transfer model and rotational multi zone interface conditions. This simplification is accurate providing much better performance as the number of mesh nodes is much smaller. The methodology of the model setup is presented.

1. INTRODUCTION

The industrial rotary heat exchanger is intended to retrieve the heat from the exhaust gases and transfer it to the cold inlet air. This increases the combustion efficiency of the furnace. In order to maximize the heat transfer with minimum pressure drop across the exchanger the CFD simulation method is proposed. The paper presents complete simulation methods for a 5m diameter rotary heat exchanger with 1.4 m disk thickness (Figure 1). The simulation process is split into different parts. Simulating fully represented and detailed honeycomb structure heat transfer would not be feasible because of high number of channels and their complexity. Simplified porous flow and heat transfer method is implemented (Shah & Sekulic, 2003).

* Lublin University of Technology, 38D Nadbystrzycka Str. 20-618 Lublin., +48 81 538 42 50, t.tulwin@pollub.pl

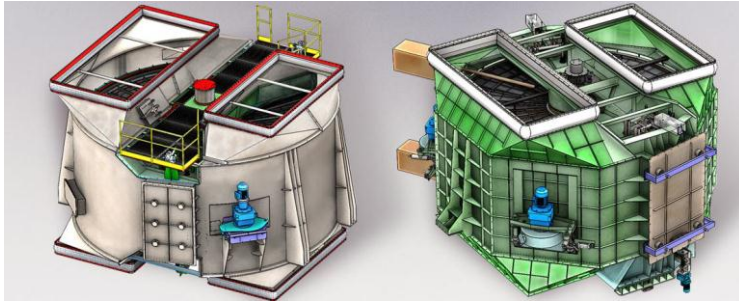


Fig. 1. A large rotary heat exchanger for industrial application (Rotor, 2016)

A large rotary heat exchanger requires a conjugate heat transfer simulation in order to find out its transient characteristics. There are a lot of factors that influence the heat transfer. Some simplifications are made in order to make a robust simulation. The results show how the rotary heat exchanger heats up in time. The heat transfer and air flow conditions are presented for different types of heat exchanger fins. Calculations of temperature data approximation with an aid of lumped heat transfer model are presented. The resultant turbulence conditions are presented showing the relationship between the heat transfer and flow conditions.

2. MATERIALS AND METHODS

2.1. Partial channel model

The circular honeycomb matrix of the rotary heat exchanger consists of two parts: hot end and cold end (Fig. 2). The hot end is made of corrugated steel elements in cross pattern. This type of channels is proven to have a good heat transfer characteristics compared to the pressure drop. It forces some mixing of gas throughout the channels. The thickness of corrugated steel plates is 0.7 mm. The cold end plates are set in a parallel pattern as they are prone to the atmospheric effects like condensation and corrosion. The channels are represented by small section cutouts split in symmetry and periodic planes. Those regions are later treated by respective boundary conditions (Ciofalo, Stasiek & Collins, 1996).

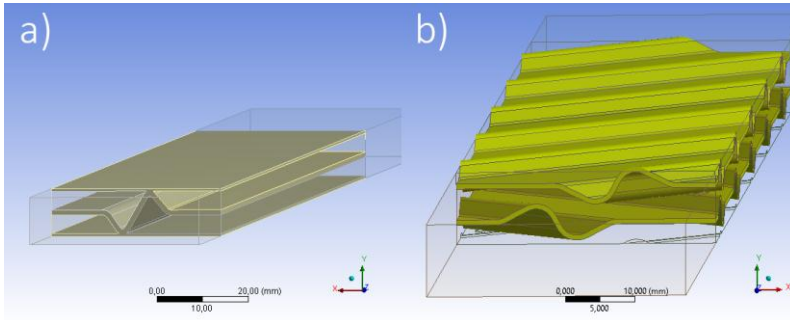


Fig. 2. Hot end channels and cold end channels respectively; single channels section cut-outs as the computational domain

Table 1 presents geometrical information about hot and cold end channels. Porosity and interfacial area density are needed in porous model simulations. Interfacial area density is the ratio of the area of the fluid/solid (“Ansys”, 2016).

Tab. 1. Geometrical properties of the heat exchanger channels

Property		Hot end	Cold end
Overall channel surface area	m ²	8.07E-02	6.3248E-02
Overall channel volume	m ³	1.92E-04	1.5244E-04
Frontal channel surface area	m ²	3.84E-04	3.8110E-04
Frontal solid surface area	m ²	5.68E-05	9.0440E-05
Channel length	m	0.5	0.4
Channel width	m	0.037247	0.0370
Channel height	m	0.0103	0.0103
Porosity	–	0.851975811	0.762687
Interfacialareadensity	m ⁻¹	4.21E+02	4.15E+02

The CFD simulation requires domain discretization into small elements. The computational mesh for the hot end channel consists of mostly tetragonal mesh between the passages and hexagonal in inlet and outlet volumes (Fig. 3a). The cold end mesh consists of hexahedral swept mesh (Fig. 3b). The side walls are represented by linear periodic boundary condition. For both cases, top and bottom walls are symmetry boundary conditions. The hot end grid has 1’517’021 nodes and 3’431’863 elements. The cold end grid has 720’225 nodes and 850’040 elements.

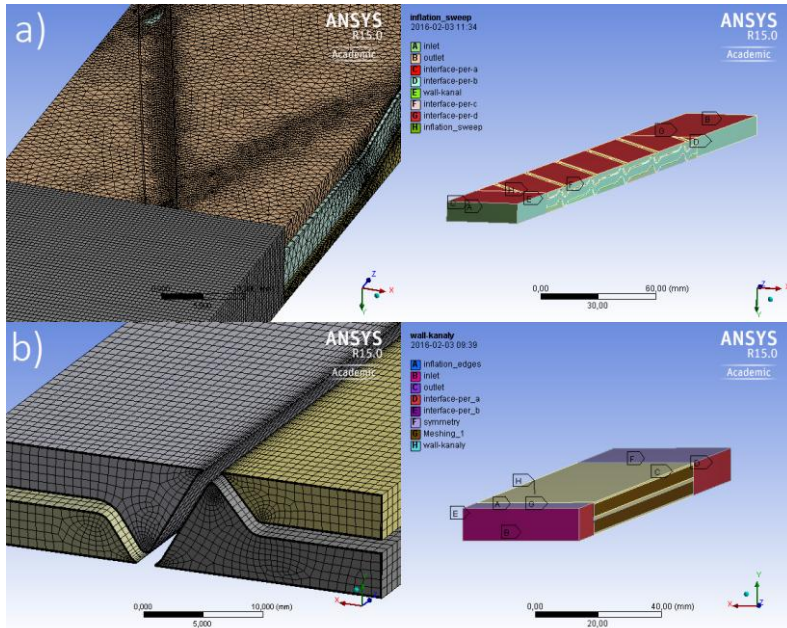


Fig. 3. The computational mesh for the hot partial channel domain

The simulation for both cases is steady state with viscous and compressible fluid. The heat capacity is set as constant. The viscosity and conductivity is represented by the linear function according to the values in table 2.

Tab. 2. Gas properties for different temperatures: conductivity and viscosity

T [K]	k [W/mk]	u [kg/ms]
300	0.02624	1.846e-05
600	0.04661	3.017e-05

Similar method was proposed in the paper (Alekseev, Kostukov, Makarov & Merzlikin, 2016).

2.2. Porous stack model

The resultant pressure drop and heat transfer coefficient from previous partial simulations are the input conditions for the simplified simulation if porous stack model. The simplification is made in means of replacing numerous and dense channels by the porous model. With proper input parameters, the pressure drop characteristics should be matching the results of the partial channel simulation.

The heat transferred model is considered as well by the non-equilibrium thermal model equations. In this case a dual cell approach is used. A solid zone domain is coincident with the fluid zone domain. The only interaction between the zones is the heat transfer solved by conservation equations. The source terms are represented by the equation 1. The transient conduction in the solid region is represented as well as the heat capacity of the solid material. The turbulence is modeled as there would be no effect of solid medium. In this case, such simplification is justified as the main region of interest is the heat transfer. The turbulence effect is included in the heat transfer coefficient calculated in the previous partial models. The porous model together with non-equilibrium thermal model and source terms allow for transient heat transfer considerations (“Ansys”, 2016).

3. RESULTS

3.1. Channel flow characteristics

For each channel 30 different cases of gas temperature and flow velocity were analysed. The parameters that are transferred to the nest porous stack simulation are heat transfer coefficient and pressure drop. The heat transfer coefficient's reference temperature is the average gas temperature in the channel. The heat transfer coefficient is calculated from the basic convection equation. The boundary condition for solid contact is the heat flux density. It is set as constant value of 160 W/m² for the experiment so that the htc can be calculated in every part of the model.

$$Q = A \cdot h (T_{\infty} - T) \quad (1)$$

where: Q – heat flux (W), A – heat transfer area (m²), T_{∞} – reference temperature, T – average solid surface temperature.

Figure 4 shows the results of pressure drop across channels.

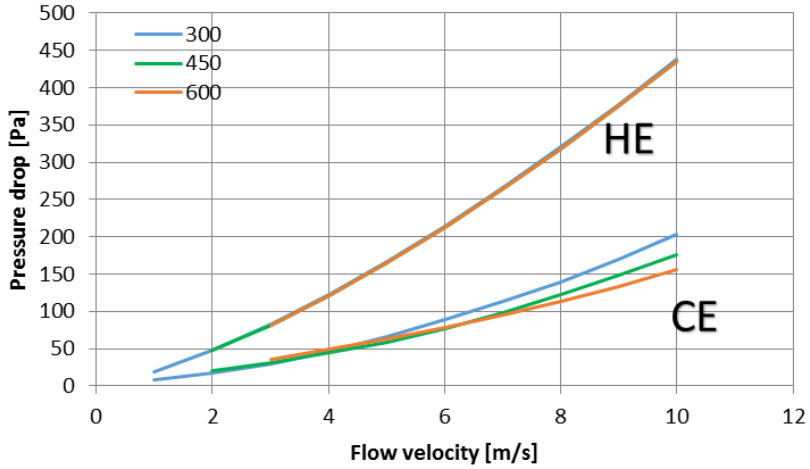


Fig. 4. Pressure vs velocity for hot end and cold end channels for 3 different temperatures

The pressure rise in respect to inlet velocity can be closely represented by the 2nd order polynomial for each case. For hot end channels the pressure drop doesn't change much with temperature change in range of 300–600K ($\ll 1\%$ change). For cold end channels the pressure drop changes with temperature. The increase of temperature decreases the flow resistance. The hot end channels produce much higher pressure drop than the cold end channels. Table 3 and 4 show derived coefficients of viscous resistance C2 and $1/a$ for cold and hot end, based on velocity and pressure data.

$$y = X1 \cdot x + X2 \cdot x^2 \quad (2)$$

They are calculated with the formula 2 based on X1 and X2 values being 2nd degree polynomial curve fit constants. The parameters: Δm – porous media thickness, ρ – gas density and μ – viscosity.

Tab. 3. Parameters for channel flow resistance calculations – hot end (own study)

X2	ρ	Δm	C2
2.2354	1.147664	0.5	7.791130505
X1	μ	Δm	$1/a$
20.544	1.78E-05	0.5	2.31E+06

**Tab. 4. Parameters for channel flow resistance calculations
– cold end (own study)**

X2	ρ	Δm	C2
1.4304	1.16085	0.4	6.161
X1	μ	Δm	1/a
5.7929	1.78E-05	0.4	8.14E+05

The porous resistance is calculated based on combination of Darcy’s law and internal loss source term (formula 3) (“Ansys”, 2016; Whitaker, 1985).

$$\Delta p = - \left(\frac{\mu}{a} v + C_2 \frac{1}{2} \rho v^2 \right) \Delta m \quad (3)$$

Figure 5 presents the heat transfer coefficient in respect to flow velocity for the hot and cold end channels. Three different flow temperatures were analysed. The heat transfer coefficient for the hot end channels can be represented by the 2nd order polynomial function for the whole range of temperatures.

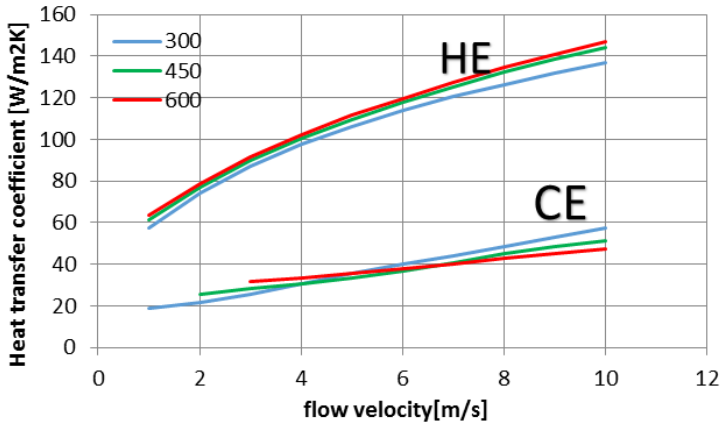


**Fig. 5. The heat transfer coefficient in respect
to flow velocity for 3 different temperatures**

The higher the temperature the higher the heat transfer coefficient for each flow velocity ranging from 1–10 m/s. For the cold end channels the htc function can be represented by the linear function for velocity range of 1–10 m/s and 3 different temperatures 300, 450 and 600 K respectively. Below around 5 m/s the increase of temperature result in increase of the htc. Above 5 m/s this relation is opposite. The heat transfer coefficient is higher for the hot end channels than for the cold end channels. Generally increasing the porosity of channels increases the heat transfer effectiveness (Mahesh, Jayaraman & Madhumitha, 2016).

The effectiveness can reach values as high as 50%. The leakage between zones can vary from 4 to 50% (Alonso, Lui, Mathisen, Ge & Simonson, 2015). Latent heat recovery is also possible using the thermal wheel with an aid of special condensation coating (Nasr, Fauchoux, Besant & Simonson, 2013).

3.2. Transient stack heating

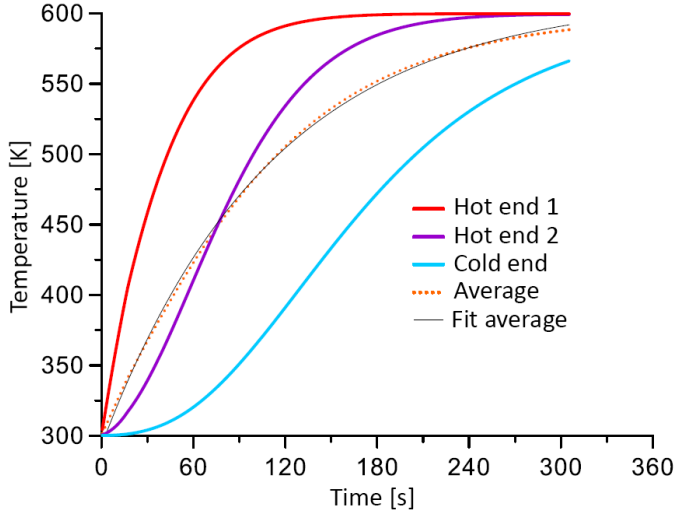


Fig. 6. The heat exchanger disk matrix average temperatures for different layers in respect to simulation time

Figure 6 shows the change of temperature in respect to simulation time for 3 different layers of the heat exchanger disk. First two layers consist of the hot end channels being 500 mm thick. 3rd layer is 400mm thick and consist of the cold end channels. The first hot end channel layer heats up first and reaches the gas temperature after around 180s. The second hot end layer heats up after around 250s. The 3rd cold end layer takes more than 400 s to reach the gas temperature.

The average disk temperature can be approximated by the power-law function:

$$y(x) = A \cdot B^x + C$$

The curve fit constants can be used in the lumped heat transfer model as the Biot-number doesn't exceed the value of 0.1 (Campo, 2012; Cengel & Ghajar, 2014). It must be noted that increasing the rotational speed of rotor can decrease the efficiency of the heat transfer (Grzebielec, Rusowicz & Rucinski, 2014).

4. CONCLUSION

The hot end type channels are more efficient in means of the heat transfer and pressure drop by approximately 25% to 10% with the flow velocity ranging from 1 to 10 m/s respectively. The reason why cold end channels are used is the corrosive nature of the inlet gases. The low temperature of the flowing as can cause water condensation and excessive corrosion and erosion. The turbulence only amplifies these effects so channels are made to cause as little disturbance to the flow as possible gently heating preheating the air. The cold end channels usually have special coating to prevent corrosion. The proposed porous model can describe the transient heat transfer well (Fig. 6). The temperature data can be used to find out the transient constant in the lumped system model formula.

REFERENCES

- Alekseev, R. A., Kostukov, A. V., Makarov, A. R., & Merzlikin V. G. (2016). Simulation of Characteristics of Thermo-Hydraulic Process in Porous-Net Matrix of Rotary Heat Exchanger. *Global Journal of Pure and Applied Mathematics*, 12(4), 2829–2838.
- Alonso, M. J., Lui, P., Mathisen, H. M., Ge, G., & Simonson, C. (2015). Review of heat/energy recovery exchangers for use in ZEBs in cold climate countries. *Building and Environment*, 84, 228–237. doi:10.1016/j.buildenv.2014.11.014
- Ansys. (n.d.). Program documentation.
- Campo, A. (2012). A new 1-D composite lumped model facilitates the algebraic calculation of local temperatures, mean temperatures, and total heat transfer in simple bodies. *Heat Mass Transfer*, 48(9), 1495–1504. doi:10.1007/s00231-012-0994-x
- Cengel, Y. A., & Ghajar, A. J. (2014). *Heat and Mass Transfer: Fundamentals & Applications* (5 ed.). McGraw-Hill.
- Ciofalo, M., Stasiek, J., & Collins, M. W. (1996). Investigation of flow and heat transfer in corrugated passages—II. Numerical simulations. *International Journal of Heat and Mass Transfer*, 39(1), 165–192. doi:10.1016/S0017-9310(96)85014-9
- Grzebielec, A., Rusowicz, A., & Rucinski, A. (2014). Analysis of the performance of the rotary heat exchanger in the real ventilation systems. *The 9th International Conference. Environmental Engineering, VGTU, Vilno*. doi:10.3846/enviro.2014.259
- Mahesh, S., Jayaraman, B., & Madhumitha, R. (2017). Analysis of Air-to-Air Rotary Regenerator for HVAC Systems Using CFD. In Bajpai R., & Chandrasekhar U. (Eds.) *Innovative Design and Development Practices in Aerospace and Automotive Engineering. Lecture Notes in Mechanical Engineering*. (pp. 455–462). Springer. doi:10.1007/978-981-10-1771-1_49
- Nasr, M. R., Fauchoux, M., Besant, R. W., & Simonson C. J. (2013). A review of frosting in air-to-air energy exchangers. *Renewable and Sustainable Energy Reviews*, 30, 538–554. doi:10.1016/j.rser.2013.10.038
- Rotor. (n.d.). Retrieved November 1, 2016, from Rotor website, <http://www.rotor.lublin.pl>
- Shah, R. K., & Sekulic, D. P. (2003). *Fundamentals of Heat Exchanger Design*. John Wiley & Sons.
- Whitaker, S. (1985). Flow in porous media I: A theoretical derivation of Darcy's law. *Transport Porous Media*, 1(1), 3–25. doi:10.1007/BF01036523

neural networks, fuzzy neural networks, forecasting, stock indexes

Yuriy TRYUS*, Nataliya ANTIPOVA**, Kateryna ZHURAVEL***,
Grygoriy ZASPA****

INFORMATION TECHNOLOGY OF STOCK INDEXES FORECASTING ON THE BASE OF FUZZY NEURAL NETWORKS

Abstract

In this research the information technology for stock indexes forecast on the base of fuzzy neural networks was created. The possibility of its use for multi-parameter short-time stock indexes forecasts, in particular S&P500, DJ, NASDAC was checked. The created information technology is used making several consequential steps. The stock indexes forecast numeral experiment based on real data for period of several years with use of the technology offered was made.

* Computer Science and Information Technology Department, Cherkasy State Technological University, 460 Shevchenko Blvd, 18006, Cherkasy, Ukraine, +380 978885231, tryusyvv@gmail.com

** Computer Science and Information Technology Department, Cherkasy State Technological University, 460 Shevchenko Blvd, 18006, Cherkasy, Ukraine, +380 663056089, LesleyRoot1726@gmail.com

*** Computer Science and Information Technology Department, Cherkasy State Technological University, 460 Shevchenko Blvd, 18006, Cherkasy, Ukraine, +380 966172088, k_galasun@mail.ru

**** Software Department, Cherkasy State Technological University, 460 Shevchenko Blvd, 18006, Cherkasy, Ukraine, +380 97 2609085, gzaspa@ukr.net

1. INTRODUCTION

The task of future time series values forecasting on the base of its history is the basis for financial planning at economics and trade, for manufacturing volume planning, management, and optimization etc. Recently fuzzy neural network based forecast gets more and more popular among forecast methods (Jang, 1993; Jang & Sun, 1995, 1997; Svalina, Galzina, Lujić, & Šimunović, 2013; Wang, 1994; Wang and Elhag, 2008; Zhang & Hu, 1998). Forecast results received using fuzzy neural networks are often more accurate in comparison with regression methods, for instance, Auto-Regressive Integrated Moving Average (ARIMA) Model (Mohaddes & Fahimifard, 2015).

The research goal is creation the information technology for stock indexes forecast on the base of fuzzy neural networks and checking the possibility of its use for multy-parameter short-time stock indexes forecasts, in particular S&P500, DJ, NASDAQ.

2. FORECAST REALIZATION STAGES

The use of information technology offered is made in several stages:

1. Downloading data, for instance, from <http://finance.yahoo.com> ("YahooFinance", 2016);
2. Preparing data for inputting into Fuzzy Logic Toolbox Matlab ("Adaptive Neuro-Fuzzy Modeling", 2016) (here the software module developed with the authors is used; it helps to prepare input data using time windows method);
3. Creating fuzzy neural networks ANFIS ("Adaptive neuro-fuzzy inference system", 2016; "Toolbox fuzzy-logic Matlab", 2016) and inputting data including stock index value at trading beginning, maximal and minimal index value on the day, value at trading closing;
4. Configuring the fuzzy neural network (generating the fuzzy output system with given parameters, choosing the type and number of membership functions for every in, choosing the membership function type for network out);
5. Modeling on test data;
6. Stock index value forecast for trading beginning for several future days; forecast result analysis.

Neural networks work with systems which have inputs and the output which depends on inputs variables values set and their work is in building the system which produces maximally close out value for all sets training sample input data on the base of some input data sample. For stock indexes forecast the system with the following variables set was used:

- input variables are the values of some stock index for current day stock exchange opening and closing and the highest and lowest index values for current day;
- output variable is the value of some stock index for the following day stock exchange opening (tab. 1).

So, system output is a stock index value forecast for the trading opening in the day following after the current day.

Tab. 1. Input and output variables for forecast

Input variables				Output variable
$Open_i$	$High_i$	Low_i	$Close_i$	$Open_{i+1}$
$Open_{i+1}$	$High_{i+1}$	Low_{i+1}	$Close_{i+1}$	$Open_{i+2}$
$Open_{i+n}$	$High_{i+n}$	Low_{i+n}	$Close_{i+n}$	$Open_{i+n+1}$

3. DATA DOWNLOAD

The data for neural networks learning, for forecast and results comparison were downloaded from «YahooFinance – BusinessFinance, StockMarket, Quotes, News» (“YahooFinance”, 2016). For stock indexes values downloaded the following steps are needed:

1. Open web site (“YahooFinance”, 2016), in search field enter stock index name, chose the necessary index from the list (Fig. 1).

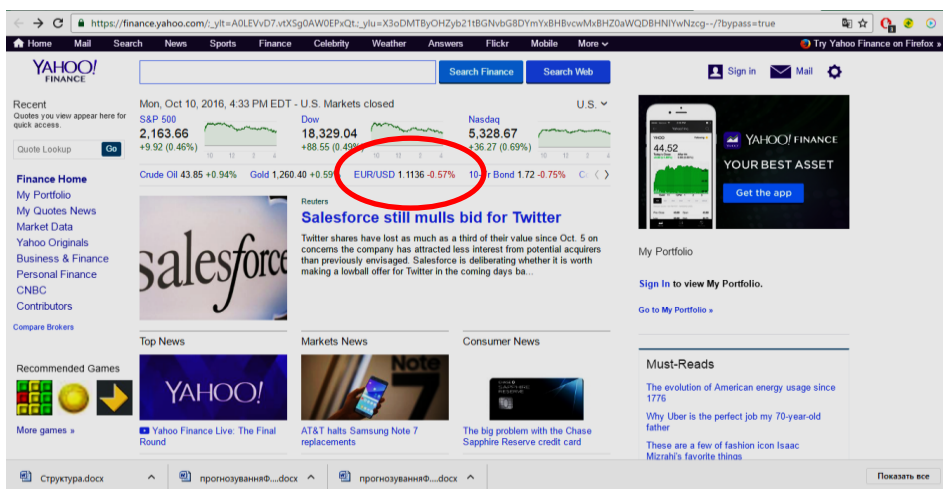


Fig. 1. Yahoo!Finance internet resource for downloading stock indexes values (source: <http://finance.yahoo.com>)

2. After opening the page of the stock index chosen open «Historical data» tab, enter data for download time period («Time Period»), press «Apply» button and download the data (Fig. 2).

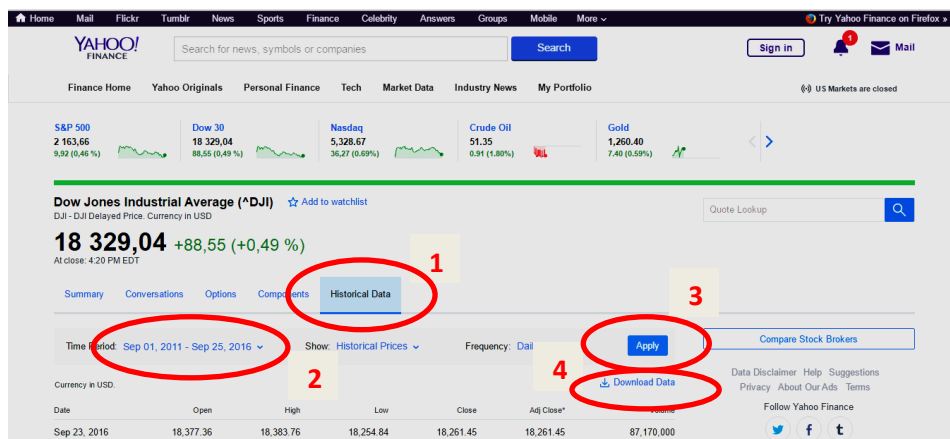


Fig. 2. Stock indexes values downloading stages
(source: own work using Internet resource <http://finance.yahoo.com>)

4. DATA PREPARATION AND FORMATTING

The following step is to enter the folder with downloaded file, open the file in text editor, replace all symbols «,» for tab «^t» and save as plain text with tab delimiters. After saving we open file in a spreadsheet application (for instance, MS Excel), remove columns with average value data (AdjClose) and sales volume (Volume), delete first row with columns headers, sort all data on first column ascending from the earliest date to the oldest, remove first column with information on date (Date) and save the file.

Forecasting on the base of fuzzy neural networks was made using Anfis editor (Adaptive Neuro Fuzzy Inference System) (“Adaptive Neuro-Fuzzy Modeling”, 2016; “Adaptive neuro-fuzzy inference system”, 2016) from the toolkit Fuzzy Logic Toolbox of Matlab software (“Toolbox fuzzy-logic Matlab”, 2016).

The forecasting results for indexes Dow Jones, S&P 500, NASDAQ were researched. The study samples were got for period from September 1st, 2011 to September 7th, 2016. For every index the forecast for 12 days was made, so, from September 8th, 2016 to September 23rd, 2016.

Before fuzzy output system study start the file data must be transformed to form given in tab. 1. For this function CreateAModelOfTheRowNnet can be used (it is presented in listing 1). The following parameters are passed to the function: Row – the file with formatted data from site name, NameOfFile – the file

in which the study sample data will be saved name, NumOfTail – days number for which the forecasting will be made (some rows are truncated in study sample file), NameOfTailFile – name of file for saving data for checking. The example of function call from Matlab command line:

```
>>CreateAModelOfTheRowNnet('tableDJ.txt', 'DJ_train.dat', 12, 'DJ_tail.dat');
```

Listing 1

```
function [ output_args ] = CreateAModelOfTheRowNnet(Row, NameOfFile, NumOfTail, NameOfTailFile)
try
    Row = load(Row);
catch
end

[m,n] = size(Row);

LengthOfRow = length(Row);
NumOfInputs = 4;

fori = 2:LengthOfRow
    output_args(i-1, 5) = Row(i, 1);
    forIDInside = 1:NumOfInputs
        output_args(i-1, IDInside) = Row(i-1, IDInside);
    end
end

if (nargin> 1)
    ifnargin == 2
        NumOfTail = 0;
    end;

    filess = fopen(NameOfFile,'wt');
    [m, n] = size(output_args);
    fori = 1 : m - NumOfTail
        for j = 1:n
            fprintf(filess,'%10.10f\t',output_args(i,j));
        end;
        fprintf(filess,'\n');
    end;
    fclose(filess);

    ifnargin>= 4
        filess = fopen(NameOfTailFile,'wt');
        StartNum = m - NumOfTail + 1;
        fori = StartNum:m
            for j = 1:n
                fprintf(filess,'%10.10f\t',output_args(i,j));
            end
            fprintf(filess,'\n');
        end
        fclose(filess);
    end
end
end
```

5. FUZZY NEURAL NETWORK STUDY

For fuzzy logical output system study the following actions must be executed:

1. Open Anfis editor (in Matlab command line write: `>>anfisedit`).
2. Download to Anfis editor (Load data) the study sample data (Training) from Matlab working area or from file, for example, DJ_train.dat (Fig. 3, item 1–2).
3. Build the initial system of fuzzy logical output. It can be made in several ways:
 - download the system created before (Load from file or Load from workspace) (Fig. 3, item 3);
 - generate the system (Generate FIS) with full rules set on inputs and output membership functions number which are given the user for input in «Grid partition» mode. In this case membership functions will be located equidistant from each other on all in/out variable range of (Fig. 3, item 4);
 - generate the system (Generate FIS) using study sample values clusterization (Sub. clustering) and creation on its base the membership function (Fig. 3, item 5).
4. Execute the fuzzy neural network study (Train Now) using hybrid algorithm (Optim. method: hybrid) or converse error spread algorithm (Optim. method: backpropa) (Fig. 3, item 6).
5. After system study it is possible to compare system outputs values with real data in «Training data» (Test Now) mode (Fig. 3, item 7).

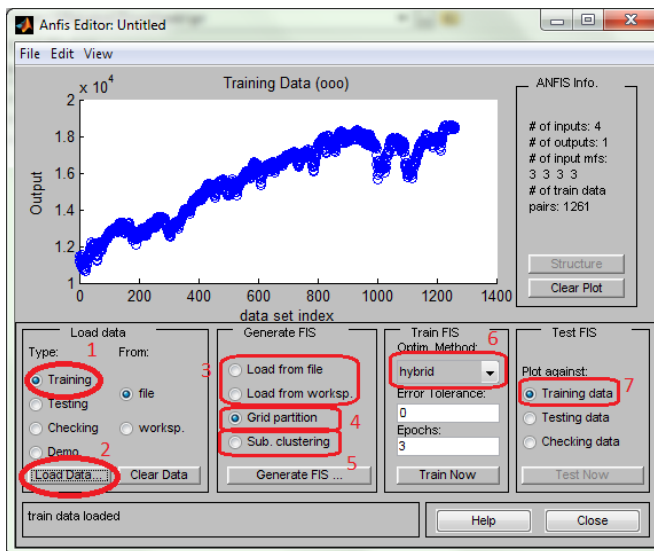


Fig. 3. Fuzzy logical output system study stages

The received system of fuzzy logical output can be used for stock indexes forecasting. To check the forecasting efficiency the data from file should be downloaded (Load data) to the editor for checking (for example, DJ_tail.dat) in Checking mode. Then real data diagrams and fuzzy output system generated data diagrams should be superimposed (Fig. 4 item 1–2).

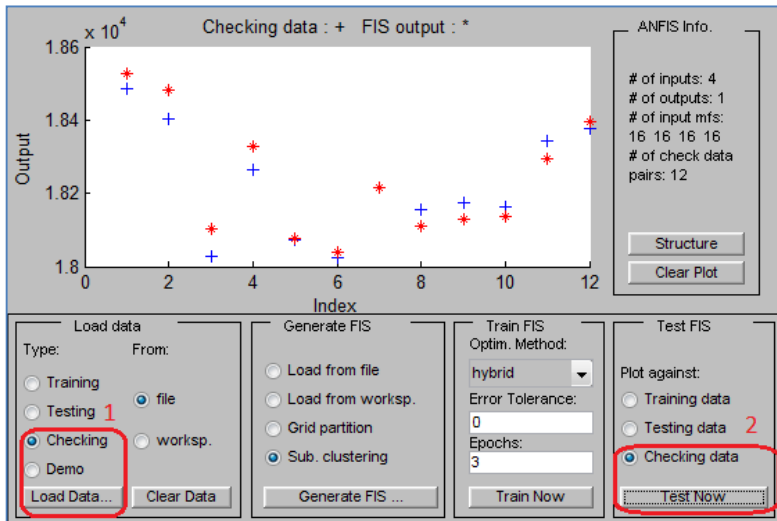


Fig. 4. Checking the efficiency of forecasting using fuzzy neural network

Classic neural network uses the same stages. But for it NNTool app from Matlab package should be used. First, the data must be loaded into Matlab working area and then the data must be transposed. For instance, for DJ index data the following commands should be executed in command line:

```
>>loadDJ_train.dat;
>>loadDJ_tail.dat;
>>input_train = DJ_train(:,1:4)';
>>input_sim = DJ_tail(:,1:end-1)';
>>target_train = DJ_train(:,5)';
>>target_sim = DJ_tail(:,5)';
```

For loading NNTool application the following command must be written in command line: >>nnntool. Then in NNTool editor window the data are loaded and neural network is created with configuration given in Fig. 5.

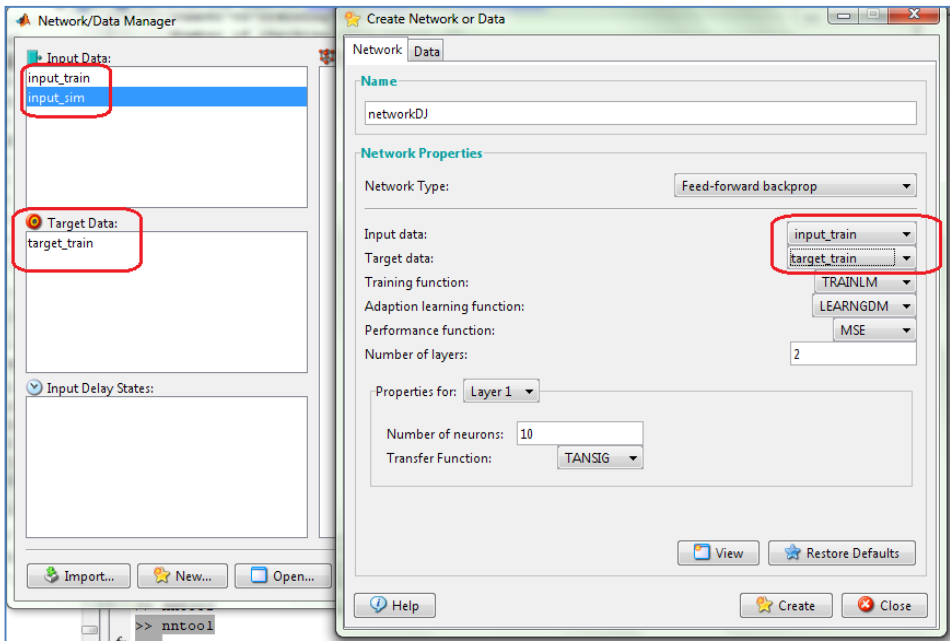


Fig. 5. Loading data to NNTool and neural network creation

Then one should go to neural network study control window and execute the study having selected the proper analysis parameters (Fig. 6).

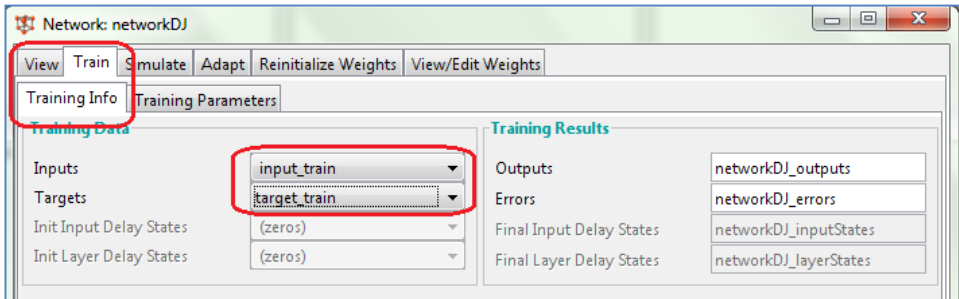


Fig. 6. Neural network study

After the study one can generate system output for data which were selected for checking forecast effectiveness (Fig. 7). Then the result can be loaded to Matlab working area using «Export...» function in NNTool application command panel. The comparison of forecast data and real data is given in diagram (Fig. 8).

In Fig. 9 and 10 the real values of S&P 500 stock index for the period from September 8th, 2016 to September 23rd, 2016 and forecast result using fuzzy neural network and classical neural network respectively.

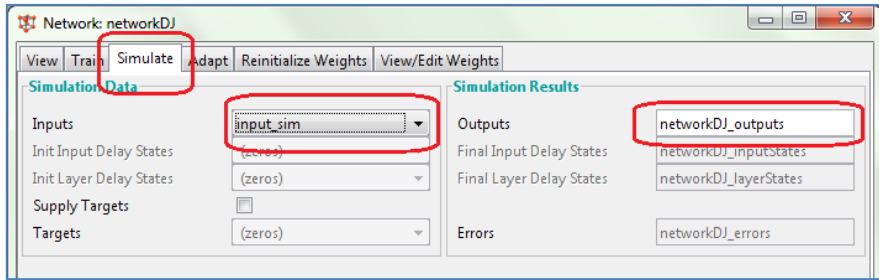


Fig. 7. Neural network output generation for forecast efficiency checking data

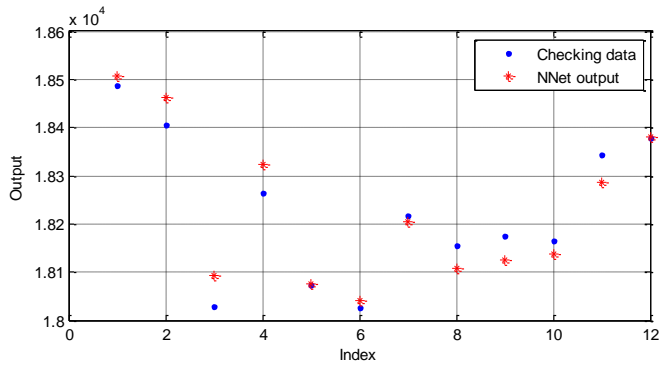


Fig. 8. Real values of DowJones stock index for the period from September 8th, 2016 to September 23rd, 2016 and forecast result using classical neural network

In Fig. 11 and 12 the real values of NASDAQ stock index for the period from September 8th, 2016 to September 23rd, 2016 and forecast result using fuzzy neural network and classical neural network respectively.

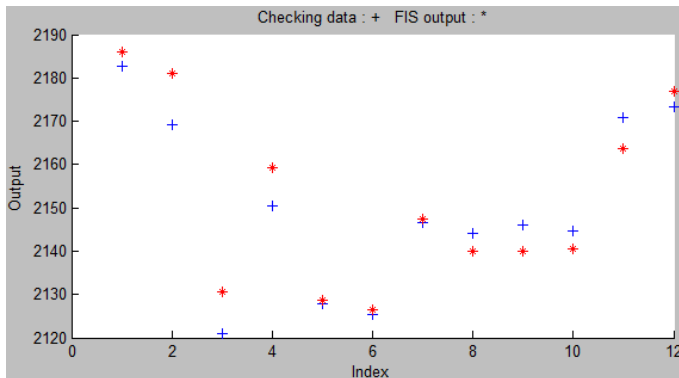


Fig. 9. Real values of S&P 500 stock index for the period from September 8th, 2016 to September 23rd, 2016 and forecast result using fuzzy neural network

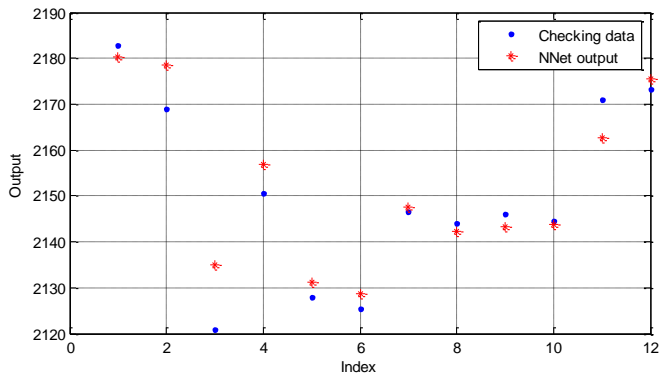


Fig. 10. Real values of S&P 500 stock index for the period from September 8th, 2016 to September 23rd, 2016 and forecast result using classical neural network

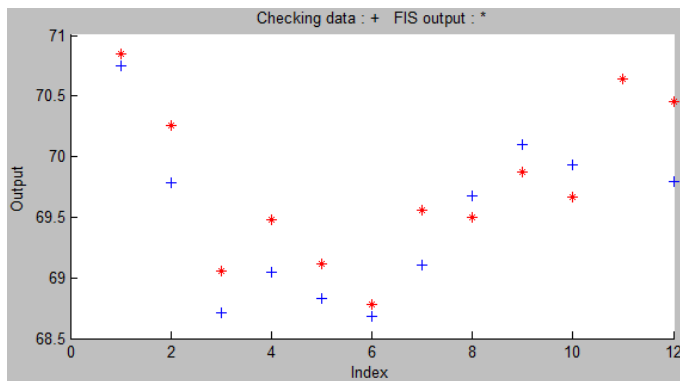


Fig. 11. Real values of NASDAQ stock index for the period from September 8th, 2016 to September 23rd, 2016 and forecast result using fuzzy neural network

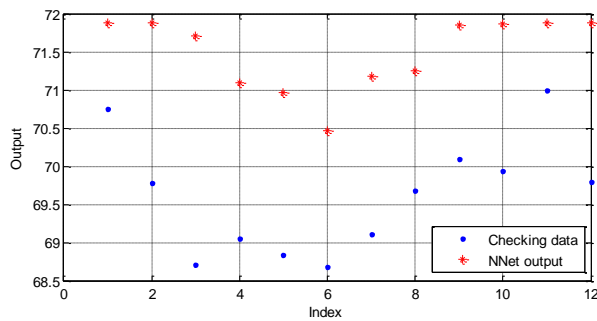


Fig. 12. Real values of NASDAQ stock index for the period from September 8th, 2016 to September 23rd, 2016 and forecast result using classical neural network

The forecast errors using both methods are given in tab. 2. Classical neural network produced better result for stock indexes Dow Jones and S&P 500 but fuzzy neural network produced better result for NASDAQ index.

The success in classical neural network study depends significantly on generation the initial system parameters, so, sometimes the study doesn't produce even satisfactory result. Fuzzy neural networks in given experiment produced forecasts with almost the same error that classical neural network did but the forecast accuracy was more stable.

Tab. 2. Forecast errors of fuzzy and classical neural networks for different indexes

Error Index	Fuzzy neural networks error		Classical neural networks error	
	Absolute	Relative	Absolute	Relative
DowJones	45,6767	0,002456	34,7843	0,00187
S&P 500	6,2105	0,002836	4,6235	0,002111
NASDAQ	0,36032	0,005075	1,8733	0,026385

6. CONCLUSION

1. The results of numeric experiment in stock indexes forecast on real data for period of several years on the base of proposed technology has shown the possibility and expediency of fuzzy neural networks use short-term stock indexes forecast and their advantage over common artificial neural networks on criterion of forecast accuracy and stability.
2. The information technology offered can be used for single parameter and multi-parameter short term forecasting of currency rates and shares price if data in form of time series are available.

REFERENCES

- Adaptive Neuro-Fuzzy Modeling*. (n.d.). Retrieved September 26, 2016, from MathWorks website, <https://www.mathworks.com/help/fuzzy/adaptive-neuro-fuzzy-inference-systems.html>
- Adaptive neuro-fuzzy inference system*. (n.d.). Retrieved September 26, 2016, from MathWorks website, <https://www.mathworks.com/help/fuzzy/neuro-adaptive-learning-and-anfis.html>
- Jang, J.-S. R., (1993). ANFIS: Adaptive-Network-based Fuzzy Inference Systems. *IEEE Transactions on Systems, Man, and Cybernetics*, 23(3), 665–685.
- Jang, J.-S. R., & Sun, C.-T. (1995). Neuro-fuzzy modeling and control. *Proceedings of the IEEE*, 83(3), 378–406.
- Jang, J.-S. R., & Sun, C.-T. (1997). *Neuro-Fuzzy and Soft Computing: A Computational Approach to Learning and Machine Intelligence*. Upper Saddle River, NJ: Prentice Hall.
- Mohaddes, S. A., & Fahimifard, S. M. (2015). Application of Adaptive Neuro-Fuzzy Inference System (ANFIS) in Forecasting Agricultural Products Export Revenues (Case of Iran's Agriculture Sector). *Journal of Agricultural Science and Technology*, 17(1), 1–10.

- Svalina, I., Galzina, V., Lujić, R., & Šimunović, G. (2013). An adaptive network-based fuzzy inference system (ANFIS) for the forecasting: The case of close price indices. *Expert Systems with Applications*, 40(15), 6055-6063. doi:10.1016/j.eswa.2013.05.029
- Toolbox fuzzy-logic Matlab*. (n.d.). Retrieved September 28, 2016, from MathWorks website, <http://www.mathworks.com/products/fuzzy-logic/>
- Wang, L.-X. (1994). *Adaptive fuzzy systems and control: design and stability analysis*. Upper Saddle River, NJ: Prentice Hall.
- Wang, Y. M., & Elhag, T. (2008). An Adaptive Neuro-fuzzy Inference System for Bridge Risk Assessment. *Expert Systems with Applications*, 34(4), 3099–3106. doi:10.1016/j.eswa.2007.06.026
- YahooFinance – BusinessFinance, StockMarket, Quotes, News*. (n.d.). Retrieved September 21, 2016, from YahooFinance website, <http://finance.yahoo.com>
- Zhang, G., & Hu, M. Y. (1998). Neural Network Forecasting of the British Pound/US Dollar Exchange Rate. *Omega The International Journal of Management Science*, 26(4), 495–506. doi:10.1016/S0305-0483(98)00003-6

broaching, broach, FEM, ABAQUS, alloy EN-AW 6061-T6

Stanisław BŁAWUCKI*, Kazimierz ZALESKI**

CONSTRUCTION AND TECHNOLOGICAL ANALYSIS OF THE BROACH BLADE SHAPE USING THE FINITE ELEMENT METHOD

Abstract

The paper presents results of numerical FEM analyses of the process of broaching the groove using the Explicit module of the ABAQUS program. The impact of the blade geometry was presented and of the selected technological parameters of processing when cutting the aluminium EN-AW 6061-T6 alloy on the load of the broach blade during its operation. This article shows influence of value of rake and clearance angle onto deformations of the tool's cutting edge in the transverse direction. An interaction between broach blade shape and reduced stress in the area of cutting edge was presented. The optimum geometry of the cutting tool was proposed.

1. INTRODUCTION

Broaching is a method of the loss shaping of machine parts. This treatment involves the removal of the material layer with next blades, which are arranged in series. The broach blades, wedge-shaped, perform the rectilinear motion and delving into the treated material they cause its separation. This way, the object gets the final desired shape and dimensions. Broaching is used especially when the processing of parts with other methods is difficult.

In the works, which were created in the 60s of the XX century (Górski, 1967; Monday, 1960), a technology was described, tools and machines used for broaching. In the following years, studies were created on the optimisation of the broaching process (Belov & Ivanov, 1975; Kokmeyer, 1984). Scientific works

* Politechnika Lubelska, Nadbystrzycka 36, 20-618 Lublin, 514 849 284, s.blawucki@pollub.pl

** Politechnika Lubelska, Nadbystrzycka 36, 20-618 Lublin, 81 5384238, k.zaleski@pollub.pl

using the finite element method for the analysis of the broaching were created during the last two decades, with the development of the numerical computational methods. Subsequent citation: Sajeev, Vijaraghavan & Rao (2000) in their research performed the analysis of stress caused in the tool and the workpiece during the simulated cutting of the single broach blade. The cutting model was brought to the issue of free cutting process, also called orthogonal cutting, where the width of the tool blade is greater than the width of the cut layer of the processed object. The works (Schulze, Zanger & Boev, 2013; Xiangwei, Bin, Zhibo & Wenran, 2011; Zhang, Outeiro & Mabrouki, 2015) dealt with the impact of the workpiece's geometry on the dimension and location of the shear plane and on the components of the cutting forces during orthogonal machining. A simplified model was adopted for numerical calculations, in which the width of the tool was equal to the width of the workpiece.

One can encounter many publications from recent years (Kokturk & Budak, 2004; Vogtel, Klocke, Lung & Terzi, 2015) on the optimisation of the blade shape of the broach, based on the strength calculations. However, the strength calculations require knowledge of analytical methods and they assume some safety factors, which leads to the increased size and weight of the tool, as well as deterioration of the technology of the execution of the broach blade.

In the present work, the issue of geometry optimisation of the broach blade to splineways was undertaken, when the criteria included the improvement of performance technology and the reduction of dimensions of the blade cross-sectional area at its basis, in order to shorten the working part of the broach. Decision variables in the computing task include the angles γ and δ , which control the dimensions of the cross-section of the working part. The size of the cross-section of the broach blade at the base affects the value of maximum reduced stress in arrears. The model of orthogonal constrained cutting was used.

2. RESEARCH METHODOLOGY

2.1. Workpiece and tool geometry

The research was carried out on numerical models using the finite element method in the Explicit module of the ABAQUS program. The dimensions of the workpiece and tool were adopted as in figure 1. The scope of the analysed angles of the broach blade was presented in table 1. The reference geometry (d) was selected based on literature recommendations by Górski (1967). The material of the workpiece was chosen for the research – aluminium EN-AW 6061-T6 alloy and the tool material – tungsten carbide (WC) with characteristics given in table 2.

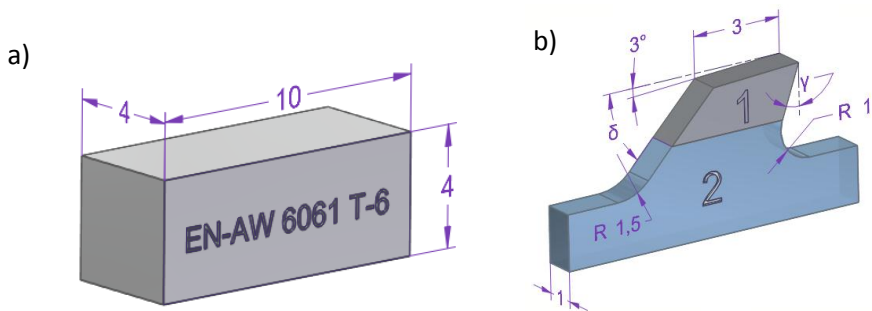


Fig. 1. Characteristic dimensions: a) of the workpiece, b) of the tool: 1 – broach blade, 2 – working part of the broach (excluding the blade) with the chip space

Tab. 1. The values of angles γ and δ of the broach blade defined during numerical analyses

Angle	Values of angles								
γ	0°			10°			20°		
δ	45°	60°	9°	45°	60°	90°	4°	60°	9°
Symbol	a	b	c	d (reference)	e	f	g	h	i

Figure 2a presents the way of restraining the tool and the workpiece. The movement of the workpiece was limited in three directions. The movement of the tool was limited in two directions, a possibility of blade movement was only kept in the parallel direction to the work plane and perpendicular to the cutting edge. A constant thickness of the cutting layer was assumed at 0,25 mm and a constant cutting speed at the level of 50 m/min. The width of the cutting edge results from the length of the cutting edge of the tool and is 1 mm.

Geometrical models of the tool and the work piece (fig. 2b) were divided into finite cubic elements of the C3D8R type with eight nodes and with the side dimension of 0,1 mm. Additionally, at the depth of 0,5 mm from the surface a local density was performed for the mesh in the machined layer of the work-piece to the side dimension of 0,01 mm.

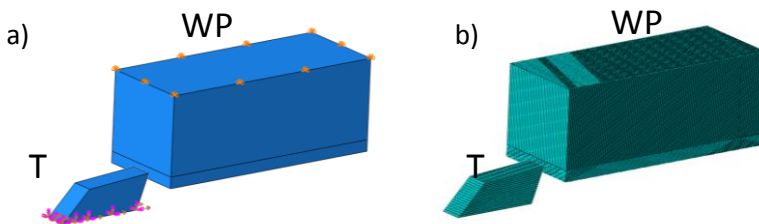


**Fig. 2. The system of the workpiece (WP) – tool (T):
a) restraint, b) finite element mesh**

2.2. Model of the material

With numerical calculations of the cutting process, the constitutive model of the material of Johnson-Cook was implemented (Boldyrev, Shchurov & Nikonov, 2016; Grzesik, 2010; Kosmol & Mieszcza, 2009; Zhang, Outeiro & Mabrouki, 2015) due to very large plastic deformations in the area of chip formation. The equations for the material takes the form:

$$\bar{\sigma} = \left[A + B \cdot (\bar{\varepsilon})^n \right] \cdot \left[1 + C \cdot \ln \left(\frac{\dot{\bar{\varepsilon}}}{\dot{\bar{\varepsilon}}_0} \right) \right] \cdot \left[1 - \left(\frac{T - T_0}{T_{melt} - T_0} \right)^m \right] \quad (1)$$

where: $\bar{\sigma}$ – equivalent plastic stress,
 A – initial yield stress,
 B – hardening modulus,
 $\bar{\varepsilon}$ – equivalent plastic strain,
 n – work - hardening exponent,
 C – coefficient dependent on the strain rate,
 \ln – natural logarithm,
 $\dot{\bar{\varepsilon}}$ – equivalent plastic strain rate,
 $\dot{\bar{\varepsilon}}_0$ – reference equivalent plastic strain rate,
 T – temperature in the cutting zone,
 T_0 – ambient temperature,
 T_{melt} – melting temperature of the workpiece,
 m – thermal softening coefficient.

Tab. 2. Material properties of workpiece and tool (Boldyrev et al., 2016)

Property or material coefficient	Workpiece	Tool
<i>Density</i> [kg/m ³]	2700	15500
<i>Young's modulus</i> [Pa]	$7 \cdot 10^{10}$	$6,5 \cdot 10^{11}$
<i>Plasticity</i> [Pa]	A=324,1 · 10 ⁶ B=113,8 · 10 ⁶	–
$\dot{\bar{\varepsilon}}$ [s ⁻¹]	10 ⁵	
$\dot{\bar{\varepsilon}}_0$ [s ⁻¹]	1	–
<i>Poisson's ratio</i>	0,33	0,21
<i>Friction coefficient</i>	0,15	
C	0.002	–
n	0,17	–
T_0 [°C]	25	–
T_{melt} [°C]	580	–
m	1,34	–

The Johnson-Cook model does not define the beginning of the material destruction, hence the need to use the function describing the initiation of destruction, as well as knowledge of parameters describing the failure process is required. The determination of the five parameters (d_1, \dots, d_5) involves a series of experimental fracture tests, varying the stress triaxiality, strain-rate and temperature (Boldyrev, Shchurov & Nikonov, 2016; Grzesik, 2010; Kosmol & Mieszcak, 2009; Zhang, Outeiro & Mabrouki, 2015). Destruction parameters are summarised in table 3, while the ductile fracture model is described by the equation (2) below:

$$\bar{\varepsilon}_f = [d_1 + d_2 \cdot \exp(d_3 \cdot \eta)] \cdot \left[1 + d_4 \cdot \ln\left(\frac{\dot{\bar{\varepsilon}}}{\dot{\bar{\varepsilon}}_0}\right) \right] \cdot \left[1 + d_5 \cdot \left(\frac{T - T_0}{T_{melt} - T_0} \right) \right] \quad (2)$$

where: $\bar{\varepsilon}_f$ – equivalent fracture strain,
 d_1, \dots, d_5 – damage parameters
 η – stress triaxiality parameter,
 \ln – natural logarithm,
 $\dot{\bar{\varepsilon}}$ – equivalent plastic strain rate,
 $\dot{\bar{\varepsilon}}_0$ – reference equivalent plastic strain rate,
 T – temperature in the cutting zone,
 T_0 – ambient temperature,
 T_{melt} – melting temperature of the workpiece.

Tab. 3. Parametre values of the failure process initiation, (Boldyrev et al., 2016)

Parameter	d_1	d_2	d_3	d_4	d_5
Value	-0,77	1,45	-0,47	0	1,6

In numerical calculations the regeneration function of the mesh of the damaged elements was not used, which in the case of the conducted calculations has got aesthetic qualities and does not impact the results of calculations. Moreover, there is a possibility of the destruction analysis when cutting the composite materials. Then, one should apply the material model described by Dębski & Sadowski (2014).

3. DISCUSSION OF THE RESULTS

The applied material model and the destruction model allowed the analysis of deformations and reduced Huber-Mises stress in spatial system, which were obtained on the cutting edge zone and in the cross-section of the blade of the broach. Due to a small value of deformations of the broach blade (fig. 4), their value can be regarded as negligible.

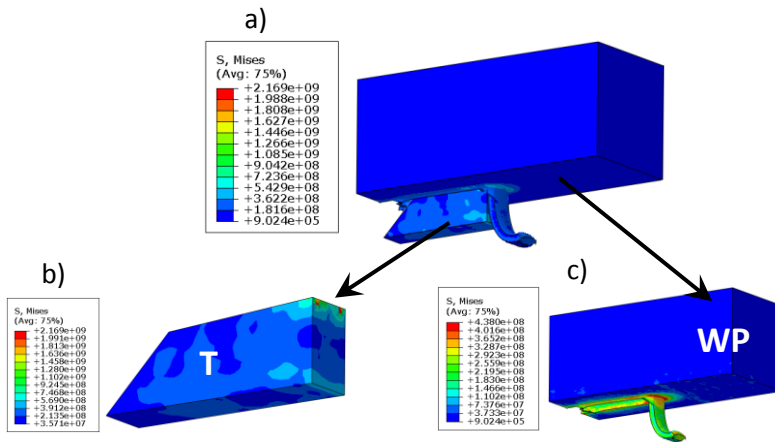


Fig. 3. Examples of the MES analysis results showing the distribution of maximum reduced stresses: a) in the system the workpiece - tool, b) in the tool (T), c) in the workpiece (WP); expressed in Pascals

The reference geometry (d) (fig. 4, 5, 6) of the tool's blade, with the angles of $\gamma = 10^\circ$ and $\delta = 45^\circ$, was characterised by a deformation in the nodes in the zone of the cutting edge at the level of $0,000002$ mm, maximum reduced stress in the tool's cross-section base of $2 \cdot 10^9$ Pa and reduced stress within the cutting edge zone of $8 \cdot 10^9$ Pa.

It was noted that along with the change of angles γ and δ a change of reduced stress took place in the cross-section of the broach blade at the base and in the zone of the cutting edge (fig. 5 and fig. 6). There has been a simultaneous impact of the pair of the studied angles on the value of reduced stress. With the angles $\gamma=0^\circ$ and $\delta=45^\circ$ the maximum reduced stress in the blade's cross-section reaches the lowest value from all analysed cases. With these geometry, the cross-section area of the blade at the base is the largest of the contemplated combinations of pairs of angles.

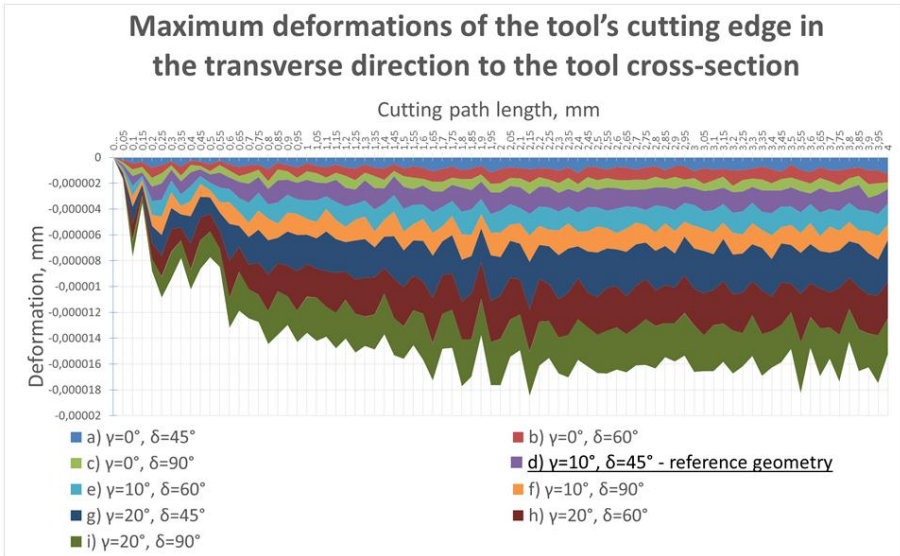


Fig. 4. The curves of maximum deformations of the tool's cutting edge in the transverse direction to the cross-section, in the cutting path function for different angles of the tool's working part

Taking into account the producibility of the performance of the working part of the broach, the best structural solution seems to be the set of blade's angles $\gamma = 0^\circ$ and $\delta = 90^\circ$. This would allow a considerable shortening of the working part of the tool. However, Lipski et al. (2002) says, that with these parameters an adverse build-up edge phenomenon occurs, as well as the rise of temperature on the blade due to the intense chip friction on the tool face. Therefore, one should carry out further explorations of the optimal geometry of the broach blade.

Taking into account the above observations, one can conclude that the optimal solution is a pair of angles of the reference geometry (d). Given that the change of the angle δ from 45° to 90° will increase the stress in the blade's cross-section by 50%, while the producibility of the tool will be improved, and its length will be reduced, this type of compromise is worth noticing, especially for the machining of the aluminium alloy, due to low cutting forces.

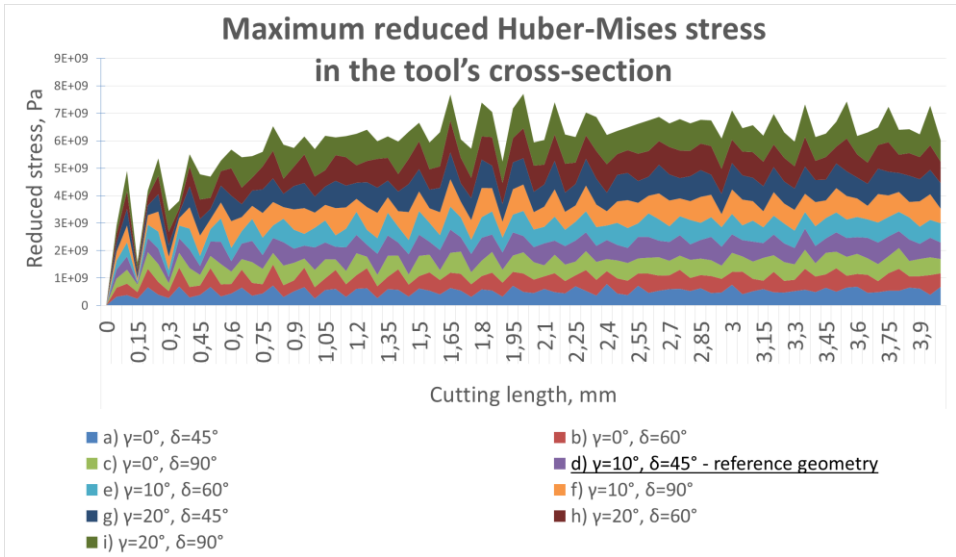


Fig. 5. Curves of the reduced Huber-Mises stress course in the tool's blade cross-section in the function of the cutting length for different angles of the tool's blade

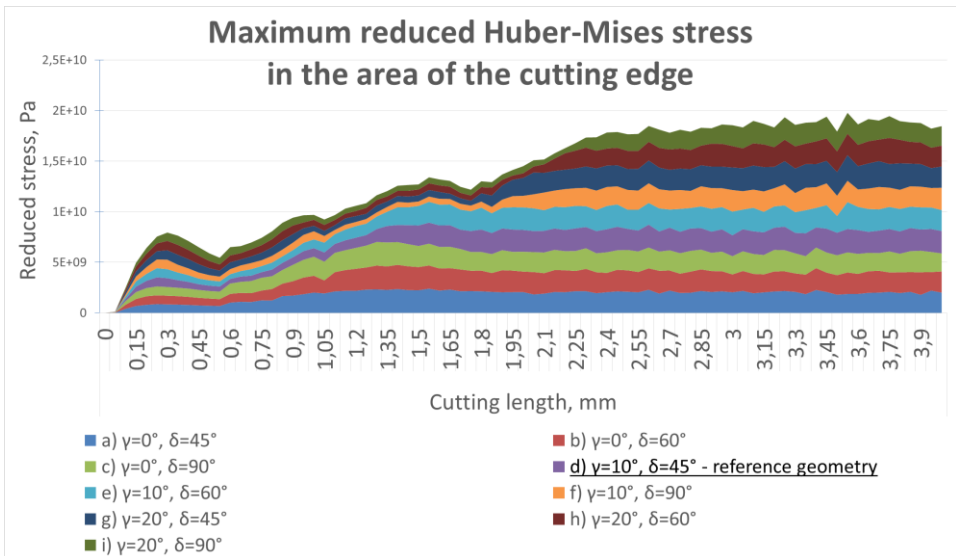


Fig. 6. Curves of the reduced Huber-Mises stress course in the zone of the cutting edge in the function of the cutting path for different angles of the tool's blade

3. CONCLUSIONS

On the basis of numerical analyses and literature review one can draw the following conclusions concerning the analysed geometry of the blade of the broach.

1. Distribution of the deformations and stress in MES models is in line with expectations, as assessed on the basis of gradient maps, obtained for the model of the workpiece and for the tool.
2. According to the assumptions of the numerical analysis, the processed material underwent the plastic deformation of high intensity and elastic deformation, and moreover, there were numerous failure areas of the finite elements and their permanent deformation.
3. The reference geometry (d) of the tool's blade, with the angles $\gamma = 10^\circ$ and $\delta = 45^\circ$ was characterised by a deformation in the cutting edge nodes at the level of 0,000002 mm, maximum reduced stress in the tool's cross-section of $2 \cdot 10^9$ Pa and reduced stress in the zone of the cutting edge of $8 \cdot 10^9$ Pa.
4. Some of the analysed pairs of angles of the working part of the broach exhibit better properties in terms of ultimate strength on the complex condition of stress created in the studied cross-section of the tool during the process of spatial broaching with the carbide blade into the groove of the aluminium EN-AW 6061-T6 alloy.
5. The analysed geometries of the broach's blade (e), (f), (g), (h) and (i) show worse properties in the aspect of ultimate strength to the complex condition of the stress formed in the studied cross-section of the tool during the broaching process.
6. Given the aspect of producibility of the performance of the working part of the broach, the geometry, which $\gamma = 0^\circ$ and $\delta = 90^\circ$, seems optimal, as it allows for a significant reduction of the total length of the broach, by reducing the length of its scale.
7. Reviewing the literature on the subject, the reference geometry, which $\gamma = 10^\circ$ and $\delta = 45^\circ$, is the best solution, taking into account the strength of the tool's blade and the processes occurring in the cutting zone, such as the built-up on the blade.
8. The presented numerical model of broaching the splineways can be of practical use when designing tools and planning of waste machining.

REFERENCE

- Belov, V. S., & Ivanov, G. M. (1975). Improving the accuracy of surface broaching machines. *Stanki i Instrumenty*, 46(7), 6–8.
- Boldyrev, I. S., Shchurov, I. A., & Nikonov, A. V. (2016). Numerical Simulation of the Aluminum 6061-T6 Cutting and the Effect of the Constitutive Material Model and Failure Criteria on Cutting Forces' Prediction. *Procedia Engineering*, 150, 866–870. doi:10.1016/j.proeng.2016.07.031

- Dębski, H., & Sadowski, T. (2014). Modelling of microcracks initiation and evolution along interfaces of the WC/Co composite by the finite element method. *Computational Material Science*, 83, 403–411. doi:10.1016/j.commatsci.2013.11.045
- Górski, E. (1967). *Narzędzia skrawające kształtowe*. Warszawa: WNT.
- Grzesik, W. (2010). *Podstawy skrawania materiałów konstrukcyjnych*. Warszawa: WNT.
- Kokmeyer, E. (1984). *Better Broaching Operations*. Society of Manufacturing Engineers Madison.
- Kokturk, U., & Budak, E. (2004). Optimization of broaching tool design. *Proceedings of the Intelligent Computation in Manufacturing Engineering – 4 Conference, CIRP ICME '04*. Sorrento.
- Kosmol, J., & Mieszczak, W. (2009). Zastosowanie metody elementów skończonych do modelowania procesu wiercenia. *Modelowanie Inżynierskie*, 37, 169–176.
- Lipski, J., Litak, G., Rusinek, R., Szabelski, K., Teter, A., Warmiński, J., & Zaleski, K. (2002). Surface quality of a work material's influence on the vibrations of the cutting process. *Journal of Sound and Vibration*, 252(4), s. 729–737. doi:10.1006/jsvi.2001.3943
- Monday, C. (1960). *Broaching*. London: The Machinery Publishing Co.
- Sajeev, V., Vijaraghavan, L., & Rao, U.R. (2000). An analysis of the effects of burnishing in internal broaching. *International Journal of Mechanical Engineering Education*, 28(2), 163–173.
- Schulze, V., Zanger, F., & Boev, N. (2013). Numerical Investigations on Changes of the Main Shear Plane while Broaching. *Procedia CIRP*, 8, 246–251. doi:10.1016/j.procir.2013.06.097
- Xiangwei, K., Bin, L., Zhibo, J., & Wenran, G. (2011). Broaching Performance of Superalloy GH4169 Based on FEM. *Journal of Materials Science & Technology*, 27(12), 1178–1184. doi:10.1016/S1005-0302(12)60015-2
- Vogtel, P., Klocke, F., Lung, D., & Terzi, S. (2015). Automatic Broaching Tool Design by Technological and Geometrical Optimization. *Procedia CIRP*, 33, 496–501. doi:10.1016/j.procir.2015.06.061
- Zhang, Y., Outeiro, J. C., & Mabrouki, T. (2015). On the selection of Johnson-Cook constitutive model parameters for Ti-6Al-4V using three types of numerical models of orthogonal cutting. *Procedia CIRP*, 31, 112–117. doi:10.1016/j.procir.2015.03.052

CAD/CAM/CAE, reverse engineering, the internal combustion engine

*Michał BIAŁY**, *Marcin SZLACHETKA***

CRANK-PISTON MODEL OF INTERNAL COMBUSTION ENGINE USING CAD/CAM/CAE IN THE MSC ADAMS

Abstract

The article presents the modeling and simulation of the crank-piston model of internal combustion engine. The object of the research was the engine of the vehicle from the B segment. The individual elements of the gasoline engine were digitizing using the process of reverse engineering. After converting the geometry, assembling was imported to MSC Adams software. The crank-piston system was specified by boundary conditions of piston forces applied on the pistons crowns. This force was obtain from the cylinder pressure recorded during the tests, that were carried out on a chassis dynamometer. The simulation studies allowed to determine the load distribution in a dynamic state for the selected kinematic pairs.

1. INTRODUCTION

Nowadays there is growing competition between car and engine manufacturers. This race generates a need to shorten the time needed for the construction and the design phases of the products. In the case of an analytical approach to the design, there is possibility to save time and costs of products production. This way is presented in the article Czyż & Magryta (2016), Wendeker & Czyż (2016)

* Department of Thermodynamics, Fluid Mechanics and Aviation Propulsion Systems, Faculty of Mechanical Engineering, Lublin University of Technology, Nadbystrzycka Street 36, 20-618 Lublin, Poland, e-mail: m.bialy@pollub.pl

** Department of Mechanics and Mechanical Engineering, Faculty of Economic Sciences and Technology, The Pope John Paul II State School Of Higher Education in Biała Podlaska, Sidorska Street 95, 21-500 Biała-Podlaska, Poland, e-mail: m.szlachetka@dydaktyka.pswbp.pl

where the loads acting on the drive unit of an unmanned helicopter during special maneuvers has been studied. However, there is no way to compare analytical results with the actual behavior of the products. On the second side, the experimental approach involves the development of a prototype or a series of prototypes. For this method, you can record the most accurate results and get the highest costs. Both approaches can be integrated into a hybrid method. This can be achieved through a combination of analytical calculations and simulation research of prototypes. Such actions, limited the duration of the measurements and their costs. In case of an experienced researcher, you can get results at a similar level to real studies. Properly built solid model makes it possible to analyze its mechanical properties in the states of static and dynamic operating conditions, which translates into a large number of design solutions before building the final model (Apanowicz, 2002; Chang, 2014; Ionescu, 2007; Troncossi, Ricci & Rivola, 2011).

2. MSC ADAMS SOFTWARE

To determine the mechanical load response of the crankshaft main bearings of the engine, the MSC Adams simulation software was used. Multibody environment allows for simulation of dynamic phenomena. It allows the determination of the parameters of kinematic mechanisms. It allows to analyze the distribution of forces in the nodes of kinematic pairs, at any time step. The software makes it easier to modify and optimize the performance of the designed products. In addition, MSC Adams allows to perform simulation tests of prototypes and their components. There is a possibility of solving kinematic, dynamic, static and quasi-static equations. (Balyakin & Kosenok, 2015; Hroncová, Binda, Šargaa & Kicák, 2012).

Simulation studies starts by drawing a solid model in a software module or by importing the finished geometry from the CAD (*Computer Aided Design*) environment. Solid models or entire assemblies can be imported from software such as *Catia*, *Inventor*, *Solid-Works*, *ProE* or *Unigraphics*. The *MSC Adams* software can import geometry format like: *STEP*, *IGES*, *DXF*, *Parasolid* and others. The individual elements of the simulated mechanisms may be subjected to static or dynamic loads in the form of a concentrated force or continuous loads. In addition, you can simulate the static and dynamic friction or elements contact properties. While the results of the simulations are stored in a transparent manner in the form of a graphic or numbers. (Biały, Wendeker, Szlachetka & Magryta, 2013; Tomić, Sjerić & Lulić, 2012).

3. OBJECT OF STUDY AND RESEARCH METHODOLOGY

The object of the research was the crank-piston system of internal combustion engine, codenamed *A14XER*. This drive unit is mounted in passenger vehicles of B segment (e.g. *Opel Corsa D*). It is a four-cylinder engine with Otto work cycle. The unit is equipped with a multi-point injection system. In addition, the engine has a variable geometry of intake system and has infinitely variable valve timing. Basic specifications of *A14XER* engine are summarized in table 1.

Tab. 1. Specifications of *A14XER* engine („Opel diagnostyka”, 2017)

Parameter	Value	Unit
Name	<i>A14XER</i>	[]
Displacement	1398	[cc]
Configuration	I4	[–]
Bore / Stroke	73.4 / 82.6	[mm / mm]
Compression Ratio	10.5 : 1	[–]
Power	74 at 6,000 rpm	[kW]
Torque	130 at 4,000 rpm	[Nm]
Number of valves	16	[]
Emission	EURO5	[–]

The methodology of digitization of the crank-piston *A14XER* engine is described in the next section. The model was loaded with a piston force. This force was obtained on the basis of the investigations of vehicle equipped with discussed unit. The study was conducted on a *Maha FPS 3000* chassis dynamometer. This device allows to simulate road conditions for a number of urban cycle and measurement of maximum power. In addition, chassis dynamometer allows to determine the flexibility of the engine, checking the speedometer and a number of other parameters. (Bukovan, Jakubovicova, Sapieta & Sapietova, 2017; Kolator & Janulin, 2014). Figure 1 shows the *A14XER* engine.



Fig. 1. Research *A14XER* engine (“Gmpowertrain”, 2017)

The pressure in the combustion chamber was recorded during the test bench tests. It was realized by using individual fiber optic pressure sensors from *OPTRAND* company. The sensors were placed in the spark plug, individually for each cylinder. The in cylinder pressure was recorded at a constant rotation speed of the crankshaft (1,500 rpm) and constant load (constant pressure in the intake manifold 90 kPa). The figure 2 shows the single characteristics of averaged cylinder pressure.

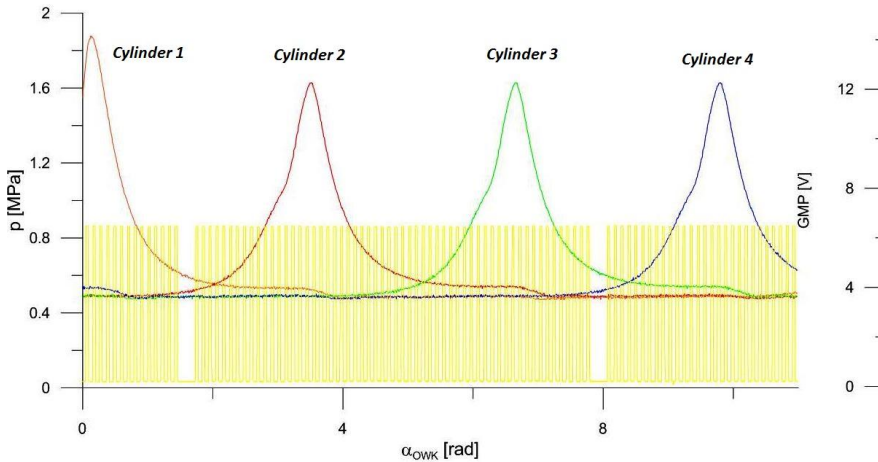


Fig. 2. The characteristic of cylinder pressure and TDC mark

4. DIGITALISATION OF THE CRANK-PISTON SYSTEM

The process of simulation tests of the *A14XER* engine using *MD Adams* software consisted of the following steps:

- surface scanning with the use of three-dimensional scanner,
- model preparation (geometry import, applying of the material characteristics, applying of degrees of freedom),
- applying the load force from the gas to each of the pistons in the form of a concentrated force; course of effective pressure for the full working cycle of the engine (Sun & Zhang, 2017).
- linking of the load value with the angle position of the crankshaft (Zhenga & Zhou, 2014),
- export of research results to a graphical or tabular form.

The virtual model of all components of the crankshaft-piston engine system was developed based on actual parts. In the first stage, using a handheld *ZScanner® 700* scanner (Figure 3), the surface of the points cloud was digitized.

This handheld scanner, due to its ability of movement relative to the object, allows one to scan the interior of an object so that the inner surface is generated. (Czyż, Kayumov & Montusiewicz, 2015).



Fig. 3. Handheld laser scanner ZScanner® 700

Then, based on the points cloud, the three-dimensional model of the crankshaft piston engine was created in *Catia v5* software. The components were developed in the form of the solid elements using the Part Design module. While the assembly of a whole unit was made using the Assembly Design module. The model of the crankshaft-piston system in *Catia v5* is shown in figure 4.

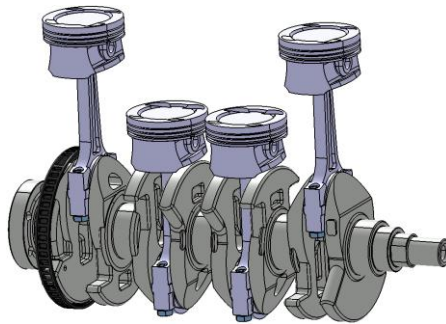


Fig. 4. Model of crankshaft-piston system in *Catia v5*

CAD model of the crank-piston system contained the following elements:

- crankshaft,
- four connecting rods with the bottom parts and screws,
- four piston pins,
- four pistons.

5. MSC ADAMS SIMULATION STUDIES

Developed three-dimensional solid model of the crank-piston system was exported from *CAD* to *MSC Adams* software. Due to the lack of a uniform data format between the two programs, an intermediate geometry translator was used. The exported model in *STEP* format (from *CAD*), was converted and imported in the form of *parasolid* to the *Adams View* module (figure 5).

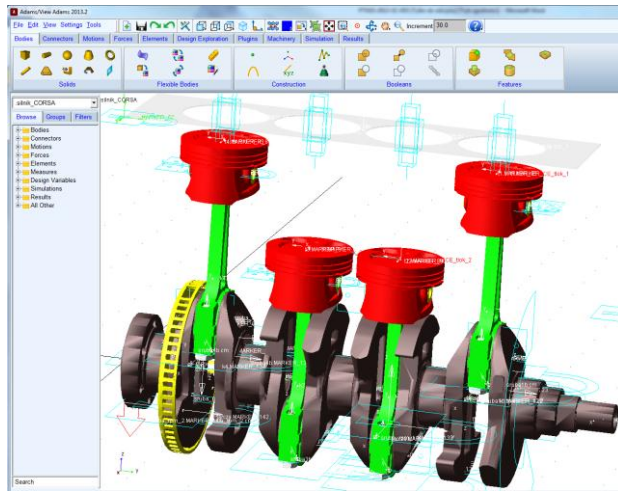


Fig. 5. Windows screenshot of MSC ADAMS software from the Adams-View module

Then specific data for all elements of the assembly were set up. Mass and material properties (Stojanovic & Glisovic, 2016) were added (table 2).

After defining characteristic data for the individual components, the process of receive degrees of freedom from kinematic pairs started. In the model we can see such pairs as rotation of: pin main shaft, rod bearing, planar motion of the piston relative to the cylinder and et cetera. For this purpose, the following features were used:

- revolute joint – to simulate the rotation,
- translation joint - to carry out reciprocating motion,
- fixed joint - in order to restrain the elements in relative motion, e.g. to the connecting rod bearings.

Tab. 2. Material properties

Name	Number	Mass	Young's modulus	Poisson's ratio
	[units]	[kg]	[N / mm ²]	[]
Crankshaft	1	9.4408	$2.07 \cdot 10^5$	0.29
Connecting rod	4	0.3261		
Cover rod	4	0.0908		
Piston	4	0.3026		
The piston pin	4	0.0695		
Bolt rod	8	0.0166		
Disk	1	0.2725		
Bolt disk	3	0.0034		

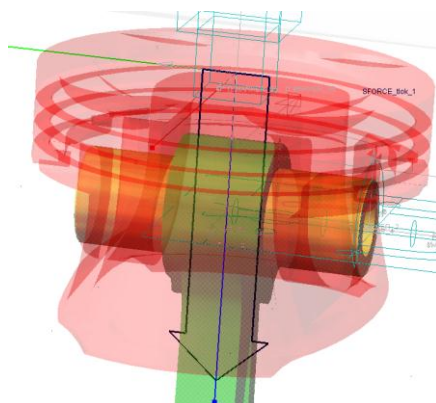


Fig. 6. Added load in the form of a concentrated force resulting from effective pressure

Before the last stage of the model preparation it was necessary to add piston forces. Those forces were calculated on the basis of the pressure measurement and in the combustion chamber. The forces were added for individual pistons, to each piston crowns. Added load in the form of a concentrated force to one of the pistons is shown in figure 6.

At the last stage, the piston forces value were related to the angle of rotation of the crankshaft. For this purpose *Akima function*, type *AKISPL* was used. The *AKISPL function* uses Akima spline interpolation to return the y values for the x variable input through the spline entity. It uses spline curve in x-y direction and linear interpolate in x-z direction. (*Basic ADAMS Full Simulation Training Guide*, 2001; “MSC Software”, 2017; Sun & Zhang, 2017).

6. RESEARCH RESULTS

Simulation tests were carried out for a fixed crankshaft rotational speed and constant load (represented by the constant pressure in the intake manifold). Simulations were realized for several consecutive cycles of the engine work. In figures 7 and 9, the results of research simulation are shown.

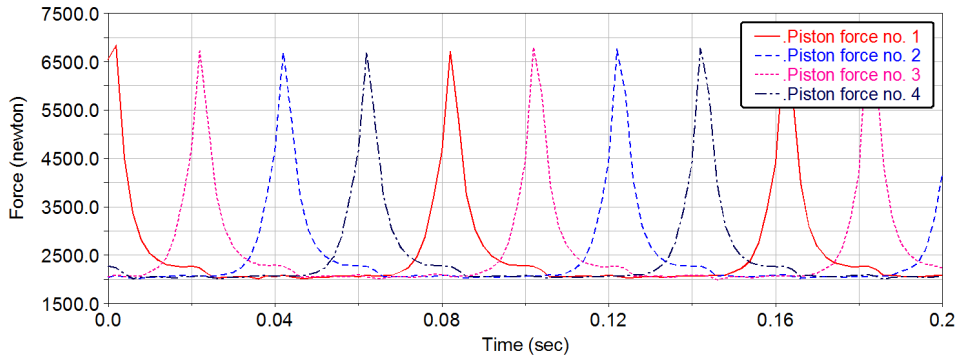


Fig. 7. Load characteristic of the piston force

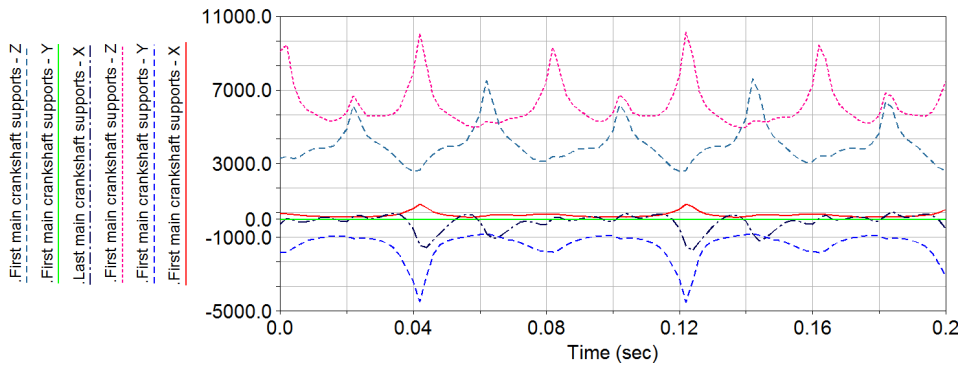


Fig. 8. Load characteristic of the main crankshaft supports (first and last)

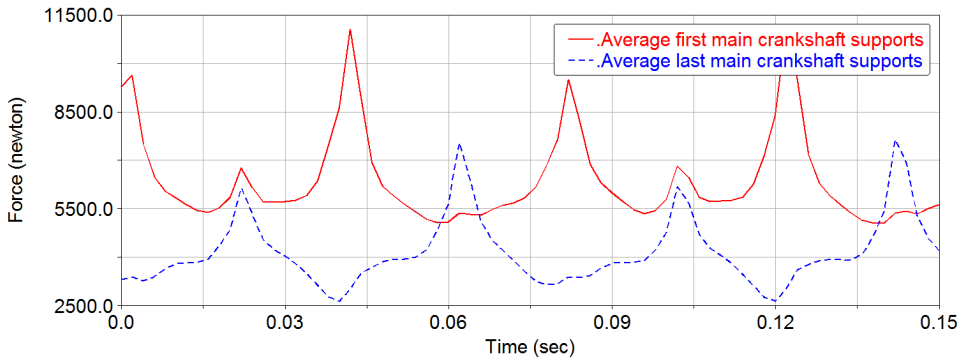


Fig. 9. Average load characteristic of the main crankshaft supports (first and last)

7. CONCLUSIONS

Simulation studies confirm the benefits of hybrid research. The cost of hybrid testing is significantly reduced as compared to the real tests. Besides of the purchase of software, the hybrid tests does not require the construction of a measuring station equipped with measurement and control equipment. There is no need to purchase a number of samples, filling the media (fuel, oil etc.). Furthermore, there is a time shortening. The model construction using scanning process and *CAD* modeling lasts from a few to dozen days (depending on the complexity of the model). The biggest difficulty in modeling, becomes the choice of materials and factors characteristic for solid parts e.g. the selection of the parameters of friction in the kinematic nodes.

On the basis of performed simulation studies, the load of the crankshaft of the internal combustion engine was determined. This load is transmitted further into the engine body, and then, via flexible supports to the bodywork of the vehicle and consequently to the passenger area. Knowledge of the course of load spectrum transferred from the engine to its mounting points allows for the selection or design of the new flexible elements. A further phase of work involves the selection of stiffness and damping parameters of supports for such an internal combustion engine. It should be noted that the simulation studies were carried out only on the basis of several successive cycles of engine operation in a steady state. However, the primary objective of the studies was to present the ideology of the model development of the crank-piston system from the internal combustion engine.

This work was funded under the Research Project 4519/B/T02/2010/39: “Zasilanie wodorem silników spalinowych”, financed from Polish Ministry of Science and Higher Education.

REFERENCES

- Apanowicz, J. (2002). *Metodologia Ogólna*. Gdynia: Wydawnictwo Diecezji IV pińskiej „BERNARDINIUM”.
- Balyakin, V., & Kosenok, B. (2015). Study of the Dynamic Characteristics of a Two-Cylinder Internal Combustion Engine Using Vector Model. *Procedia Engineering*, 106, 183–191. doi: 10.1016/j.proeng.2015.06.023
- Basic ADAMS Full Simulation Training Guide* (2001). Version 11.0 part number 110viewtr-03. Mechanical Dynamics, Incorporated
- Biały, M., Wendeker, M., Szlachetka, M., & Magryta, P. (2013). Knocking combustion influence on the load of the piston-crank system using MSC ADAMS software. *Combustion Engines*, 52(3), 421–427.
- Bukovan, J., Jakubovicova, L., Sapieta, M., & Sapietova, A. (2017). Analysis and implementation of input load effects on an air compressor piston in MSC.ADAMS. *Procedia Engineering*, 177, 554–561. doi: 10.1016/j.proeng.2017.02.260
- Chang, K.-H., (2014). Assembly Modeling. Chapter 4. In *Product Design Modeling Using CAD/CAE* (pp. 169–232). Boston: Academic Press. doi:10.1016/B978-0-12-398513-2.00004-X
- Czyż, Z., & Magryta, P. (2016). Analysis of the operating load of foil-air bearings in the gas generator of the turbine engine during the acceleration and deceleration maneuver. *Eksploatacja i Niezawodność – Maintenance and Reliability*, 18(4), 507–513. doi:10.17531/ein.2016.4.5.
- Czyż, Z., Kayumov, R., & Montusiewicz, J. (2015). Selected methods of making three-dimensional virtual models of museum ceramic objects. *Applied Computer Science*, 11(1), 51–65.
- Gmpowertrain*. (n.d.). Retrieved February 2, 2017, from Gmpowertrain website <http://gmpowertrain.com>
- Hroncová, D., Binda, M., Šargaa, P., & Kicák, F. (2012). Kinematical analysis of crank slider mechanism using MSC Adams/View. *Procedia Engineering*, 48, 213–222. doi:10.1016/j.proeng.2012.09.507
- Ionescu, F. (2007). Modelling and simulation in mechatronics. *IFAC Proceedings Volumes*, 40(18), 301–312. doi:10.3182/20070927-4-RO-3905.00051
- Kolator, B., & Janulin, M. (2014). Wyznaczanie stanów trakcyjnych pojazdu za pomocą hamowni podwoziowej LPS 3000. *Studies & Proceedings of Polish Association for Knowledge Management*, 139–150.
- MSC Software*. (n.d.). Retrieved February 2, 2017, from MSC Software website <http://www.mssoftware.com>
- Opel diagnostyka*. (n.d.). Retrieved February 2, 2017, from Opel website <https://opel2015.wordpress.com>
- Stojanovic, B., & Glisovic, J. (2016). Automotive Engine Materials. In *Reference Module in Materials Science and Materials Engineering*. Elsevier.
- Sun, Z., & Zhang, C. (2017). Trajectory-based combustion control for renewable fuels in free piston engines. *Applied Energy*, 187, 72–83. doi:10.1016/j.apenergy.2016.11.045
- Tomić, R., Sjerić, M., & Lulić, Z. (2012). The optimization of crankshaft offset of spark ignition engine. *Journal of Trends in the Development of Machinery and Associated Technology*, 16(1), 211–214.
- Troncossi, M., Ricci, R., & Rivola A. (2011). Model Reduction of the Flexible Rotating Crankshaft of a Motorcycle Engine Cranktrain. *International Journal of Rotating Machinery*, 2011, Article ID 143523, 9 pages. doi: 10.1155/2011/143523
- Wendeker, M., & Czyż, Z. (2016). Analysis of the bearing nodes loads of turbine engine at an unmanned helicopter during a jump up and jump down maneuver. *Eksploatacja i Niezawodność – Maintenance and Reliability*, 18(1), 89–97, doi:10.17531/ein.2016.1.12
- Zhenga, E., & Zhou, X. (2014). Modeling and simulation of flexible slider-crank mechanism with clearance for a closed high speed press system. *Mechanism and Machine Theory*, 74, 10–30. doi: 10.1016/j.mechmachtheory.2013.11.015

*Fireworks algorithm, Function optimization, Swarm intelligence,
Mathematical programming, Natural computing*

Evans BAIDOO*

FIREWORKS ALGORITHM FOR UNCONSTRAINED FUNCTION OPTIMIZATION PROBLEMS

Abstract

Modern real world science and engineering problems can be classified as multi-objective optimisation problems which demand for expedient and efficient stochastic algorithms to respond to the optimization needs. This paper presents an object-oriented software application that implements a firework optimization algorithm for function optimization problems. The algorithm, a kind of parallel diffuse optimization algorithm is based on the explosive phenomenon of fireworks. The algorithm presented promising results when compared to other population or iterative based meta-heuristic algorithm after it was experimented on five standard benchmark problems. The software application was implemented in Java with interactive interface which allow for easy modification and extended experimentation. Additionally, this paper validates the effect of runtime on the algorithm performance.

1. INTRODUCTION

Function optimisation problems have been solved by many different techniques. Optimization in operation research explains a process of finding the high value of a function in a domain definition which is subject to numerous constraints on the variable values. As a rule of thumb, function optimization problem finds the optimal solution of an objective function definition by means of iteration (Ren & Wu, 2013). Characters of these optimisation problems are mostly identified as linear or non-linear, continuous or discrete, concave or convex functions etc.

* Kwame Nkrumah University of Science and Technology, Department of Computer Science, PMB, KNUST, Ghana, Email: ebaidoo2.cos@st.knust.edu.gh

In such instances conversion from constraint function optimization problem into an unconstrained problem is implemented by focusing on the designed special operators and penalty functions so as to enable the feasibility of the solution at all times.

There are a wide range of mathematical programming algorithms which offer various techniques to control various optimization problems as numerical, discrete or combinatorial optimization problems, but most of the methods at most times fail to return satisfactory results. In operations research, as an alternative to the mathematical programming methods, bio-inspired optimization algorithms have become very popular. Over the last decade, researchers are paying attention to nature-inspired heuristics. These algorithms centre on the cooperative intellectual behaviours of animal groups, insects, bee or ant colonies etc and its problem solution abilities. Swarm system as mostly referred have lots of advantages in finding solutions to many optimization problems (Bonabeau, Dorigo & Theraulaz, 1999). As applied in many technical fields, such as data mining, signal processing, network routing, pattern recognition and others, this system is a kind of random search algorithm that simulates the biological population evolution and hence solves complex stochastic optimization problems through cooperation of individuals and species competition (Yuan, de Oca, Birattari & Stutzle, 2012). Typical among the swarm intelligence algorithms are the ant colony optimization (ACO) algorithm (Chandra et al., 2012), the bee colony (ABC) algorithm (Karaboga & Basturk, 2007) particle swarm optimization (PSO) algorithm (Kennedy & Eberhart, 1995), and the genetic algorithm (GA) (Tang, Man, Kwong & He, 1996) enthused by the Darwinian law. Among the listed SI algorithms, PSO is one of the largely accepted algorithms for probing optimal locations in an undefined dimensional space.

A new swarm intelligence algorithm which aroused worldwide concern in 2010 with an excellent optimisation performance was one proposed by Ying Tan. This algorithm which inspired by the emergent swarm behaviour of fireworks is referred to as Fireworks algorithms. This algorithm follows in the tradition of swarm intelligence (Tan & Zhu, 2010).

In this paper an object-oriented implementation of fireworks algorithm is tested on unconstrained function optimization problems. A software program was developed in Java to solve the function optimisation problem, test the results of benchmark functions and also to test the system robustness and performances. The remaining of the paper is organised as follows: In section 2 Fireworks algorithm is introduced followed by section 3 with a brief explanation of five standard unconstrained Benchmark functions. Section 4 details the software implementation of the fireworks algorithm with Section 5 presenting the simulation experiment and results. Finally the paper concludes with Section 6.

2. FIREWORKS ALGORITHM

2.1. Background

A novel swarm intelligence algorithm, Fireworks Algorithm (FA), over the past decade has been implored to solve universal optimisation problems although research of various works according to survey, have shown few implementation. Proposed by Tan and Zhu, this algorithm mimics fireworks explosion activity and behaviour. Its first implementation was to identify its superior performance over Standard PSO and Clonal PSO (Tan & Zhu, 2010). Zheng et al. (2012) put forward a hybrid fireworks-differential evolution (FWA-DE) algorithm. They use the crossover, mutation and selection operators in the Differential evolution algorithm. An enhanced fireworks algorithm (EFWA) presented by Zheng et al. (2013) was used to improve the least radius detection rate, the rules of mapping and spark selection approach of the explode sparks. In 2014, a Hybrid approach which put together FWA and differential mutation (FWA-DM), was formulated. Having successfully experimented on CEC 2014 benchmark functions, it proves to be a good solution. Another proposed solution is the dynamic search firework algorithm (DFWA) (Zheng et al., 2014). This algorithm works by dividing the fireworks population into basic fireworks with optimal fitness value and non-core fireworks. This strategy enables the algorithm to undertake local search and global search efficiently and effectively. As put forward by Ding et al. (2013), the parallelized GPU-based Fireworks Algorithm (GPU-FWA) proficiently exploit graphical processing unit (GPU), to solve large-scale problems. In a research paper by Li et al. (2014), they propose the adaptive firework algorithm (AFWA) to carry out self-tuning of blast radius. They measure the distance involving the best individual and the discussed individual by setting the distance as the next blast radius of the best individual. From this kind of technique, the adaptive step size adjustment shows good optimization performance on the improved FWA.

The focal source of motivation for the FA is the process of starting out a firework. Any time a firework is start out, shower of sparks consume the local space in the region of it. Tan disclose that, the explosion progression of a firework can be analyse as an exploration in the local space about an exact point where the firework left through the sparks created in the explosion (Tan & Zhu, 2010). The explosion of Firework reveals two specific behaviours. A healthy created fireworks, presents numerous sparks and the sparks tends to be engulf in the centre of the explosion. The fireworks is mostly found in areas in the search space which tends to promising and may possibly be close to optimal solution. Therefore it is ideal to produce enough sparks to locate the best spot in the region of the firework. In contrast, poor quality fireworks demonstrate divergent behaviour. Mostly in such instances, sparks generated are relatively few and scattered in the local space. This activity indicates that, the best solution

to the problem is distant away from the spot of the firework and for that matter, the radius of the search could be larger.

2.2. Algorithm attitude

The fireworks algorithm (FA) is a novel iterative-based disperse optimization algorithm approach that imitates the behaviour of fireworks explosion that identifies the equilibrium between global search and local exploration by means of regulating the explosion method of fireworks bombs. The overall algorithm is stochastic in nature. When there is an explosion of fireworks, the sparks produced spread in the air filling their immediate region. For this matter to locate a point x in the specified function $f(x) = y$, fire explosion can be created in the area which is possible to search continually until sparks locates the point close to x or find the x space. In every generation of explosion, N positions of the fireworks are chosen. Then after N other positions are chosen from the recent sparks and fireworks positions for the next firework explosion. From the results obtained after the explosion, a rough estimation of the position is recorded until the finest position is recorded else fireworks explosions are continued with explosion locations of N selected again. A graphical clarification is expressed in figure 1.

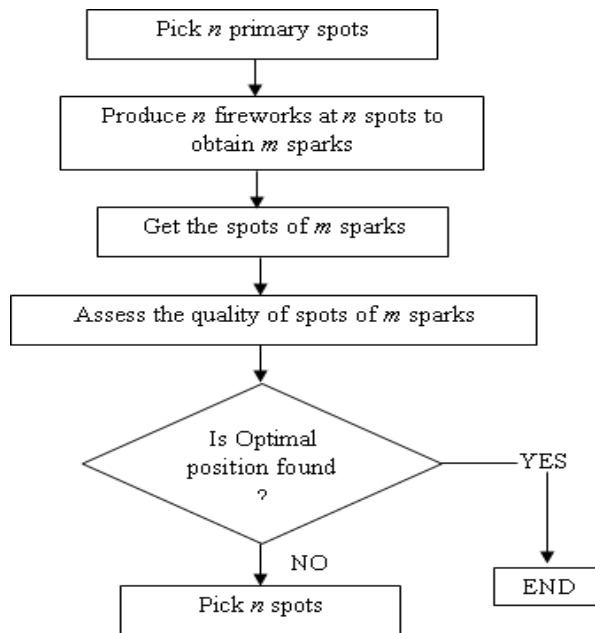


Fig. 1. Flowchart of Fireworks Algorithm

2.3. Algorithm Structure

Two important elements of the FA are the number of sparks and the amplitude of explosion. To illustrate the first element of the algorithm, assuming that FA is intended for some kind of optimisation problem:

$$\text{Minimize } f(x) \in \mathbb{R}, x_{\min} \leq x \leq x_{\max}, \quad (1)$$

in this case $x = x_1, x_2, \dots, x_n$ represent a probable solution, with $f(x)$ being the objective function and x_{\min} and x_{\max} denoting extent of the solution search space. So therefore the number of sparks that can be produced by each single firework x_i can be stated as:

$$S_i = m \frac{y_{\max} - f(x_i) + \xi}{\sum_{i=1}^n (y_{\max} - f(x_i)) + \zeta'} \quad (2)$$

Where m symbolize a parameter which take care of the general number of sparks generated by n fireworks, with $y_{\max} = \max(f(x_i))$ ($i = 1, 2, \dots, n$) being the worst value of the target function amongst the n fireworks, and ξ , is the least computer constant exploited to evade zero-division-error. From experimentations by (Tan & Zhu, 2010), S_i needs to be smaller so as to avoid devastating outcomes under terrible firework explosions, therefore bounds on S_i are created as expressed in 3.

$$\hat{S}_i = \begin{cases} \text{round}(a \cdot m) & \text{if } S_i < a \cdot m \\ \text{round}(b \cdot m) & \text{if } S_i > b \cdot m \\ \text{round}(S_i) & \text{otherwise } a < b < 1, \end{cases} \quad (3)$$

where a and b represent preset constant parameters. The second important element of FA defines the amplitude of explosion. A well created firework amplitude usually is smaller compared to that of a terrible one. The expression defined in 4 illustrates the amplitude of each explosion.

$$A_i = \hat{A} * \frac{f(x_i) - y_{\min} + \xi}{\sum_{i=1}^n (f(x_i) - y_{\min}) + \zeta'} \quad (4)$$

where \hat{A} refers to the value of the highest explosion amplitude with $y_{\min} = \min(f(x_i))$ ($i = 1, 2, \dots, n$) representing best firework of the target function in n fireworks. In the course of an explosion, the z direction (dimension) of sparks is affected. The number of randomly affected directions is obtained by

$$z = \text{round}(d \cdot \chi), \quad (5)$$

where d denotes the optimisation problem number dimension of location x , with χ being a uniform distribution of a random number ranging from 0 and 1. With the aim of determining the x_i firework location of a spark, a spark location x_j is first generated. The entire process is made known in pseudo-code 1.

Pseudo-code 1

```

Find the initial spark's location:  $x_j = x_i$ 
Choose random  $z$  dimensions of  $x_j$  by adopting Eq. (5)
Compute the displacement:  $h = A_i \cdot \sigma$ ;
for each chosen dimension  $x_k^j$  of  $x_j$  do
     $x_k^j = x_k^j + h$ 
    If  $x_k^j < x_k^{min}$  or  $x_k^j > x_k^{max}$ 
        map  $x_k^j$  to the promising space:
         $x_k^j = x_k^{min} + |x_k^j| \%(x_k^{max} - x_k^{min});$ 
    end if
end for

```

From the pseudo-code 1, σ represent a random number of intervals (-1, 1). To maintain the goal of diversity of sparks, a second approach to establishing sparks generation is implemented - Gaussian explosion as illustrated in Pseudo-code 2. A Gaussian (1, 1) function which refers to the Gaussian distribution with a single standard deviation and mean is adapted to describe the explosion coefficient. With this approach m^{\wedge} sparks are generated in every Gauss explosion.

Pseudo-code 2

```

Establish the initial spark's location:  $\hat{x}_j = x_i$ 
Choose arbitrary  $z$  dimensions of  $\hat{x}_j$  by adopting Eq. (5)
Compute the coefficient of Gauss explosion:  $g = \text{Gaussian}(1, 1)$ 
for each chosen dimension  $\hat{x}_k^j$  of  $\hat{x}_j$  do
     $\hat{x}_k^j = \hat{x}_k^j \cdot g$ 
    If  $\hat{x}_k^j < x_k^{min}$  or  $\hat{x}_k^j > x_k^{max}$  in that case
        map  $\hat{x}_k^j$  to the promising space:
         $\hat{x}_k^j = x_k^{min} + |\hat{x}_k^j| \%(x_k^{max} - x_k^{min});$ 
    end if
end for

```

At the start of every iteration, n fireworks locations are chosen. The finest position x^* according to the best target function $f(x^*)$ is always kept and reassigned for the next iteration. At this point, the selection of $n-1$ locations are

chosen rooted on their distance with other locations to maintain sparks diversity. The measure of distance between a location or spot and other spots/locations is generally determined in FA as:

$$R(x_i) = \sum_{j \in K} d(x_i, x_j) - \sum_{j \in K} \|x_i - x_j\|, \quad (6)$$

where K is the set of all present locations of both fireworks and sparks. At this point the probability of selecting location x_i can be expressed in (7) as:

$$P(x_i) = \frac{R(x_i)}{\sum_{j \in K} R(x_j)}, \quad (7)$$

where $P(x_i)$ indicate the probability that the location x_i will be chosen. Putting all together Pseudo-code 3 illustrates the build up of Fireworks algorithm in high level language.

Pseudo-code 3 in High level language

```

Arbitrarily establish  $n$  location of fireworks
iterate until complete
  for every individual firework
    determine the firework amplitude
    determine the total of regular sparks
    Create the regular sparks
  end for
  create special Gauss sparks
  calculate every individual spark from sparks list,
    choose  $n$  to serve as new fireworks locations
  generate  $n$  new fireworks
end iteration
present the finest spark location found

```

The function estimations of the FA are such that there are about $n + m + \hat{m}$ carried out by each generation. Assuming the optimum of a target function can be identified in generation T, the FA complexity will be $O(n + m + \hat{m})$. A further explanation of the behaviour of the algorithm process is demonstrated in the graph in Figure 2 taken from James McCaffrey (2016).

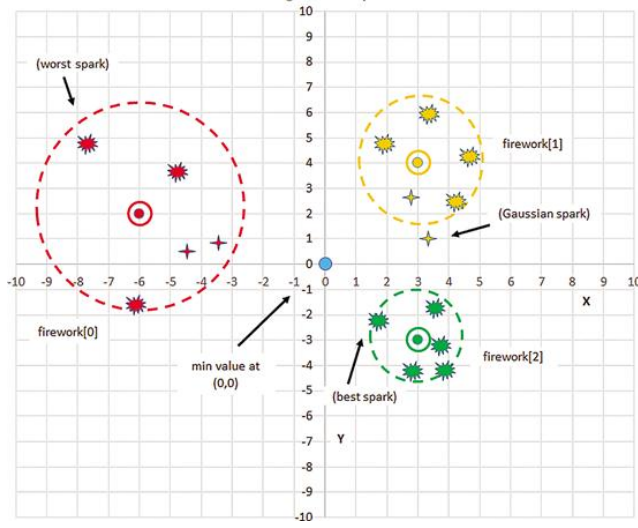


Fig. 1. Fireworks optimization algorithm

In summing up, pseudo-code 1 and 2, presents two sorts of sparks which are respectively generated in each of the iteration. In the first spark kind, the sparks number and explosion amplitude depend to a larger extent the worth of the fireworks. This is sharply in contrast with other sparks which are created using the Gaussian explosion process for firework searching in the local Gauss space. Subsequently, the n positions of the succeeding explosion are chosen once the two kinds of spark positions are obtained. Pseudo-code 3 put together the overall structure of FA.

3. BENCHMARK FUNCTIONS

Numerous benchmark functions have been reported in literature over the years yet; there have not been an accepted standard list. This paper experimented five rich set of popular benchmark functions with varied qualities in terms of valley landscape, separability, and modality to assess the character traits of the solution algorithm adopted – in this case check its correctness, toughness and general performance of the implementation program as adopted in Virtual Library of Simulation Experiments: “Test Functions and Datasets” (2016) and Bacanin et al (2014). In this paper the unconstrained function optimization problems used is of the form:

$$\begin{aligned} & \underset{x}{\text{minimize}} \quad f(x) \\ & \text{Subject to: } x \in \omega \leq 0, i = 1 \dots m \\ & \quad x_j^l \leq x_j \leq x_j^u, j = 1 \dots n \end{aligned}$$

Where, $f(x)$ represent the objective function to be minimized, with x being the continuous vector variable of domain $\omega \subset \mathbb{R}^n$ and $f(x): \omega \rightarrow \mathbb{R}$ representing a continuous real-valued function. The lower and upper bounds defined within each function dimension is represented by ω .

The first is the Dixon-Price test function, f_1 . This function is a continuous, non-separable and multimodal minimization test operation. It search domain lies in $-10 \leq x_i \leq 10, i = 1, 2, \dots, n$ with its global minimum, $f(x)$ at 0.

Griewank function, f_2 which has its global minimum value at 0 with the function initialization range from $[-600, 600]$, is second. It is a continuous and differentiable function which has a corresponding universal optimum solution as $x_{opt} = (x_1, x_2, \dots, x_n) = (100, 100, \dots, 100)$. This function although multimodal, its multimodality diminishes with high dimensionalities ($n > 30$) and therefore appears uni-modal.

Rosenbrock, f_3 makes the list as third. It is a well-known traditional optimization problem with a 2 dimensional function which describe a deep valley with a parabola form of the shape $x_1^2 = x_2$ that results to the global minimum. Owing to the non-linearity of the valley, lots of algorithms converge slowly since they vary the direction of the search constantly and for this reason this problem has been repetitively used in assessing gradient-based optimization algorithms performance. Valley function is unimodal with the initialization interval of X $[-30, 30]$.

The fourth test function is the Schwefel function, f_4 . This function is complex, with many local minima. Initialization range for the function is $[-500, 500]$. The surface of Schwefel function is made up of a large amount of peaks and valleys. It is a deceptive function which possesses two global minimum with its global minimum over the parameter space from the succeeding best local minima geometrically far-off. Thus its search algorithm is ably susceptible to converging in a wrong direction. It has its global minima $x^*at = \pm[\pi(0.5 + k)]^2, f_4(x^*) = -418.983$. The difficulty with this test function is that its gradient cannot bend along their axis owing to the epistasis with their variables. For this reason, most algorithms that make use of the gradient leisurely converge.

The Sphere concludes the benchmark functions. This function has the properties of being separable, scalable, continuous and multimodal. Its interval range lies in the region of $0 \leq x_i \leq 10$ with its universal minimal value at 0 and optimum solution being $x_{opt} = (x_1, x_2, \dots, x_n) = (0, 0, \dots, 0)$.

The functions expression, its initialization and intervals are further expressed in Table 1.

Tab. 1. Benchmark functions expression and initialisation

Function	Expression	Initialisation
Dixon-Price	$f_1(x) = (x_1 - 1)^2 + \sum_{i=2}^n i(2x_i^2 - x_{i-1})^2$	$[-10, 10]$
Griewank	$f_2(x) = \sum_{i=1}^n \frac{x_i^2}{4000} - \prod_{i=1}^n \cos\left(\frac{x_i}{\sqrt{i}}\right) + 1$	$[-100, 100]$
Rosenbrock	$f_3(x) = \sum_{i=1}^{n-1} [100 \cdot (x_{i+1} - x_i^2)^2 + (x_i - 1)^2]$	$[-30, 30]$
Schwefel	$f_4(x) = \sum_{i=1}^n -x_i \sin(\sqrt{ x_i })$	$[-500, 500]$
Sphere	$f_5(x) = \sum_{i=1}^n x_i^2$	$[0, 10]$

4. eFIREWORKS IMPLEMENTATION

This paper implements a software program which uses an object oriented approach to its execution of the fireworks algorithm. The developed software is named eFireworks (explosive Fireworks). When an objected oriented approach is adopted there is improvement in the software scalability and therefore there is lesser time execution even when there is an implementation of different optimization problems of new programming concept. Object oriented capabilities allow for addition of varying optimization functions and lots more benchmark problems with little or no effort. Additionally, object oriented implementation allows for easy modification of the behaviour of algorithm functions. Similar works have been suggested for artificial fish swarm algorithm in James McCaffrey (2016) and ABC in Virtual Library of Simulation Experiments: “Test Functions and Datasets” (2016). The developed software with its graphical user interface is created in Java programming language. Java was chosen partly due to the fact that its paradigm entirely imitates object-oriented and the ability that it is based on classes, concurrent and is general purposed. Additionally, its implementation dependencies can be as few as possible. An added advantage that java has is its ability to allow application developers to ”write once, run anywhere.” This consequently makes most Java application convenient and portable thus allowing software – eFireworks – to be executed on varying computer system. The software adopts a graphical user interface. The graphical user interface among other qualities enables easier control of parameters and test function to optimize.

The software application is deeply adopts the theory of tightly connected abstract classes and inheritance. This concept enables easy adaptation to new functional problems and the future extendibility of the program. eFireworks is developed using java 1.7.0.25, NetBeans 7.1. 2 with Windows 8 operating system of x64 bit. Figure 2 illustrate a Screenshot of the vital Graphical user interface (GUI) of eFireworks.

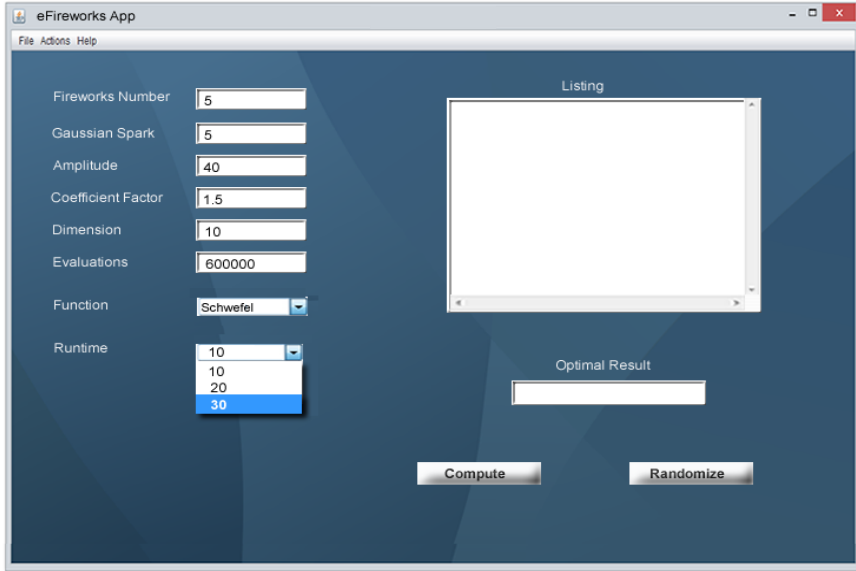


Fig. 2. Screenshot of eFireworks User interface

5. OPTIMIZATION TEST AND RESULTS

All tests were executed on intel(R) Core (TM_i3-3110M CPU@ 2.40GHz laptop equipped with 4GB RAM on Windows 8 x64 Operating System in NetBeans 7.1.2 IDE. The NetBeans IDE and operating system were the only processes running during test execution. To validate the algorithm and examine runtime effects on the algorithm performance, two sets of test was conducted on each of the five benchmark functions. 10 runs was set for the first execution and 30 runs for the second, each using different random seeds. The best, statistical mean and standard deviation results were the indicators that were observed from the problem solution. The bounds used for the upper and lower parameters were the default values from Table 1. The benchmark dimensionality for all functions is set to 10 ($D = 10$) with the maximum number of function evaluation perked at 600,000 for all functions. The parameter settings of FA used are same as in Tan and Zhu (2010): number of fireworks, $n = 5$,

total number of regular sparks, $m = 50$, special Gaussian spark, $\hat{m} = 5$, amplitude, $A = 40$, maximum spark of firework, $b = 0.8$ and minimum spark of firework, $a = 0.04$. Results of test values are shown in Table 2 for runtime of 10 and Table 3 for runtime of 30.

Tab. 2. Experimental results of 10 runs

Function	Best cost function	Statistical Mean	Standard Deviation
Dixon-Price	4.7E-10	2.01E-01	0.321355
Griewank	0.00172	0.0273431	0.017826912
Rosenbrock	0.02364	0.19397877	0.087896961
Schwefel	-4489.82887	-4309.82887	103.2795559
Sphere	2.048E-09	0.025760842	0.081249567

As can be identified from Table 2 and 3, the optimization obtained with Fireworks algorithm presents satisfactory results for all under listed benchmark problems. Comparison can be drawn with other famous heuristic or bio-inspired algorithms and software systems such as Karaboga and Basturk (2007) & Bacanin (2014). The algorithm proves to be robust in its operations and presents optimal results.

Tab. 3. Experimental results of 10 runs

Function	Best cost function	Statistical Mean	Standard Deviation
Dixon-Price	3.66E-10	0.135119376	0.27035624
Griewank	0.0001125	0.019550378	0.022130294
Rosenbrock	0.010225	0.103153984	0.107639116
Schwefel	-5389.82887	-4547.919763	369.4342795
Sphere	0	0.008030625	0.043813971

Drawing comparison from Table 2 and Table 3 it can be deduce that as the number of runs are increased, results obtained tends to be slightly better. It can therefore be concluded that the performance of the optimization solution, Fireworks algorithm is marginally affected by alteration of number of runs although it may be disregarded since the results presented is of tiny deviation.

6. CONCLUSIONS

In this paper, an implementation of a population based swarm intelligence algorithm, Fireworks algorithm was adopted to solve unconstrained function optimization problems using a developed object-oriented graphical user interface application. The application presents a much more expedient way to work and allows for easy modification for other optimization problems as compared to the original version. The algorithm was tested on five benchmark functions and performance recorded. The optimization solution algorithm demonstrated its ability to contain several benchmark problems but there is some margin of improvement. In future, the study can be extended to investigate and study other global and real life problems such as urban traffic regulation, job scheduling, parcel delivery etc.

REFERENCES

- Bacanin, N., Tuba, M., & Stanarevic, N. (2012). Artificial Fish Swarm Algorithm for Unconstrained Optimization Problems. *Applied Mathematics in Electrical and Computer Engineering*, 405–410.
- Bonabeau, E., Dorigo, M., & Theraulaz, G. (1999). *Swarm Intelligence: From Natural to Artificial Systems*. New York: Oxford University Press Inc.
- Ding, K., Zheng, S. Q., & Tan, Y. (2013). A GPU-based Parallel Fireworks Algorithm for Optimization. *Gecco'13: Proceedings of the 2013 Genetic and Evolutionary Computation Conference*, 9–16.
- Karaboga, D., & Basturk, B. (2007). A powerful and efficient algorithm for numerical function optimization: artificial bee colony (ABC) algorithm. *Journal of Global Optimization*, 39(3), 459–471. doi:10.1007/s10898-007-9149-x
- Kennedy, J., Eberhart, R. C. (1995). Particle swarm optimization. *Proceedings of IEEE International Conference on Neural Networks*, 4, 1942–1948.
- Li, J., Zheng, S., & Tan, Y. (2014). Adaptive Fireworks Algorithm. *2014 IEEE Congress on Evolutionary Computation (CEC)*, 3214–3221. doi:10.1109/CEC.2014.6900418
- McCaffrey, J. (2016, September). *Fireworks Algorithm Optimization*. Retrieved from <https://msdn.microsoft.com/en-us/magazine/dn857364.aspx>
- Mohan, B. C., & Baskaran, R. (2012). A survey: Ant Colony Optimization based recent research and implementation on several engineering domain. *Expert Systems with Applications*, 39(4), 4618–4627. doi:10.1016/j.eswa.2011.09.076
- Ren, Y., & Wu, Y. (2013). An efficient algorithm for high-dimensional function optimization. *Soft Computing*, 17, 995–1004. doi:10.1007/s00500-013-0984-z
- Tan, Y., & Zhu, Y. (2010). Fireworks Algorithm for Optimization. In: Y. Tan, Y. Shi, & K.C. Tan (Eds.), *Advances in Swarm Intelligence. ICSI 2010. Lecture Notes in Computer Science* (vol. 6145, pp. 355–364). Springer.
- Tang, K. S., Man, K. F., Kwong, S., & He, Q. (1996). Genetic algorithms and their applications. *IEEE Signal Processing Magazine*, 13(6), 22–37. doi:10.1109/79.543973
- Virtual Library of Simulation Experiments: Test Functions and Datasets* (n.d.). Retrieved August, 2016, from <https://www.sfu.ca/~ssurjano/optimization.html>
- Yuan, Z., de Oca, M. A. M., Birattari, M., & Stutzle, T. (2012). Continuous optimization algorithms for tuning real and integer parameters of swarm intelligence algorithms. *Swarm Intelligence*, 6(1), 49–75. doi:10.1007/s11721-011-0065-9
- Zheng, S. Q., Janecek, A., Li, J. Z., & Tan, Y. (2014). Dynamic Search in Fireworks Algorithm. *2014 IEEE Congress on Evolutionary Computation (Cec)*, 3222–3229.

- Zheng, S., Janecek, A., & Tan, Y. (2013). Enhanced Fireworks Algorithm. *2013 IEEE Congress on Evolutionary Computation*, 2069-2077. doi:10.1109/CEC.2013.6557813
- Zheng, Y. J., Xu, X. L., & Ling, H. F. (2012). A hybrid fireworks optimization method with differential evolution operators. *Neurocomputing*, 148, 75–80. doi:10.1016/j.neucom.2012.08.075

modal analysis, stability, milling process, surface roughness

Paweł PIEŚKO, Magdalena ZAWADA-MICHAŁOWSKA**

USEFULNESS OF MODAL ANALYSIS FOR EVALUATION OF MILLING PROCESS STABILITY

Abstract

The paper presents evaluation of modal analysis usefulness for determination of milling process stability. In the first phase of the study experimental modal analysis was performed and using CutPro 9.5 software, stability lobes were generated. In the next step, machining tests were carried out. The last stage of the experiment involved verification of modal analysis usefulness for evaluation of milling process stability based on surface roughness measurements. Conducted research allowed to state that modal analysis can be a useful tool for determining milling process stability.

1. INTRODUCTION

Machining is one of the fastest growing methods of manufacturing. Effective type of cutting is milling where it is necessary to determine the appropriate process conditions, ensuring its stable course. The stability of process is significant mainly in the context of obtaining maximum machining capability as well as avoidance of surface quality deterioration, resulting from vibrations of both the tool and the workpiece (particularly during cutting of thin-walled elements). Additionally, they generate accelerated wear of cutting tools and high-frequency noise (Bojanowski & Pawłowski, 2011; Budak, Tunc, Alan & Ozguven, 2012; Campa, de Lacalle & Celaya, 2011; Sun & Xiong, 2017).

*Department of Production Engineering, Lublin University of Technology, Nadbystrzycka Street 36, 20-618 Lublin, Poland, e-mail: m.michalowska@pollub.pl, p.piesko@pollub.pl

Milling process stability is understood as a condition wherein self-excited vibrations do not occur or emerging oscillation is extinguished. This phenomenon is very complex and it depends on many factors. The most important of them are presented in Fig. 1 (Kilic & Altintas, 2016; Maamar, Bouzgarrou, Gagnol & Fathallah, 2017; Płodzień & Żyłka, 2013).



Fig. 1. Factors affecting milling process stability (Płodzień & Żyłka, 2013)

Recently a dynamic development of issues related to machining stability has been observed. Currently, the appropriate definition of process condition, ensuring its stable course and avoidance vibrations is possible by using specialized software (e.g.: ShopPro, CutPro) that allows the selection of optimal technological parameters (Płodzień & Żyłka, 2013; Totis, Albertelli, Sortino & Monno, 2014).

The most widely used stability forecasting method of OUPN system (machine-clamping-workpiece-tool) is to determine stability lobes for settled process conditions. Stability lobes present the dependence of rotation speed n usually in function of depth of cut a_p (or width of cut a_e) defining stable and unstable areas. Experimental modal analysis is used for obtaining these curves (Totis et al., 2014; Totis, Albertelli, Torta, Sortino & Monno, 2017; Zhang, Xiong, Ding, Feng & Xiong, 2012).

The issue with OUPN system during milling proceeds mainly from the intermittent work of mill, causing the periodic tool deflection from the workpiece. As a result of this, corrugated structure is formed on work surface after the pass of cutting tool. To sum up, if frequency of entering blade is not equal to frequency

of natural vibrations, phase displacement is formed between the tool and the workpiece. Consequently, the effect is a variable value of width of cut layer h , resulting in various cutting forces and generating negative self-excited vibrations (Ahmadi & Ismail, 2012; Ciurana & Quintana, 2011; Lehrich & Lis, 2014; Twardowski, 2006; Zhang et al., 2012).

2. METHODOLOGY

The aim of the study was to evaluate modal analysis usefulness for determination of milling process stability. In the first stage of the study, modal analysis was carried out and based on stability lobes, technological parameters corresponding to stable and unstable ranges of tool work were read. On the grounds of the obtained results, machining tests were made. Then, the verification of modal analysis usefulness for determination of milling process stability was performed, based on surface roughness measurements.

The study was conducted on vertical machining centre AVIA VMC 800 HS with application of set for modal analysis (Fig. 2), where main elements were: modal hammer with force measurement sensor, accelerometer, data acquisition module and a computer with CutPro 9.5 software, among others.

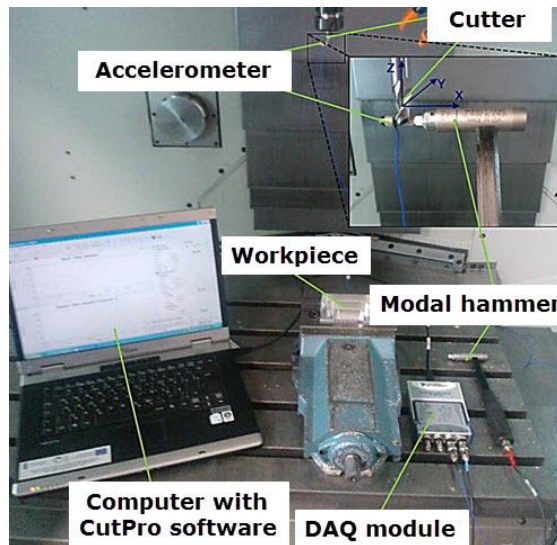


Fig. 2. Set for modal analysis (own study)

Constant technological parameters were defined in CutPro 9.5 program, i.e.: width of cut $a_e = 1$ mm and feed per tooth $f_z = 0.04$ mm/tooth, properties of workpiece material and tools geometry.

Aluminum alloy EN AW-2024 T351 (chemical symbol: EN AW-AlCu4Mg1) that is widely applied in industry, especially aerospace, was used for the study. Its chemical composition and selected properties are presented in Table. 1.

Tab. 1. Chemical composition and selected properties of alloy EN AW-2024 (PN-EN 573-3:2014-02; PN-EN 485-2:2016-10)

Chemical composition	Si	Fe	Cu	Mn	Mg	Cr	Zn	Ti
	0.5	0.5	3.8 – 4.9	0.3 – 0.9	1.2 – 1.8	0.1	0.25	0.15
Properties	Density, ρ		Young's modulus, E		Tensile strength, R_m		Yield strength, $R_{p0.2}$	
	2.78 g/cm ³		73 GPa		430 MPa		290 MPa	

Two solid end mills destined for aluminium alloys machining were used in the experiment:

- Seger (PUN-12-00-24/50-100-3AL),
- SGS Solid Carbide Tools (44748).

Mill of Seger (PUN-12-00-24/50-100-3AL) that was made on special order is shown in Fig. 1, and Table 2 presents its technical specifications.

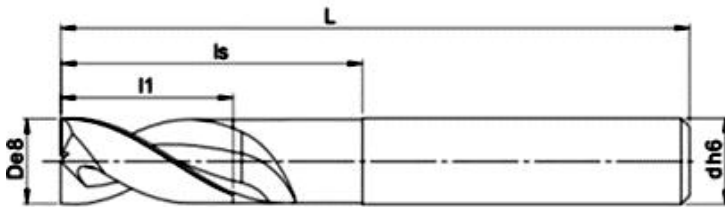


Fig. 3. Mill of Seger PUN-12-00-24/50-100-3AL (“Seger online catalog”, 2016)

Tab. 2. Technical data of Seger mill PUN-12-00-24/50-100-3AL (“Seger online catalog”, 2016)

Symbol:	PUN-12-00-24/50-100-3AL
Number of milling inserts z:	3
Cutting diameter D [mm]:	12
Overall length L [mm]:	100
Length of cut l₁ (a_p) [mm]:	50
Shrank diameter d [mm]:	12

Mill of SGS Solid Carbide Tools (44748) destined for high performance machining is presented in Fig. 4. Its technical parameters are shown in Table. 3.

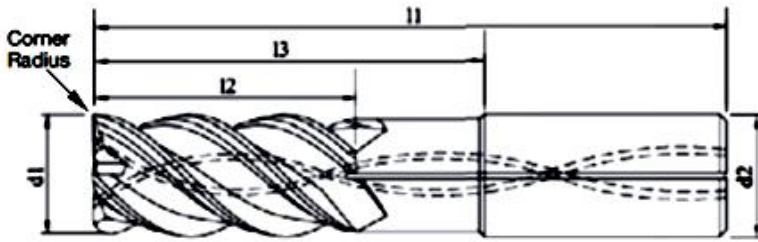


Fig. 4. Mill of SGS Solid Carbide Tools 44748 (“SGS online catalog”, 2016)

Tab. 3. Technical data of SGS Solid Carbide Tools mill 44748 (“SGS online catalog”, 2016)

Symbol:	44748
Number of flutes z :	4
Cutting diameter d_1 [mm]:	12
Length of cut l_2 (a_p) [mm]:	48
Overall length l_1 [mm]:	100
Shrank diameter d_2 [mm]:	12
Corner radius R [mm]:	2

Machining tests were carried out with technological parameters corresponding to stable and unstable ranges of work:

- for mill of Seger:
 - parameters of stable work:
 - $n = 19\,700$ rpm,
 - $a_p = 20$ mm,
 - parameters of unstable work:
 - $n = 12\,800$ rpm,
 - $a_p = 20$ mm,
- for mill of SGS:
 - parameters of stable work:
 - $n = 20\,400$ rpm,
 - $a_p = 15$ mm,
 - parameters of unstable work:
 - $n = 14\,400$ rpm,
 - $a_p = 15$ mm.

The cuboidal samples were machined during milling. They were mounted in a vice as is presented in Fig. 5.

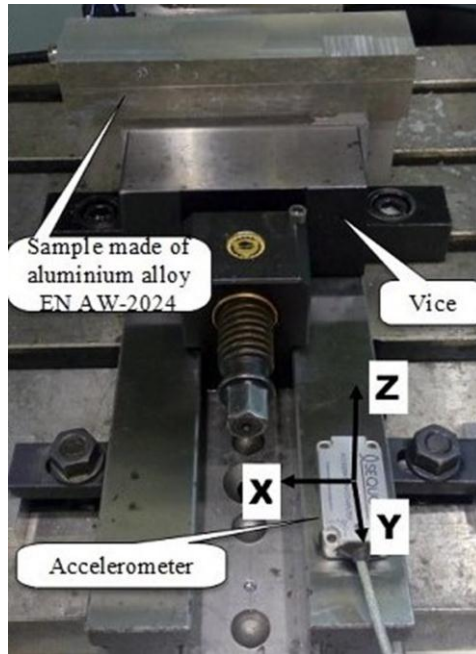


Fig. 5. Method of sample fixing

Surface quality was adopted as a criterion for evaluation of milling process stability. For this purpose, parameter Ra was measured by using a contact profilometer – Hommel Tester T1000 (Fig. 6).



Fig. 6. Hommel Tester T1000 profilometer

Measurements of surface roughness were repeated five times for each tested tool.

3. RESULTS

Based on the collected signals and defined parameters, stability lobes were generated by means of CutPro software. These charts were used for the determination of stable and unstable areas.

The obtained graphs were modified by adding the values of technological parameters for machining tests:

- stable work – green colour,
- unstable work – red colour.

The obtained stability lobes for mill of Seger is presented in Fig. 7 and Fig. 8 for mill of SGS.

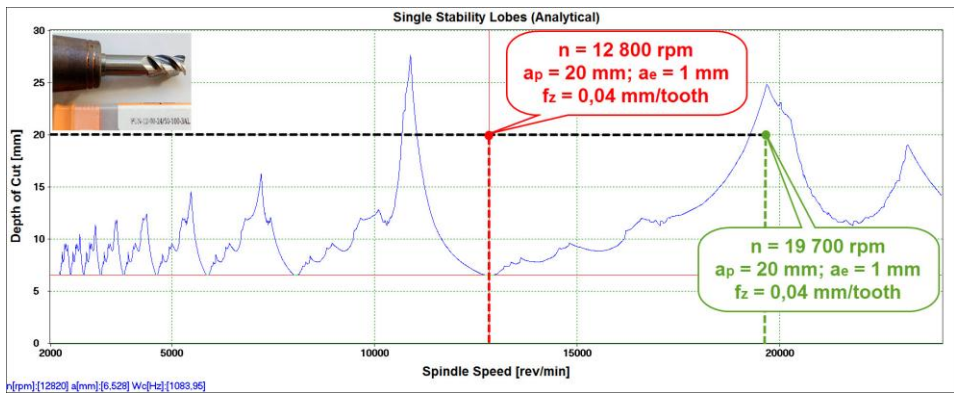


Fig. 7. Obtained stability lobes for mill of Seger

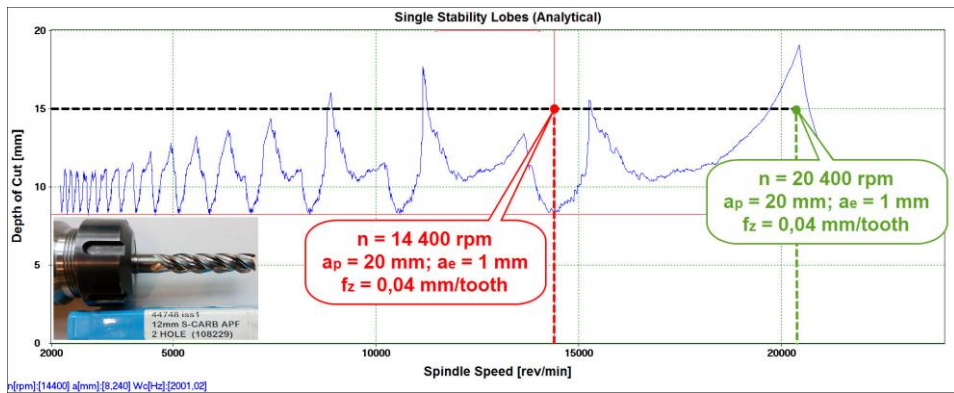


Fig. 8. Obtained stability lobes for mill of SGS (own study)

The range of stable tool work corresponds to the areas that are located under stability lobes. Based on graphs, the existence of liminal depth of cut a_p is noted below where theoretically machining is stable, regardless of cutting speed v_c . The characteristic increase of width range of stable and unstable areas with growth of rotation speed n is also visible. It facilitates the selection of machining parameters (rotation speed n), to ensure that they are located in the range of stable or unstable machining, therefore, the highest values of rotation speed n were selected for the verification. Additionally, the points corresponding to the central positions of both stable and unstable areas were taken.

Another phase of study was the verification of modal analysis usefulness for determination of milling process stability based on surface roughness measurements. The values of R_a surface roughness parameter for examined mills and technological parameters corresponding to stable and unstable machining are shown in Fig. 9.

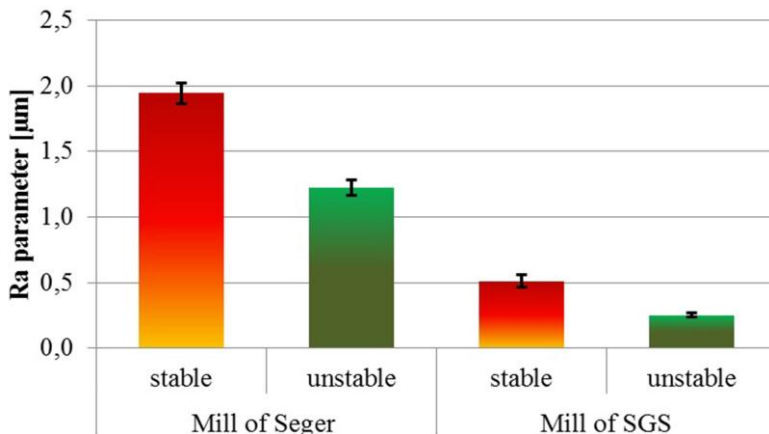


Fig. 9. The values of R_a surface roughness parameter for two tested mills and technological parameters corresponding to stable and unstable machining

With regard to graph (Fig. 9) the green columns present the obtained roughness values which according to the results of modal analysis corresponding to machining parameters ensure stable work. Unstable conditions were marked with red colour. The higher values of R_a parameter were obtained for unstable conditions of machining for both mills.

4. CONCLUSION

The conducted analysis allowed to formulate following conclusions:

- On graphs generated from CutPro software, the existence of liminal depth of cut a_p has been noted, where theoretically machining is stable, regardless of rotation speed n .

- The characteristic increase of width range of stable and unstable areas with growth of rotation speed n has been also visible.
- The higher values of R_a parameter were obtained for unstable conditions of machining for both cases.
- The performed verification allows to state that experimental modal analysis using CutPro software can be a useful tool for evaluation of milling process stability.
- The results of modal analysis help to determine machining ensuring required machining quality.

REFERENCES

- Ahmadi, K., & Ismail, F. (2012). Stability lobes in milling including process damping and utilizing Multi-Frequency and Semi-Discretization Methods. *International Journal of Machine Tools & Manufacture*, 54-55, 46–54. doi:10.1016/j.ijmachtools.2011.11.007
- Bojanowski, S., & Pawłowski, W. (2011). Teoretyczna analiza modalna zespołu wrzeciennika przedmiotu szlifierki do otworów. *Mechanik*, 84(11), 870-873.
- Budak, E., Tunc, L. T., Alan, S., & Ozguven, H. N. (2012). Prediction of workpiece dynamics and its effects on chatter stability in milling. *CIRP Annals-Manufacturing Technology*, 61(1), 339–342. doi:10.1016/j.cirp.2012.03.144
- Campa, F. J., de Lacalle, L. N. L., & Celaya, A. (2011). Chatter avoidance in the milling of thin floors with bull-nose end mills: Model and stability diagrams. *International Journal of Machine Tools & Manufacture*, 51(1), 43–53. doi:10.1016/j.ijmachtools.2010.09.008
- Ciurana, J. & Quintana, G. (2011). Chatter in machining processes: A review. *International Journal of Machine Tools and Manufacture*, 51(5), 363–376. doi:10.1016/j.ijmachtools.2011.01.001
- Kilic, Z. M., & Altintas, Y. (2016). Generalized mechanics and dynamics of metal cutting operations for unified simulations. *International Journal of Machine Tools & Manufacture*, 104, 1–13. doi:10.1016/j.ijmachtools.2016.01.006
- Lehrich, K., & Lis, K. (2014). Analiza modalna korpusu stojaka obrabiarki CNC. *Inżynieria Maszyn*, 19(1), 20-33.
- Maamar, A., Bouzgarrou, B. C., Gagnol, V., & Fathallah, R. (2017). Time Domain Stability Analysis for Machining Processes. *Advances in Acoustics and Vibration*, 5, 77–88. doi:10.1007/978-3-319-41459-1_8
- Płodzień, M., & Żyłka, Ł. (2013). Stabilność 5-osiowego frezowania stopów aluminium. *Mechanik*, 86(2), 1–12.
- Polish Norm: PN-EN 485-2:2016-10. Aluminium and aluminium alloys. Sheet, strip and plate. Part 2: Mechanical properties.
- Polish Norm: PN-EN 573-3:2014-02. Aluminium and aluminium alloys. Chemical composition and form of wrought products. Part 3: Chemical composition and form of products.
- Seeger online catalog. (n.d.). Retrieved November 30, 2016, from Seeger website, <http://www.seger.net.pl/pl>
- SGS online catalog. (n.d.). Retrieved November 30, 2016, from SGS Solid Carbide Tools website, <http://sgstool.com>
- Sun, Y., & Xiong, Z. (2017). High-order full-discretization method using Lagrange interpolation for stability analysis of turning processes with stiffness variation. *Journal of Sound and Vibration*, 386, 50–64. doi:10.1016/j.jsv.2016.08.039
- Totis, G., Albertelli, P., Sortino, M., & Monno, M. (2014). Efficient evaluation of Process stability in milling with Spindle Speed Variation by using the Chebyshev Collocation Method. *Journal of Sound and Vibration*, 333(3), 646–668. doi:10.1016/j.jsv.2013.09.043

- Totis, G., Albertelli, P., Torta, M., Sortino, M., & Monno, M. (2017). Upgraded stability analysis of milling operations by means of advanced modeling of tooling system bending. *International Journal of Machine Tools & Manufacture*, 113, 19–34. doi:10.1016/j.ijmachtools.2016.11.005
- Twardowski, P. (2006). Stabilność procesu frezowania stali na twardo w warunkach HSM. *Archiwum Technologii Maszyn i Automatyzacji*, 26(2), 93–101.
- Zhang, X. J., Xiong, C. H., Ding, Y., Feng, M. J., & Xiong, Y. L. (2012). Milling stability analysis with simultaneously considering the structural mode coupling effect and regenerative effect. *International Journal of Machine Tools & Manufacture*, 53(1), 127–140. doi:10.1016/j.ijmachtools.2011.10.004

remote laboratory, iLab , virtual experiment

Tomasz CHMIELEWSKI, Katarzyna ZIELIŃSKA***

SURVEY OF REMOTELY CONTROLLED LABORATORIES FOR RESEARCH AND EDUCATION

Abstract

This paper presents the recent advances in development and utilization of remote laboratories, which can be controlled without physical access to the equipment. Currently observed rapid increase of number of such systems is mostly owed to high-speed Internet expansion, as well as the continuous tendency to ensure the open access to modern knowledge. In this paper, various arrangements of equipment in such testing rooms are addressed in areas such as electrical engineering, electronics, mechanical engineering. A comprehensive survey of currently most popular remote laboratories worldwide is provided. The paper is concluded by the discussion that presents the authors' view point on how remote laboratories may evolve in the future.

1. INTRODUCTION

Nowadays, the computers have dominated almost each and every stage of research and education in technology or medicine. Looking back, however, the experimental work has always been a foundation of science. Therefore, despite the development of powerful virtual instruments (such as simulations) that allow engineers, researchers and students to solve variety of problems, the laboratory work, real-time measurements are still a state-of-the-art standard for introducing any kind of innovation. This can be identified at the research work flowchart presented in Figure 1.

* Electrical Engineering and Computer Science Faculty, Lublin University of Technology, Nadbystrzycka 38A, Lublin, Poland, tomasz.chmielewski@pollub.pl

** Electrical Engineering and Computer Science Faculty, Lublin University of Technology, Nadbystrzycka 38A, Lublin, Poland, katarzyna.zielinska@pollub.pl

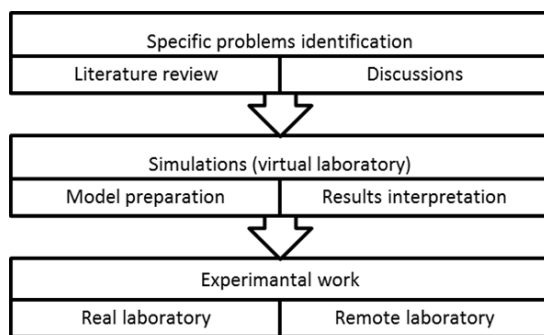


Fig. 1. Experiments in standard research approach

Furthermore, the flowchart in Figure 1 clearly displays a certain classification of carrying out the research or educational experiments. One should notice that there is a clear division on real and virtual environment laboratories with the remote technology being a mix of both (Barrios et al., 2013; Guimaraes, Cardozo, Moraes & Coelho, 2011; Henke, Ostendorff, Wuttke & Vogel, 2012; Nafalski, 2012; Nedic, Machotka & Nafalski, 2003; Orduna, Garcia-Zubia, Irurzun, Lopez-de-Ipina & Rodriguez-Gil, 2011; Tirado, Herrera, Marquez, Mejias & Andujar, 2015). Each way of conducting laboratory work has its pros and cons that may affect the choice of the methodology for a given problem. Nonetheless, it can be noticed that when the experiment is based purely on the computer tools (simulations, virtual lab) one of the research work stages is skipped, which should result in time savings, but also somewhat lower credibility of the outcome. The advantages and disadvantages of each method are listed in Table I.

Tab. 1. Pros and cons of using various types of laboratories for research and education (Nafalski, 2011)

Lab type	Pros	Cons
Real	<ul style="list-style-type: none"> • Interaction with equipment • Work in groups • Flexibility • Confirmation of hypothesis 	<ul style="list-style-type: none"> • Cost • Place restrictions • Low accessibility • Supervision required
Remote	<ul style="list-style-type: none"> • Good for concept explanation • No place restrictions • Medium cost • High accessibility 	<ul style="list-style-type: none"> • Lower flexibility • Indirect interaction with equipment
Virtual	<ul style="list-style-type: none"> • Good for concept explanation • No place and time restrictions • Low cost • High accessibility 	<ul style="list-style-type: none"> • Idealized data • Results have limited credibility • No interaction with equipment

Due to the increasing complexity, accuracy and consequently cost of today's lab equipment, the standard approach of arranging test rooms has evolved. Constant tendency of cost reduction and simultaneously rising demand of knowledge, especially in modern technology field, calls for alternatives that may meet all of above-mentioned requirements (German-Sallo, Grif & Gligor, 2015; Orduna et al., 2012, 2015; Sivakumar, Robertson, Artimy & Aslam, 2005).

One of the solutions that may address this issue and provide a remedy to the short-comings of experimental work are remote laboratories. In short, the general idea behind the remotely controlled laboratory is to create a hybrid system that utilizes hardware and software. Both of those layers are necessary and equally important in ensuring its proper operation. The software in this case is essentially the interface and the control panel that allows interacting with the hardware. This interaction should be interpreted at few levels that are characteristic to any experiment theses, i.e.: planning, assets assembly and connection, measurements and parameters variation. Software is essential also due to the fact that it guarantees the basic feature of herein discussed concept of experiment which is remote access. Today's remote laboratories are mostly web based, which means that they can be accessed worldwide via internet. The general idea behind the remote laboratory in its modern form is presented in Figure 2. As can be observed, such system operation consists in remote control over physical equipment, such as various measurement equipment, parts, connection routing, experiment parameters and so on.

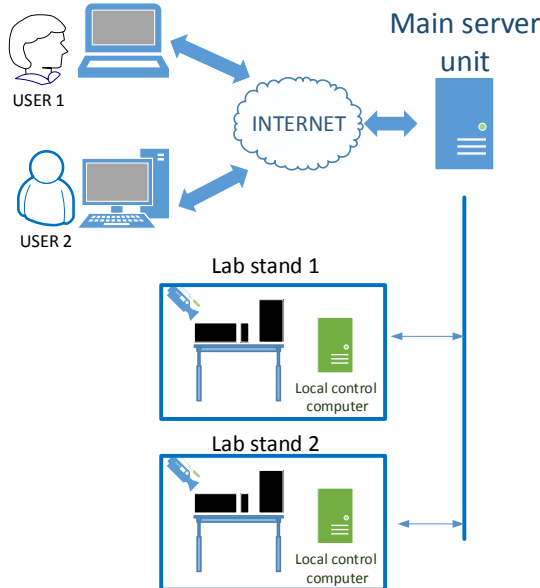


Fig. 2. Experiments in standard research approach

The entire process is supervised via camera picture and virtual interface that should be user friendly and reflect a real laboratory stand in most accurate way. Each laboratory stand needs to be designed in a way that the desired experiment can be assembled automatically. In the case of electrical circuits this means utilization of relays, transistors etc. and when it comes to, for instance, mechanical experiments, there is a need for various motors and actuators that can, for example, move certain elements. Those active parts are typically controlled by the local computer which is then connected to the main server that constitutes a gateway to the external network for all experiments. Thanks to the Internet, users may connect to their experiments regardless of their location. Moreover, the laboratory can be accessed by many users at the same time. A big advantage of such feature is the fact that those users can be only spectators, which is an interesting way of conducting, for instance, a lecture for a very large audience, hence being an excellent educational tool.

2. REMOTE LABORATORIES IN CONTROL ENGINEERING, ELECTRONICS AND PHYSICS

Due to its characteristics the area of automated control and electronics is one of the most suitable for remote laboratories implementation. The features that make those fields suitable for remote laboratories applications are most of all low power, microprocessor based solutions, easy coupling with existing software platforms such as LabView. The examples of such systems are briefly presented and described in this chapter.

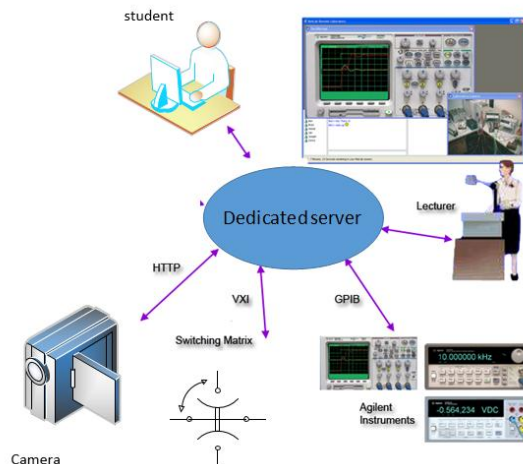


Fig. 3. NetLab architecture (source: <http://netlab.unisa.edu.au/index.xhtml>)

A good example of the remote laboratory is NetLab (Nafalski, 2011; Nedic et al., 2003), which can be used by academic staff for teaching and demonstrations during lectures, and by students for conducting their experiments remotely on real laboratory equipment (Fig. 3). The lab stand comprises passive, controllable elements, such as resistors, capacitors and inductors. The control is done by relay switching matrix from the graphical GUI prepared in Java. The measurements are taken with digital scopes. The entire experiment can be also observed via a webcam.

In (Gadzhанov, Nafalski & Nedic, 2014) an interesting concept of the laboratory is presented. It serves as a platform for motion control experiments (Fig. 4). It is based on LabView environment LabVIEW Web Services and Remote Front Panels. This not only facilitates the system implementation, but also delivers great numbers of features such as viewer mode. The entire setup comprises a 12 inch linear stage, coupled with a Brushless DC motor and controlled by a high-performance motion controller.

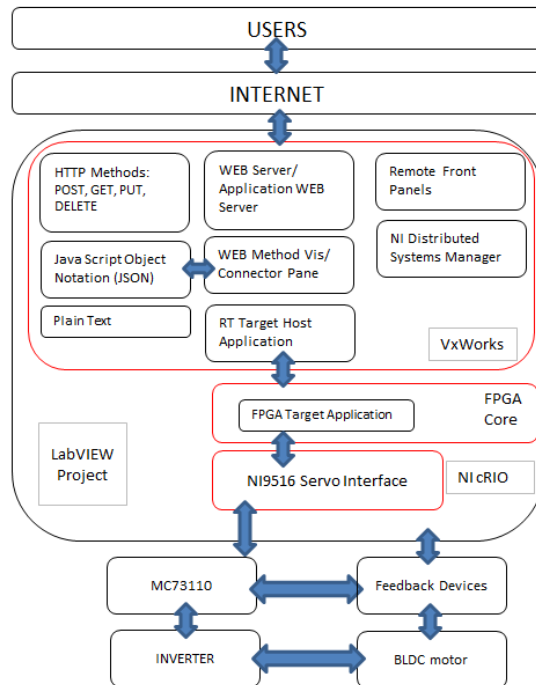


Fig. 4. Architecture of remote laboratory in proposed in (Gadzhанov et al., 2014)

High precision measurements of linear and rotary positions are fed by a resolver and resolver-to-digital converter. The entire setup is governed by the real-time controller with a Field-Programmable GateArray1 (FPGA) core from National Instruments. Such system allow to work with PID controllers and set up desired

experiments using user friendly GUI which also displays the measurements. Similar laboratory was described in (Hercog, Gergic, Uran & Jezernik, 2007) where the controlled object is a small DC motor (Fig. 5). The LabView was also used in this case; however, the entire structure of the system is slightly different. It utilizes DSP controllers that are programmed using code generated from Matlab.

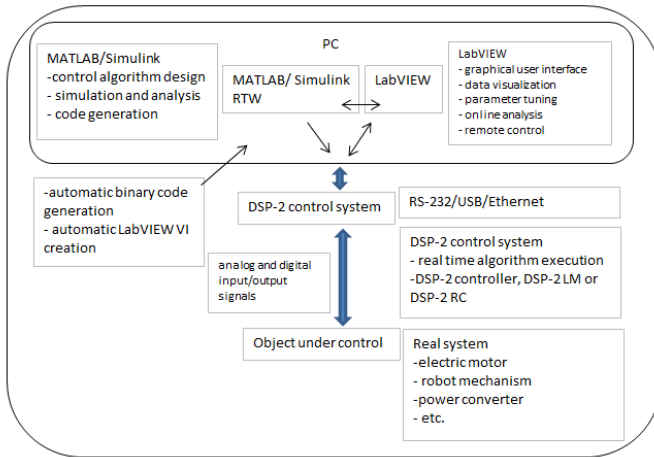


Fig. 5. Architecture of remote laboratory as proposed in (Hercog et al., 2007)

Another example of the remote laboratory which is especially useful for education is described in (Chen & Gao, 2012). PLC controllers are a crucial part of many industry applications and the laboratory described in (Chen & Gao, 2012) allows students to get some more practical knowledge about their operation and programming (Fig. 6). The authors also present a comparative study of learning effectiveness using remote lab which clearly indicates that in this case it could be a solid alternative for a real laboratory.

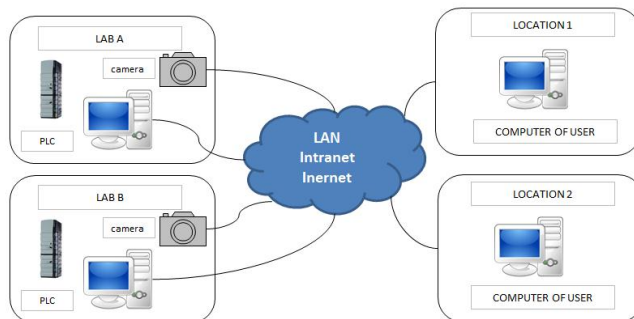


Fig. 6. Architecture of PLC remote laboratory in proposed in (Chen & Gao, 2012)

More examples of how the remote laboratories can be utilized as a tool for control engineering education can be found in (Ayodele, Inyang & Kehinde, 2015; Beghi, Cervato & Rampazzo, 2015; Exel, Gentil, Michau & Rey, 2000; Santana, Ferre, Izaguirre, Aracil & Hernandez, 2013).

Alongside control engineering, there are many other fields that can be experimentally aided by remote laboratories technology. Some of the examples are briefly described in this chapter.

As it is presented in (Del Canto, Prada, Fuertes, Alonso & Dominguez, 2015), certain aspects of cyber security can be also analyzed using the remote laboratory. The authors have proposed a test stand whose main active components are PLC controllers and network scanner. The laboratory uses two virtual machines one of which is responsible for general control over PLC and SCADA signals whereas second one is a vulnerability scanner used for testing safety protocols. The stand is also equipped in a web camera that allows observing the current status of PLC devices.

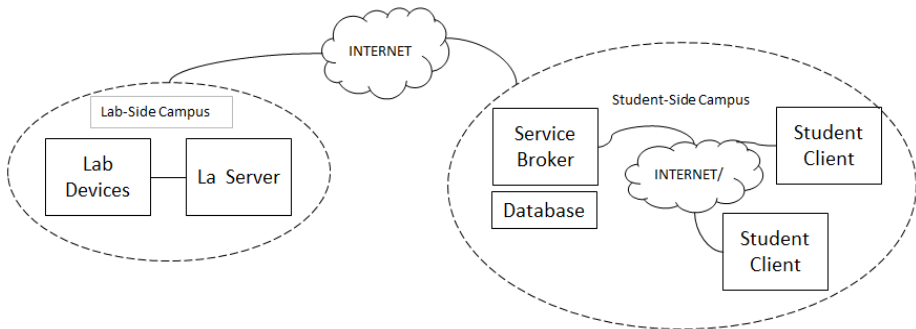


Fig. 7. MIT's iLab architecture (Hardison et al., 2008)

The work from MIT exemplifies how the remote laboratories can be applied even for nuclear (neutron) physics experiments (DeLong et al., 2010; Hardison, DeLong, Bailey & Harward, 2008). The iLab platform (presented in Fig. 7) in this case is used for experiments on the neutron beam that can be generated by the equipment installed therein. The neutron beam is generated by the 5 MW nuclear reactor that may sustain it continuously. Other elements of the lab stand are crystal, detectors, chopper and attenuation materials placed under the support structure (DeLong et al., 2010). Unfortunately, the laboratory has some limitations, namely the neutron beam is not open constantly, but it has to be manually switched on by the lab staff when the experiment is scheduled.

The mechanical systems can be as well experimentally tested in remote laboratories. A very simple test stand for oscillating beam is controlled by LabView installed on the computer. The measurements are performed by two accelerometers. The user may control the beam stimulus with few signals e.g. sinewave, triangle, saw tooth. The user accesses the experiments using LabView due to the fact that the GUI is based on LabView web UI Builder with LabView web services (Cazacu, 2014).

3. ENVIRONMENTAL AND SOCIAL ASPECTS OF REMOTE LABORATORIES

The idea of remote and the technology behind it may and already have influenced the society and its view on knowledge and education. The concept of nearly unlimited access to the lab resources may in a future evolve to change of education and research that will affect the daily activities of a students and researchers. Should the remote laboratories were applied on the wider scale, the frequency of students' attendance on traditional classes may be significantly reduced. Considering the fact that students are large group of modern society such change may lead to common benefits. For example decreased number of classes reduces the need for commuting which for some universities whose facilities are spread over large area is at high rate. Reduced number of actively commuting people can be translated to lower traffic which in turn is a direct source of pollution. Another aspect is more efficient use of laboratory space and equipment. The remote laboratory which cannot be physically accessed by the student will not be required to provide the same space as a conventional. It will also apply different health and safety rules. The effect of increased efficiency can be twofold. First is due to the fact that the remote laboratory can be used by more students because of no time restrictions the energy use can be easily managed. This can be especially important for high power tests which could be done in most convenient moment both economically and environmentally. For instance the test can be correlated in time with large energy production from renewables in order not to employ conventional power plants for this purpose.

This extends also on other aspects such as environment. Remote laboratory can be classified as a part of internet of things (IoT). IoT is basically a network of interconnected physical objects that are embedded with electronics, sensors and software that are used for data acquisition and exchange. Those devices can be used for variety of purposes this includes also the water, soil and atmosphere quality and pollution, radiation, electromagnetic fields etc. from the environmental point of view. The wide range of applications related to environmental topics is presented in (Estevez & Wu, 2015). Those are related to sensors and their coordination for energy management (e.g. lights control), harvesting the energy from renewables (e.g. PV panels and energy storage monitoring and optimization). The author of (Estevez & Wu, 2015) provides also the application

of remote measurements. One of the best example is the air pollution measurement which consequently leads to better monitoring and alerts that when announced lead to pollution reduction e.g. by means of traffic restriction. Based on remote sensors coupled via internet the services can act fast when for instance the weather conditions change and the air pollution rises.

In (Wong, MatJafri, Abdullah & Lim, 2009) authors also propose to apply remote measurements of air pollution by means commonly used internet protocol (IP) camera. The solution utilizes an advances image processing algorithms for determination of PM10 particles concentration in air. Such solution is especially beneficial and cost efficient for highly urbanized areas where the image monitoring (e.g. security, traffic control etc.) is nowadays common. Taking into account the numbers of IP cameras installed in a modern cities the pollution measurement grid could be greatly extended, yielding more data nearly as accurate as the one obtained from the dustmeter. Hence m the research on air pollution could benefit from such measurement system data the research. The access to the measurement and possible image processing algorithm modification is essentially unlimited via the internet. Similar idea was presented in (Wang, Zhang, Huang & Li, 2010) however the “sensors” were in a way aggregated i.e. satellite image was used instead of number of cameras.

One of the finest examples of remote laboratories and how it is indispensable for environmentally related research is presented in (Richter et al., 2016). The authors describe the complex system for research on Bioenergy production from agricultural crop. The system included number of steps such as modeling and observations as well as on site measurements on each considered farm. However, what makes it unique is that the remote control via satellites was performed. Based on the images the farm productivity could be constantly monitored and assessed. Bearing in mind that the research included 23 farms conduction of on-site monitoring would be problematic and time consuming.

In general the remote laboratories and measurements concerning the environmental aspects can be classified as follows:

- Air, water and soil pollution monitoring,
- Whether and lighting contains monitoring for energy management,
- Research on aboveground biomass,
- Remote laboratory for biomass energy heating,
- Research on farming for better biomass production.

Additionally the applications of remote laboratories presented in the preceding sections indirectly affect the environment by decreasing pollution and increasing the energy efficiency. The research and resulting innovations in the area of electronics and control engineering were in fact among the most important factors that reduced e.g. greenhouse gases by the automotive transport. The efficiency of modern petrol and diesel engines is far better than few decades ago.

This is mainly to be owed to the modern electronics that monitors and control the combustions process to make it more efficient. The remote laboratories with the unlimited access for the students and researchers are great stimulant for an innovation also for such applications as energy efficiency and lowering the fuel usage.

4. FUTURE OF REMOTE LABORATORIES

As the technology evolves it provides new, innovative tools that may also affect the way that we think about the remote laboratories. One of the examples of such effect on herein discussed topic are mobile technologies that have recently taken over many areas of our life. Such approach was presented in (Orduna et al., 2011), where the concept of the access via mobile phone was presented. If we could assume that the mobile devices will continue to develop at this pace, then their role as a tool for remote laboratory control will grow. Thanks to that the user could supervise or modify the experiment easily but also receive online notifications about recent parameters of the given process.

Another tool that could revolutionize the remote lab is “virtual reality”. Using devices such as Oculus Rift, one could imagine that the user could actually increase the interaction with the laboratory without physical presence in the test room. This function could be also realized by the holographic 3D imaging. Robotics could also play a big role in remote lab development. Precise robots could be useful, for example, in chemistry related experiments or in other fields where physical interaction with the equipment is necessary. Remotely-controlled humanoid robots – which could act as a user’s avatar – is not an impossible scenario. Such approach would be especially beneficial for the experiments that have to be performed in clean or hazardous environment.

Last but not least, all the above-mentioned tools could be aided by artificial intelligence (AI). AI protocols could actually help with design of experiment and then, at least in some portion, with the execution e.g. parts or ingredients gathering and delivering to the test stand.

5. SUMMARY

The authors have presented the issue of remote laboratory in research and education with strong focus on showing the wide range of science fields that can make use of this emerging technology. Advantages and disadvantages of remote labs were also compared with simulations and hands-on experiments. The paper discusses also the impact of remote experiments and measurements on environment and prospects for improvement of overall factors that are affecting the environment. Moreover, the authors have speculated on how the remote laboratory topic may evolve in the future.

REFERENCES

- Ayodele, K. P., Inyang, I. A., & Kehinde, L. O. (2015). An iLab for Teaching Advanced Logic Concepts With Hardware Descriptive Languages. *IEEE Transactions on Education*, 58(4), 262–268. doi:10.1109/te.2015.2395996
- Barrios, A., Panche, S., Duque, M., Grisales, V. H., Prieto, F., Villa, J. L., Chevrel, P., Canu, M. (2013). A multi-user remote academic laboratory system. *Computers & Education*, 62, 111–122. doi:10.1016/j.compedu.2012.10.011
- Beghi, A., Cervato, A., & Rampazzo, M. (2015). A Remote Refrigeration Laboratory for Control Engineering Education. *IFAC PapersOnLine*, 48(29), 25–30. doi:10.1016/j.ifacol.2015.11.208
- Cazacu, D. (2014). A remote laboratory for frequency-response analysis of vibrating mechanical systems. *7th International Conference Interdisciplinarity in Engineering (Inter-Eng 2013)*, 12, 675–680. doi:10.1016/j.protcy.2013.12.548
- Chen, X. M., & Gao, H. Y. (2012). A Remote PLC Laboratory Design and Realization. *International Conference on Advances in Computational Modeling and Simulation*, 31, 1168–1172. doi:10.1016/j.proeng.2012.01.1158
- Del Canto, C. J., Prada, M. A., Fuertes, J. J., Alonso, S., & Dominguez, M. (2015). Remote Laboratory for Cybersecurity of Industrial Control Systems. *IFAC PapersOnLine*, 48(29), 13–18. doi:10.1016/j.ifacol.2015.11.206
- DeLong, K., Harward, V. J., Bailey, P., Hardison, J., Kohse, G., & Ostrotsky, Y. (2010). Three online neutron beam experiments based on the iLab Shared Architecture. *IEEE EDUCON 2010 Conference*, 7(1), 145–150. doi:10.1109/EDUCON.2010.5492587
- Estevez, C., & Wu, J. (2015). Recent advances in Green Internet of Things. *2015 7th IEEE Latin-American Conference on Communications (LATINCOM)*, 1–5. doi:10.1109/LATINCOM.2015.7430133
- Exel, M., Gentil, S., Michau, F., & Rey, D. (2000). Simulation workshop and remote laboratory: Two web-based training approaches for control. *Proceedings of the 2000 in American Control Conference*, 5, 3468–3472. doi:10.1109/ACC.2000.879213
- Gadzhanov, S. D., Nafalski, A., & Nedic, Z. (2014). LabVIEW based remote laboratory for advanced motion control. *2014 11th International Conference on Remote Engineering and Virtual Instrumentation (REV)*, 129–136. doi:10.1109/REV.2014.6784237
- German-Sallo, Z., Grif, H. S., & Gligor, A. (2015). Technical evaluation of remote laboratories in an engineering educational network. *8th International Conference Interdisciplinarity in Engineering, Inter-Eng 2014*, 19, 1136–1141. doi:10.1016/j.protcy.2015.02.162
- Guimaraes, E. G., Cardozo, E., Moraes, D. H., & Coelho, P. R. (2011). Design and Implementation Issues for Modern Remote Laboratories. *IEEE Transactions on Learning Technologies*, 4(2), 149–161. doi:10.1109/tlt.2010.22
- Hardison, J. L., DeLong, K., Bailey, P. H., & Harward, V. J. (2008). Deploying interactive remote labs using the iLab Shared Architecture. *2008 38th Annual Frontiers in Education Conference*, S2A-1-S2A-6. doi:10.1109/FIE.2008.4720536
- Henke, K., Ostendorff, S., Wuttke, H., & Vogel, S. (2012). A grid concept for reliable, flexible and robust remote engineering laboratories. *9th International Conference on Remote Engineering and Virtual Instrumentation*, 8, 42–49.
- Hercog, D., Gergic, B., Uran, S., & Jezernik, K. (2007). A DSP-based remote control laboratory. *IEEE Transactions on Industrial Electronics*, 54(6), 3057–3068. doi:10.1109/tie.2007.907009
- Nafalski, A., (2012). *Remote Laboratories Developments in Electrical Engineering*. Lublin: Politechnika Lubelska.
- Nedic, Z., Machotka, J., & Nafalski, A. (2003). Remote laboratories versus virtual and real laboratories. *33rd Annual Frontiers in Education*, 2003. *FIE 2003*, 1, T3E-1-T3E-6. doi:10.1109/FIE.2003.1263343
- Orduna, P., Garcia-Zubia, J., Irurzun, J., Lopez-de-Ipina, D., & Rodriguez-Gil, L. (2011). Enabling mobile access to Remote Laboratories. *2011 IEEE Global Engineering Education Conference (EDUCON)*, 312–318. doi:10.1109/EDUCON.2011.5773154

- Orduña, P., Rodríguez-Gil, L., Angulo, I., Dziabenko, O., López-de-Ipiña, D., & García-Zubia, J. (2012). Exploring students collaboration in remote laboratory infrastructures. *2012 9th International Conference on Remote Engineering and Virtual Instrumentation (REV)*, 1–5. doi:10.1109/REV.2012.6293159
- Orduna, P., Zutin, D., Govaerts, S., Zorrozuza, I. L., Bailey, P.H., Sancristobal, E., Salzmann, C., Rodríguez-Gil, L., DeLong, K., Gillet, D., Castro, M., Lopez-de-Ipina, D., & Garcia-Zubia, J. (2015). An Extensible Architecture for the Integration of Remote and Virtual Laboratories in Public Learning Tools. *IEEE Revista Iberoamericana De Tecnologias Del Aprendizaje-Ieee Rita*, 10(4), 223–233. doi:10.1109/rita.2015.2486338
- Richter, G. M., Agostini, F., Barker, A., Costomiris, D., & Qi, A. M. (2016). Assessing on-farm productivity of Miscanthus crops by combining soil mapping, yield modelling and remote sensing. *Biomass & Bioenergy*, 85, 252–261. doi:10.1016/j.biombioe.2015.12.024
- Santana, I., Ferre, M., Izaguirre, E., Aracil, R., & Hernandez, L. (2013). Remote Laboratories for Education and Research Purposes in Automatic Control Systems. *IEEE Transactions on Industrial Informatics*, 9(1), 547–556. doi:10.1109/tii.2011.2182518
- Sivakumar, S. C., Robertson, W., Artimy, M., & Aslam, N. (2005). A web-based remote interactive laboratory for Internetworking education. *IEEE Transactions on Education*, 48(4), 586–598. doi:10.1109/te.2005.858393
- Tirado, R., Herrera, R. S., Marquez, M. A., Mejias, A., & Andujar, J. M. (2015). Comparing Remote Laboratories from the Student Perspective. *IFAC PapersOnLine*, 48(29), 176–181. doi:10.1016/j.ifacol.2015.11.233
- Wang, D., Zhang, C., Huang, Y., & Li, W. (2010). Visualizing Air Pollutants through Image Processing. *2010 2nd International Conference on Information Engineering and Computer Science*, 1–4. doi:10.1109/ICIECS.2010.5678349
- Wong, C. J., MatJafri, M. Z., Abdullah, K., & Lim, H. S. (2009). Determination of aerosol concentration using an internet protocol camera. *2009 IEEE Aerospace conference*, 1–7. doi:10.1109/AERO.2009.4839344